UNIVERSITY OF SOUTHAMPTON

Faculty of Engineering and Physical Sciences
School of Engineering

A geometric model for non-equilibrium turbulence

by

James Leetch

BEng, MSc

ORCiD: 0009-0001-7963-0202

A thesis for the degree of
Doctor of Philosophy

March 2026

University of Southampton

Abstract

Faculty of Engineering and Physical Sciences
School of Engineering

Doctor of Philosophy

A geometric model for non-equilibrium turbulence

by James Leetch

This thesis presents a geometric framework for implicit large-eddy simulation (iLES) of turbulent boundary layers. By embedding the Navier-Stokes equation within a non-Euclidean manifold, an implicit description is generated in which the sub-grid stress tensor is replaced by an effective metric tensor. The manifold reframes the turbulence modelling problem, offering a novel, resolution-independent mathematical structure that connects locally universal, inertial behaviour of turbulence with the non-universal, tensor structure of general conditions. The result is a model which is strictly local, simplifying the resultant modelling problem, ensuring minimal sensitivity to the specific inhomogeneity and anisotropy of particular flow conditions, and removing reliance upon both empirical assumptions and data.

The method functions as a unified wall and sub-grid scale model which is validated across zero- and adverse-pressure-gradient (APG) flat plate boundary layers, and a NACA4412 aerofoil case. Accurate prediction of mean velocity profiles is achieved without adjustment and the method performs robustly across a large range of resolution regimes. The results confirm that the framework achieves its aim of minimising conditions-sensitivity, while maintaining accuracy in a diverse range of conditions.

Limitations remain particularly in the representation of boundary layer tripping/transition, which leaves minor issues in the prediction of specific Reynolds stress component under history-dependent APG conditions. Nonetheless, the results demonstrate that geometric iLES provides a promising alternative to the classical methodology. The work provides a unique foundation for implicit turbulence models to be equipped with the rich tensor structure that facilitates descriptions of general conditions. This contribution is particularly relevant for the predictive simulation of turbulence under general APG conditions where statistical behaviour is strongly non-universal/problem-dependent and where equilibrium assumptions crucial to the classical, explicit description break down.

Contents

List of Figures

List of Tables

Declaration of Authorship

I declare that this thesis and the work presented in it is my own and has been generated by me as the result of my own original research.

I confirm that:

1. This work was done wholly or mainly while in candidature for a research degree at this University;
2. Where any part of this thesis has previously been submitted for a degree or any other qualification at this University or any other institution, this has been clearly stated;
3. Where I have consulted the published work of others, this is always clearly attributed;
4. Where I have quoted from the work of others, the source is always given. With the exception of such quotations, this thesis is entirely my own work;
5. I have acknowledged all main sources of help;
6. Where the thesis is based on work done by myself jointly with others, I have made clear exactly what was done by others and what I have contributed myself;
7. None of this work has been published before submission

Signed:..... Date:.....

Acknowledgements

I would like to express my sincere gratitude to my supervisors. I am especially grateful for the constructive discussions, insightful input, and encouragement which played a significant part in forming this thesis.

I am deeply thankful to Bharathram Ganapathisubramani and Gabriel Weymouth through the University of Southampton, and to Vinh-Tan Nguyen through the Singapore Agency for Science, Technology and Research (A*STAR) for providing me with the opportunity to pursue this research, as well as for securing the necessary funding and coordinating this collaborative project. Their support made this work possible and is greatly appreciated.

To all three, I extend my heartfelt thanks for their time, patience, and mentorship.

To An Shu

Definitions and Abbreviations

Coordinates and spaces

t	Time
x^i	The spatial coordinate
Ω_f	The subspace of the fluid domain
Ω_b	The subspace of the body domain
Ω	The unified domain $\Omega_f + \Omega_b$
$\mathbb{R}$	The set of real numbers
y	Wall-normal distance
y^+	Non-dimensional wall-normal distance defined as $y_n u_\tau / \nu$
M	A Riemann manifold with metric tensor g

Scalar fields

p	The pressure field
Z	The configuration integral

Vector fields

u^i	The velocity field
U_i	The velocity field distribution across a finite volume

Tensor fields

τ^{ij}_{SGS}	The sub-grid scale stress tensor
τ^{ij}_{ν}	The viscous stress tensor
g_{ij}	The metric tensor
h_{ij}	The induced metric tensor on a surface
δ_{ij}	The Euclidean metric tensor
S^{ij}	The rate-of-strain tensor
Φ^{ij}	The momentum flux

Operators

$\mathbb{E}(\cdot)$ or $\langle \cdot \rangle$	The expectation operator
$\bar{\cdot}$	The LES filter operator
∇_i	The (covariant) divergence operator

Constants and other parameters

Re	Reynolds number
Re_τ	Friction Reynolds number
β	Clauser pressure gradient parameter
u_τ	Friction velocity
ν	Viscosity
m	The external velocity distribution exponent
δ_0^*	The inlet displacement thickness
δ_{99}	The 99% boundary layer thickness
U_∞	The free-stream velocity
θ	Boundary layer momentum thickness

Abbreviations

CFD	Computational fluid dynamics
LES	Large-eddy simulation
RANS	Reynolds-average Navier-Stokes
DNS	Direct numerical simulation
SGS	Sub-grid scale
WMLES	Wall-modelled large-eddy simulation
iLES	Implicit large-eddy simulation
HIT	Homogeneous, isotropic turbulence
ZPG	Zero pressure gradient
APG	Adverse pressure gradient
BDIM	Boundary data immersion method

Chapter 1

Introduction

Over the past few decades, viscous computational fluid dynamics (CFD) has become established as a valuable tool and found extensive application in both academic and industrial analysis. In view of the increasing pressure for technological progress, perhaps the single most restrictive barrier to development is the difficulty faced in dealing with wall-bounded turbulence. Together, the scientific and computational challenges of the problem and its ubiquity in both nature and engineering make research in this area important to a wide variety of fields.

Ultimately, the Navier-Stokes equation has been known since the mid-19th century and in principle provides a complete description for the fluid dynamics of turbulent flows. However, its predictive power is strongly limited by computation, because high Reynolds number solutions are described by intractable amounts of information. This distinguishes turbulence as a physical problem in which dealing with limited information is central.

> Since the inception of thermodynamics, a delicate tension between physics and information has been unfolding.
>
> (Witkowski et al. (2024))

At the time of writing, the largest computing facilities have reached exa-scale (Atchley et al., 2023). Despite the availability of such immense computing power, a direct numerical simulation (DNS) representative of airflow around a large commercial airliner in flight might still take on the order of decades to complete under optimistic assumptions. While the Reynolds number of this problem is relatively high (of the order 10^8), other practically relevant flows have yet higher complexity. For example, even for a large cargo vessel at Reynolds number of the order 10^9, a DNS might take millennia. Given the strong scaling of computational cost with Reynolds number and global atmospheric flows reaching Reynolds numbers of the order 10^{12}, full solutions

to the Navier-Stokes equation are quite often inconceivable. It is this overwhelming complexity that must be tamed in order to answer important questions about our modern world, both in engineering and in the natural sciences.

The goal of this thesis and of turbulence modelling in general is to make these turbulent solutions more and more tractable. Because a full solution to the Navier-Stokes equation requires resolution of the smallest, viscous length and time scales present in a flow, an alternative theory must be described which governs turbulent flows at observation length and time scales larger than the viscous scales. With relatively coarser resolution, the computational cost is reduced, and if the requirement for total resolution of all scales can be relaxed entirely, computational effort may then be chosen based on the precision required, rather than as a condition for accuracy. After all, the very finest details do not hold information which is worth knowing for the CFD practitioner. Approaches which aim to coarsen resolution relative to both the viscous length and time scales are collectively referred to as large eddy simulation (LES). Because LES retains both the dominant spatial and temporal dynamics, it is believed to be the most promising candidate to facilitate tractable computation of the most complex 3-dimensional and unsteady turbulent fluid flows, offering fundamental advantages in both accuracy and precision over industry-standard Reynolds-averaged Navier-Stokes (RANS) solvers (Piomelli, 2014).

Equipped with a resolution which does not necessarily capture the smallest scales of a flow, the action of unresolved scales must be represented using a "sub-grid scale" (SGS) model in order to maintain accuracy. The purpose of the LES model is to maintain conservation of both energy and momentum when the observation scale is larger than the viscous scales. If the action of the sub-grid scales can be modelled accurately, the LES approach leads to independence of computational cost from Reynolds number.

The efficient prediction of turbulent fluid flow which LES aims to achieve is highly relevant from both an industrial and societal point of view because of its direct influence on efficiency, safety, cost, and environmental impact across many sectors. Were LES made possible for general flows, such a technology would create far-reaching potential for developments over the wide range of scientific and engineering fields which deal with turbulent fluid flows. In aerospace and automotive industries, predicting turbulent effects allows engineers to design for reduced drag, improved lift and enhanced stability, overall enabling quieter, safer and more fuel-efficient designs (Hucho and Sovran, 1993). In the marine and offshore sector ship hull design, offshore platforms and subsea flows all rely on turbulence prediction for increasing durability and energy efficiency (Carlton, 2019). Understanding of turbulent dispersion is key for predicting wildfires, volcanic ash, and spread of airborne disease (Bourouiba, 2021; Nieuwstadt and Van Dop, 2012). In urban planning, modelling turbulent airflow in cities allows for the management of pollutant

dispersion, and facilitates microclimate design for healthier living spaces. Wind loads on skyscrapers, bridges, and other urban structures all depend on turbulence and must be effectively evaluated to ensure structural safety and comfort Simiu and Scanlan (1996). Climate and weather modelling also deals with atmospheric and ocean turbulence, which in combination drive transport of heat, moisture, and pollutants globally (Stevens and Lenschow, 2001). Improved LES models would directly enhance crucial forecasts and climate projections alike. Turbulent fluid flows are also central in the production of energy, particularly in steam or combustion turbines and wind farms, and turbulent flows drive a large proportion of all electrical generation (Burton et al., 2021). Where fluids need to be mixed in combustion chambers, reactors and heat exchangers, harnessing the properties of turbulent flow is essential for efficiency, with improved predictions of flow behaviour leading to higher throughput and more efficient operation (Peters, 2000). More effective turbulent mixing leads to cleaner combustion or other reactions, with reduced fuel consumption and reduced pollutant or by-product formation. Overall, turbulence modelling in CFD - especially via spatio-temporal LES - underpins a wide range of current and prospective technological innovation across modern society, with significant power to impact the environment, the economy and other aspects of life.

However, due to limitations in modelling of the sub-grid scales, independence of computational cost from Reynolds number has not yet been achieved for many problems. Particularly important in practical use cases are turbulent boundary layers formed at the interface between a fluid and solid object. At present, the computational cost of many LES boundary layer simulations still renders them impracticable or more often impossible for most potential use cases in the foreseeable future (Piomelli, 2014). Although relatively complete LES modelling has indeed proven possible under certain conditions such as for boundary layers without significant pressure gradient effects, generally effective LES modelling is not yet possible for boundary layer flows under the effects of pressure gradient, where the behaviour of sub-grid scales is often observed to be non-universal and problem-dependent (Reynolds, 1990; Chapman, 1979). In practice, pressure gradient conditions are pervasive in real-world applications, making them a significant area of focus.

In view of the significant success of LES under universal, “equilibrium” conditions, the difficulties faced under pressure gradient conditions represent a key gap in both practical capabilities and in the scientific understanding behind LES. Pressure gradient boundary layer flows are not only especially common in engineering contexts, bringing strong demand for improvements in the efficiency and accuracy of predictions, but they also present an important underlying scientific problem. While a consensus has not yet been reached, the current evidence shows that pressure gradient conditions - particularly those far from equilibrium - lead to non-universal statistical behaviour and to the collapse of the scaling laws and equilibrium assumptions

underpinning classical turbulence theory (Goldenfeld and Shih, 2017; Maciel et al., 2017; Vassilicos, 2023).

In order to approach the problems presented by non-equilibrium turbulence, the basic functions of an LES model must first be established under equilibrium. The principal task of LES modelling is to describe the turbulent energy cascade, because sub-grid scales contain flow structures in which the kinetic energy of turbulent motions is removed from the flow by viscous dissipation. Consequently, an LES model must provide energy dissipation which is physically consistent in the sense that it matches the underlying, viscous dissipation which has been left unresolved. Where wall boundaries are present, the sub-grid scales also contain the viscous wall shear stress, which acts to remove momentum from the fluid domain and transfer it to the wall. Thus, in wall bounded turbulent flows without viscous-scale resolution, an LES model must also provide a physically consistent removal of momentum from the flow.

In the literature, these two main functions - to remove energy and momentum in a physically consistent manner - are usually treated separately. For wall bounded conditions, the modelling of the viscous momentum flux is mostly if not always treated separately by using LES "wall models". These models typically provide an explicit momentum flux at the wall by imposing a modified boundary condition. On the other hand, LES modelling of viscous energy dissipation has been achieved using two major methodologies which differ significantly in their approach and philosophy. Overall, the predominant philosophical tension in the field lies here.

The two predominant methodologies differ in fundamental ways which prove crucial when they are confronted by non-equilibrium turbulence. The classical, "explicit" LES methodology chooses to derive a new governing equation from the Navier-Stokes equation. In this process, small-scale degrees of freedom present in the Navier-Stokes equation are explicitly removed, being filtered out as illustrated in Figure 1.1. The filter applied to the Navier-Stokes equation creates a sub-grid scale (SGS) stress tensor which explicitly represents the action of unresolved scales by generating an "effective" force which only appears at large observation scales. In short, because small-scale degrees of freedom are explicitly removed from the solution, their effects must be explicitly replaced. This problem is known as the closure problem, and means that the SGS stress tensor must be empirically modelled by applying correlations which have been observed beforehand under certain conditions. The implication is that energy is conserved indirectly as the result of applying an accurate empirical model. Although this methodology follows a promising line of reasoning which is very successful under certain conditions, it has proven famously difficult to pose universal, empirical statements about the behaviour of turbulent flows. Turbulence is often cited as the major unsolved problem of classical physics for this reason and the task of finding a general solution to the SGS closure problem may be a practically insurmountable challenge.

On the other hand, the "implicit" LES methodology does not explicitly remove small-scales from the theory and so does not deal with a closure problem. Nevertheless, the method aims to directly conserve energy by using mathematical constraints imposed on the large-scale solution. These constraints can be used in such a way to ensure that the coarse-grained, low resolution solution remains physically consistent with the full solution to the Navier-Stokes equation.

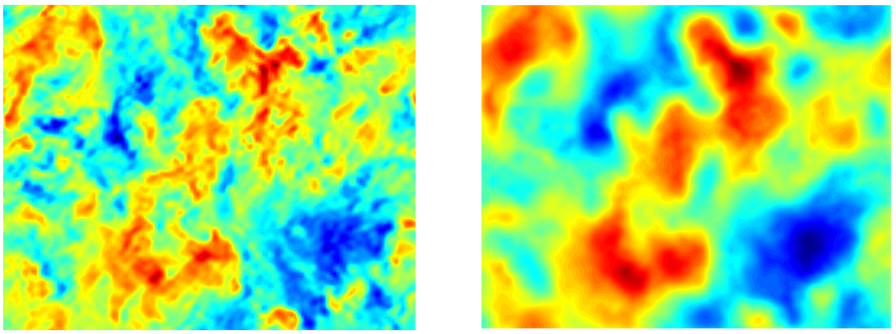

(A) Original DNS

(B) Box-filtered with length scale $L/16$

FIGURE 1.1: A velocity field created by DNS of homogeneous decaying turbulence (Lu et al., 2007) with and without filtering of small scales. The domain size is $L \times L$.

Without a general solution to the closure problem, there is no guarantee that any given explicit LES model will continue to provide accurate conservation under new conditions. Moreover, empirical models are effective where the conditions in question have already been studied and are known to have statistics compatible with the model used. Hence, the predictive capability of explicit LES models is hindered by the requirement for input of empirical data valid in the context of a particular problem. Furthermore, it is becoming increasingly apparent that the space of possible conditions is overwhelmingly large. With extensive study having been carried out over the past half a century, new exploration of this space is rapidly becoming more demanding. In earlier studies, experimental measurements or detailed numerical simulations were used to calibrate closed-form algebraic expressions for sub-grid scale closure (Lilly, 1966). Under the current regime of computational expansion and with the development of statistical models which can handle unprecedentedly large datasets, there exists an ongoing task in empirically describing more possible turbulence conditions. This has become a large scale area of research, with the increasing difficulty of further exploration being exemplified by a recent surge in popularity of machine learning techniques which offer potential for compression of larger datasets encapsulating a yet wider scope of conditions (Liu et al., 2022; Stoffer et al., 2021). Currently, there is a particularly intense focus on describing pressure gradient boundary layer flows, driven by their widespread occurrence in practical problems of interest, and by the issues encountered by present models when applied to this class of flows (Tanarro et al., 2020; Mahajan et al., 2026; Balin et al.). For example, Vinuesa et al. (2017) observe that "it is more problematic to define criteria

based on empirical correlations for general [pressure gradient turbulent boundary layers]". Despite intense and sustained research effort, a relatively complete solution to the closure problem has remained elusive under this class of conditions.

Indeed, with significant difficulties having been experienced in practice, it has also been established that pressure gradient boundary layer flows have certain properties which may fundamentally frustrate attempts to describe them empirically. While explicit LES provides a pragmatic framework for empirical modelling, there is little evidence to suggest that the closure problem it generates remains well-posed for all flows. On the contrary, pressure gradient boundary layer data in particular provides strong evidence to suggest that explicit LES may not always be an efficient approach to solving the turbulence problem.

It can be argued that non-equilibrium conditions present a fundamental problem in that their causal structure damages the efficacy of or invalidates the methodology employed by explicit LES. In short, LES fundamentally relies upon the existence of an empirical correlation which describes the small, sub-grid scales based on the large, resolved scales. Equilibrium flows naturally align with this requirement because quantities follow cascade processes.

> Big whorls have little whorls
> Which feed on their velocity,
> And little whorls have lesser whorls
> And so on to viscosity. (Richardson, 1920)

This feature of turbulence is its most well-established property and generates equilibrium fluxes of energy and momentum. In general, where the arrow of causation points from large scales to small scales, a valid correlation for LES sub-grid scale modelling can be found. In these cases, the small scales are termed "decoupled" or "separable" from the large scales, as a consequence of the fact that they do not act to determine the large scale behaviour; energy, momentum and information all flow from large scales to small scales. However, this is a simplified description valid only under specific, equilibrium conditions. In reality, it does not capture the full nature of turbulence which is in general a more complex, non-equilibrium statistical system which often temporarily reverses the arrow of causation (Goldenfeld and Shih, 2017).

The phenomenon of intermittent "feedback" from the small scales into the large scales creates a serious conceptual problem for LES. Where the details of the small scales have a significant effect the large scales, the task of solving the LES closure problem is no longer well-posed because the small scales are coupled with, and not separable from the large scales. Overall, because non-equilibrium is known to create coupling between scales, the explicit LES approach which separates and discards the small

scales is no longer consistent with the physical situation. Where it is unavoidable that the large-scale behaviour depends on non-universal small scale information, it is argued that the explicit removal of the small scales from the problem is not an efficient approach. Statistical non-equilibrium induced by pressure gradients in boundary layer flows can therefore be seen to directly hinder empirical descriptions.

At its core, the empirical method relies upon the rigorous definition of statistical ensembles. In equilibrium statistical systems, these are well-defined and produce universal probability distributions which hold regardless of microscopic details and therefore describe universal physical characteristics. This does not apply for non-equilibrium systems; yet, explicit LES relies upon the explicit sampling of a statistical ensemble. For the LES closure problem, statistics are sampled under the LES filter kernel which is typically spatial in character. Where the turbulence is homogeneous and isotropic, positions within the support of the LES kernel have identical statistics. Hence, the sampling can be interpreted to form a valid collection of statistical information. However, this remains valid only if positions within the support of the kernel have identical statistics. Under most conditions of interest, the statistical properties of the flow are neither homogenous nor isotropic. Therefore, the probability distribution which must be modelled to describe the sub-grid scale closure in most cases is not universal, but depends on the specific nature of the inhomogeneity and anisotropy present under a particular flow condition. The conditions-dependence introduced by spatial sampling is a fundamental factor limiting the generalisation of LES modelling.

Where spatial sampling cannot produce a valid ensemble, it may also be argued that temporal sampling can. In other words, while an LES model may have an effect which is not instantaneously accurate due to local inhomogeneity and anisotropy, its average effect over time may still be correct. This concept is valid for equilibrium boundary layers for example because systems in equilibrium are ergodic such that time averages are formally equivalent to ensemble averages. However, non-equilibrium systems also preclude this by exhibiting history dependency. In general for non-equilibrium statistical systems, statistics depend on the path the system took to reach to a certain state, not only on the current state itself. In the context of pressure gradient boundary layer turbulence, this is a key observed property; two boundary layers with the same local properties may behave differently depending on their evolution history (Vinuesa et al., 2017).

Overall, the combined effect of anisotropic, inhomogeneous and history-dependent conditions found in the conditions of interest is to eliminate the possibility of forming a valid statistical ensemble based on explicit spatial and/or temporal sampling. The strong implication of this observation is that the LES closure problem is left fundamentally ill-posed where a valid statistical ensemble upon which to base a model cannot be formed. Without solid statistical foundations, the turbulence

modelling problem must be reframed in order to make progress towards a methodology valid for general conditions.

This work therefore asks: how can the LES modelling problem be framed in a manner such that it remains well-posed under non-equilibrium conditions? This means framing the modelling problem in a way which cannot depend on the specific spatial anisotropy and inhomogeneity of a particular problem. It is argued that the only way to avoid dependency on spatial variations in the statistics is to produce a formulation which is fully localised in position space. It is hypothesised that a framework consistent with non-equilibrium statistical properties of turbulence must therefore: not rely on spatial filtering; and must introduce a mathematical methodology which is compatible with describing the characteristic path-dependency of the dynamics.

Accordingly, the methodology presented in this work builds upon the established methodology of implicit LES (iLES) which eliminates the need for explicit filtering. Originally, the iLES technique was motivated by the practical observation that certain finite volume schemes act as turbulence models due to their numerical energy dissipation (Margolin, 2013). Over time, the method has found a solid theoretical basis in the mathematical concept of weak solutions to the Navier-Stokes equation (Fehn and John, 2025). A weak solution satisfies the Navier-Stokes equation by conserving energy and momentum when integrated over finite volumes of space, which correspond with discrete numerical control volumes. Given the coarse, discrete resolution used by all forms of LES, this discrete description of solutions is arguably a more realistic representation than the pointwise solution described by the equation governing explicit LES.

Some properties of weak solutions have already been established which make them a physically relevant way to describe the large-scale behaviour of turbulent flows. The fundamental mathematical properties crucial to their physical meaning are their existence, regularity and uniqueness. While study of the existence and regularity of weak solutions has been well established and developed into practical modelling methodology for energy conservation (Fehn and John, 2025), the uniqueness of solutions has not yet been thoroughly investigated in the context of turbulence modelling. Moreover, the possibility for multiple possible solution trajectories is directly relevant to the crucial path-dependency property of non-equilibrium systems. This work recognises that while the causal structure of non-equilibrium flows poses a major hurdle for the explicit approach to LES which has not yet been overcome, it also represents a promising area for potential investigation as an extension to the iLES methodology. Therefore, an extension to the iLES methodology is proposed which allows the sub-grid scale modelling problem to be posed in a strictly local way, with the goal of eliminating conditions-dependence. This requires a new approach which implicitly defines a statistical ensemble without explicit sampling.

So far, it has been established that, given a certain Hölder condition on the regularity of the velocity field, weak solutions to the Navier-Stokes equation conserve energy (Fehn and John, 2025). Therefore, iLES methods use numerical schemes which have certain, physically consistent regularisation properties. As a consequence of the strong theoretical basis for energy conservation, the iLES approach has been well established as a model for turbulent energy dissipation and is often favoured in engineering applications for its simplicity and robustness (Grinstein and Drikakis, 2007). However, explicit LES is still frequently and justifiably favoured in academic analysis because it currently offers more flexible potential for adaptation to general conditions, where energy dissipation is not the only important consideration. Currently, explicit LES has greater flexibility because the SGS stress tensor can, for example, be adapted into anisotropic, inhomogeneous forms to represent complex conditions. In contrast, iLES lacks the additional tensor structure present in explicit LES. However, with the strong, mathematical foundation provided by iLES and the barriers faced by explicit LES under the conditions of interest, lack of reliance on empirical data is highly attractive. Overall, it can be concluded that there is a strong need for investigation into a form of iLES which is able to model not only unresolved energy dissipation but also momentum fluxes under general conditions. In order to achieve this, a powerful tensor structure must be introduced to LES without explicit filtering. This work presents a method which delivers the rich, tensor structure offered by explicit LES without introducing the empirical limitations which result from explicit filtering.

In order to begin conceptualising such a model, it is important to consider the conditions under which iLES models describing energy dissipation already function as stand-alone models. When considering energy dissipation, the inertial energy cascade under homogeneous, isotropic conditions (HIT) stands out as the canonical case because the distribution of velocities over a finite volume is isotropic. This means that fluctuations around the mean can be described principally in terms of their energy. In this context, it is clear why an LES model need only describe energy dissipation. However, it is well known in practice that this does not preclude an LES energy dissipation model from being applied under other conditions. A long standing controversy in the literature is the "embarrassment of success" (Kraichnan, 1974) enjoyed by Kolmogorov's theory of the energy cascade. Although Kolmogorov (1941) assumes homogeneity and local isotropy for the dimensional analysis to arrive at the turbulent energy spectrum, it has since become clear that an identical cascade picture for energy is still valid regardless in a huge range of conditions, even far from where it should be expected. In fact, even for strongly anisotropic boundary layer flows, an LES energy dissipation model remains applicable as long as the boundary layer momentum fluxes are fully resolved. In this case, the burden on the LES model is still, as intended, only to preserve energy conservation. This common setup is referred to as a "wall-resolved" LES.

This highlights a crucial link between universal, homogeneous isotropic conditions and all other conditions. Namely, it reveals that the definition of "inertial" conditions is of the greatest significance. The current work hypothesises that turbulence can always be considered "locally inertial", meaning that - over a small enough volume scale where momentum fluxes are resolved - the required sub-grid scale modelling is universal in that it pertains to a universal, local energy dissipation mechanism (since momentum conservation is already accounted for). Importantly, locally inertial conditions must be locally indistinguishable from homogeneous, isotropic turbulence. This is valid where velocity differences across a finite volume are sufficiently small (the momentum flux is resolved) and so the velocity distribution across the volume appears approximately isotropic from a local perspective and may be principally described by its energy. Given the locality of the turbulent energy cascade mechanism which has been established in the literature (Eyink and Aluie, 2009), the modelling required is therefore also likely universal under locally inertial conditions. Hence, as observed in practice, iLES may be applied as long as momentum fluxes are well-resolved.

Where the velocity field distribution is locally isotropic, the fluid within a finite volume moves together as one packet and is characterised by a single fluctuation energy and a single velocity. This view is directly compatible with that used by finite volume schemes in iLES, where the resolved values for the velocity field represent the average value of the velocity over control volumes. In this sense, finite volumes provide an inertial frame of reference for tracking the motion of the finite fluid packet. The definition of "inertial" in this context may then be specified to mean that finite packets of fluid can be characterised by a mass, an energy and a velocity. This perspective has important consequences, as it suggests that the universality of turbulence modelling is intertwined with the frame of reference under which the turbulence is observed.

The remaining issue is that of resolution. When the momentum fluxes are not fully resolved, a finite volume average is no longer valid to describe the motion of a finite fluid packet. With significant velocity gradients, the fluid within the volume is not inertial in the specific sense that its motion cannot be described by a single velocity. For example, fluid in the top portion of a volume may be moving on average at a significantly different velocity relative to fluid in the bottom portion of the volume. Thus, the finite volume no longer provides an inertial frame of reference for the finite fluid fluid packet, as there is no single velocity which faithfully describes the motion of the packet. Hence, the description of the velocity field using finite volume averages is not always realistic, as it misses the anisotropy of the velocity distribution across a finite volume.

While it is apparent that local anisotropy produces non-universal conditions within a finite volume, the appearance of anisotropy in the observed velocity distribution is

reference-frame dependent. Therefore, under a special choice of coordinate system or basis, the velocity distribution may appear isotropic and the conditions may appear locally inertial. Such a frame of reference may be referred to as a locally inertial frame of reference. While a change of reference frame holds no physical meaning on its own, the key insight which leads to a new methodology for modelling non-inertial turbulence conditions is that the locally inertial frame of reference valid for each finite volume is different. Therefore, there must exist a special system of local coordinate frames in which the flow is locally inertial at all positions. The geometrical structure which provides such a connection between different frames of reference at different positions in this sense is a metric tensor. A methodology is therefore developed in this work which replaces the sub-grid scale stress tensor (which is generated by explicit filtering) with a metric tensor which describes the sub-grid scales in a local, filter-free formulation. The metric tensor is used to describe the effects of non-inertial, non-universal conditions, while iLES is used to provide a locally universal energy dissipation mechanism.

The new geometric iLES approach produces a local modelling problem which considers only the fluid within a single finite volume. The methodology presented by this thesis proposes a solution to this local modelling problem, which is greatly simplified by the fact that it may only depend on the locally observable velocity gradient and pressure. The geometric iLES approach is therefore localised in the strictest possible sense given finite-scale of resolution. This contrasts clearly with explicit LES in which the kernel is not strictly localised. In explicit LES, sampling is carried out over neighbouring positions which may feature different local statistics. Hence, data is incorporated which is strongly influenced by conditions-dependent spatial variations in the statistics. This problem is totally avoided in the new approach, making its strict locality a key distinguishing factor and eliminating much of the conditions-dependent non-universality which troubles explicit LES methods. Unlike standard iLES, the new methodology also incorporates the key advantage of explicit LES by defining a tensor structure which is used to accurately describe non-inertial effects. Overall, this allows a broad range of conditions to be modelled, including pressure gradient boundary layers, with minimal empirical input.

After reviewing the literature relevant to LES modelling under wall-bounded conditions, key results and challenges identified in the literature are used to guide the development of a theoretical and numerical methodology based on the proposed concept of a geometric iLES model. The governing equations are derived and the meaning of the new metric tensor quantity is investigated. Next, a foundational solution is provided to the resultant local, geometric modelling problem. The proposed solution is designed to address the effects of both sub-grid scale wall momentum fluxes and of pressure gradients, so that the model functions in place of an LES wall model and is able to adapt to pressure gradient conditions. The

mathematical methodology is then developed into a numerical methodology, which is applied for the LES simulation of boundary layer flows. After validating the action of the model in modelling wall momentum fluxes under flat-plate, zero pressure gradient conditions, flat-plate adverse pressure gradient boundary layers are investigated to validate the impacts of pressure gradients. Finally, a NACA4412 simulation is carried out at high Reynolds number in order to demonstrate the flexibility of the model when faced with realistic applications.

Chapter 2

Literature Review

This chapter analyses the successes of large eddy simulation and highlights the challenges faced by current methods. The success widely found in the context of equilibrium conditions is contrasted with challenges which begin to be faced under non-equilibrium conditions generated in boundary layers by mean pressure gradients. Issues encountered by LES under the conditions of interest are discussed and evaluated in the context of the introductory remarks. Attempts made to address pressure gradient effects in current LES wall models are also discussed, with an emphasis on the key underlying assumptions being made and their validity under non-equilibrium conditions. This builds motivation and provides key area of focus for the methodology defined in the following chapter.

Under equilibrium conditions, turbulence is best characterised by cascade processes which transfer energy and momentum from larger scales of motion to smaller ones. The energy or momentum is eventually lost to viscosity at the smallest scales of motion. This feature of turbulence is its most well-established property and is known to generate equilibrium fluxes of energy and momentum. These physical features have been widely studied and their properties leveraged to construct effective empirical models for both viscous energy dissipation and viscous wall shear stress. Overall, these equilibrium cascade phenomenon are the features which make empirical modelling possible. It is shown that the basic methodology and assumptions behind LES modelling have been constructed under premises aligned with these equilibrium cascades. Under non-equilibrium conditions, it is argued that these assumptions break down, leading to the observed difficulties in producing effective and efficient models for these conditions.

In the LES literature, energy and momentum fluxes are mostly considered independently in the sub-fields of LES sub-grid scale models and LES wall models respectively. While commonly assessed separately, it has also been identified that current sub-grid scale and wall models are often incompatible - a conflict which

produces significant numerical issues for current approaches (Yang et al., 2017). These numerical difficulties are also considered and inform important decisions for the construction of the numerical methodology proposed in Chapter 4.

First, relevant aspects of the physics and modelling of the turbulent energy cascade are reviewed, focusing on the local nature of the energy cascade and the question of locally universal behaviour. The inertial turbulence energy cascade, which is widely observed and quantified by Kolmogorov's analytical result (Kolmogorov, 1941) is the keystone of turbulence research. Pioneering investigations into the turbulent energy cascade by Obukhov (1941), Onsager (1945), and Heisenberg (1948) employed a spectral description to propose a cascade mechanism. These works suggested that the transfer of energy to smaller scales by advection is principally sustained by a process where two modes of similar wave-number successively transfer their energy to a mode of twice the wave-number; this can be termed "local transfer by local triads". After considerable debate, this local description has more recently gained favour (Eyink and Aluie, 2009; Aluie and Eyink, 2009) over a competing viewpoint of "local transfer by non-local triads" proposed by various groups such as Brasseur and Corrsin (1987) and Domaradzki and Rogallo (1990). The crucial difference between the two arguments is in the dynamical importance of the interactions between ratios of wave-numbers (as in the original description) versus differences in wave-number. The conclusion that can be taken is that the important dynamical coordinate of scale must be defined in terms of ratios of wave-number (or equivalently the logarithm of wave-number).

However, it is clear that individual Fourier modes cannot be assigned physical meaning alone since they are completely de-localised in position. Moreover, the energy of a single Fourier mode is not a directly measurable quantity and so should not be assigned direct physical relevance. This is a natural concern since a visual observation of turbulence finds localised, particle-like vortex structures rather than non-local, wave-like structures. Recent work has shown that dual localisation of the cascade in both position and wave-number space is necessary for a more complete description (Eyink and Aluie, 2009; Yao et al., 2024). This description involves wave-number bands which can be interpreted with physical significance since the structures they represent are localised in space. Therefore, recent findings have established that the cascade mechanism cannot ever be fully localised in either space (in the spirit of Heisenberg's uncertainty principle). Instead, localisation is balanced between the positional and spectral spaces.

The dual localisation of the turbulent energy cascade provides explanation for important observations which were previously deemed highly surprising. Although Kolmogorov (1941) assumes homogeneity and local isotropy for the dimensional analysis to arrive at the inertial turbulent energy spectrum, it has since become clear that an identical cascade picture for energy is still valid and can be observed

regardless under a huge range of conditions. The inertial cascade picture still appears to apply even when the conditions cannot be considered homogeneous or isotropic (Kraichnan, 1974).. In fact, it has been argued that conditions which strictly fulfil Kolmogorov's assumptions only occur under such extremely large Reynolds numbers that they are generally not achieved (Kraichnan, 1974). Kolmogorov's theory has therefore been said by Kraichnan (1974) to have had an "embarrassment of success", applying in conditions even far from where it should be expected. Based on recent evidence, this observed universality is most likely a result of the localisation of the energy cascade mechanism. Where the mechanism is local, spatial inhomogeneities and variations in the flow statistics with position are irrelevant to the cascade mechanism itself. Therefore, given a lack of dependence on wider flow conditions, strongly universal behaviour is a direct implication of locality. Although homogeneity is not a requirement for universality where the cascade mechanism is localised, conditions must remain in "local isotropy". A careful definition of local isotropy is therefore crucially important in defining the universality of the local energy cascade. The exact conditions under which local isotropy is valid appear as an important feature of the present work.

When considering numerical models for the energy cascade under locally isotropic conditions, implicit LES modelling provides arguably the simplest effective model, with strong mathematical justification. The function of these models can be understood in the context of Onsager's seminal work on singular behaviour of the Euler equation (Fehn and John, 2025). Onsager (1949) conjectured that turbulence dissipation can be understood geometrically through a Hölder condition on the velocity field defined by

$$|u(x) - u(y)| \leq C||x - y||^{\alpha} \quad \forall \quad x, y \in \Omega. \tag{2.1}$$

The recently proven Onsager conjecture (Onsager, 1949) states that solutions with $\alpha > 1/3$ obey energy conservation, while those with $\alpha \leq 1/3$ do not and exhibit "anomalous" energy dissipation. This regularity condition for energy conservation has eventually translated into numerical iLES modelling (Fehn and John, 2025). The correspondence can be explained through the observation that the critical exponent $\alpha = 1/3$ is compatible with the Kolmogorov scaling behaviour of the turbulent energy cascade. This can be seen by examining the Kolmogorov structure function

$$\left\langle (\delta u(r))^2 \right\rangle = C_2 \, (\epsilon r)^{\zeta_2} \tag{2.2}$$

where $\delta u(r)$ is the difference in velocity over radial distances r, and $\langle \cdot \rangle$ is an ensemble averaging operator. With the theoretical exponent $\zeta_2 = 2/3$ (Kolmogorov, 1941), the scaling corresponds with the limiting Hölder exponent. In the Hölder sense, the least smooth velocity field which conserves energy has scaling properties which match the canonical turbulence energy cascade. Therefore, iLES methods are often explained by

stating that they seek to dissipate the minimum amount of energy possible in order to maintain regularity of the solution, because this mathematically provides a valid model for the turbulence energy cascade. It is also noteworthy that this understanding aligns well with the principle of least action; the minimum energy dissipation per unit volume and per unit time corresponds with the least action exerted by the numerical model.

Because iLES by definition seeks to be minimally dissipative, it is often able to achieve better effective resolution than explicit LES approaches which rely upon artificial smoothing of the velocity field over length scales larger than the grid scale (Volpiani et al., 2024). However, the iLES methodology remains strictly valid where the velocity field is locally isotropic and the energy cascade mechanism may be considered locally universal. Therefore, the question of handling conditions which are not locally isotropic is also central in generalising the iLES methodology.

While the dynamics of locally isotropic turbulence are principally described by a universal energy cascade, energy is not the only conserved quantity, and other mechanisms are also at play. This is particularly apparent in the context of turbulent boundary layers, where the wall sets up a strong cascade of momentum flux in the wall-normal direction. In analogy to the energy cascade, a similar equilibrium cascade concept is available for the momentum flux in some boundary layers (Marusic et al., 2013) as sketched in Figure 2.1. However, it must immediately be noted that this process is fundamentally different with regard to the fact that it is certainly not local, but occurs by transferring momentum over a range of wall-normal positions. Nevertheless, the equilibrium turbulent cascade of momentum towards the wall which is found under zero pressure gradient boundary layer conditions has been leveraged with great success in empirical modelling (Cebeci, 2013). Unlike the energy cascade, the lack of locality does not offer strong potential for universal application and generalisation. As a result, significant difficulties are encountered under pressure gradient conditions, which disrupt the momentum and energy balance of the boundary layer.

Because of the viscous nature of the no-slip boundary condition, its application and therefore the conservation of momentum normally requires the resolution of the near-wall, viscous length scale (Davidson, 2009). As a consequence, for a resolved numerical simulation, resolution near a wall scales in viscous units, which become very small with increasing Reynolds number (Re). In the context of wall-resolved LES, momentum transfer in a boundary layer means that a model for the energy cascade only is not sufficient; the processes which transfer momentum must still be resolved. Therefore, a model for the energy cascade may be used but the momentum fluxes must still be fully resolved down to the viscous sub-layer. Resolution of the viscous sub-layer is disastrous for wall-resolved LES and the cost of resolving the viscous sub-layer dominates so that the overall cost scales like $Re^{2.4}$ in a boundary

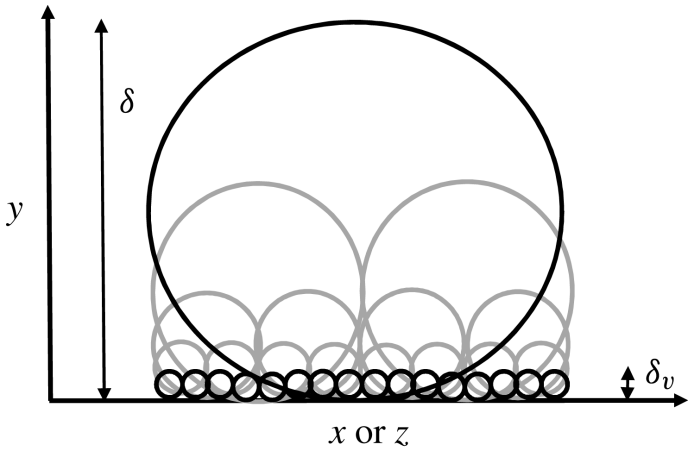

FIGURE 2.1: A schematic of the attached-eddy hypothesis (Marusic and Monty, 2019) by Hwang (2015). Each of the circles represents an attached eddy where the smallest eddies scale in the viscous, inner length scale (δ_v) and the largest scale in the outer length scale (δ).

layer (Reynolds, 1990; Chapman, 1979) with only modest improvement over direct numerical simulation. Taking into consideration that an LES which does not resolve the viscous sub-layer would have a cost that scales like $Re^{0.5}$ (Reynolds, 1990) demonstrates very unfavourable scaling due to the need to resolve momentum transfer in the boundary layer, especially in the near-wall region.

Consequently, wall models have been developed for LES in an attempt to alleviate the resolution requirement near the boundary and therefore abate or eliminate the strong scaling with Reynolds number. Essentially, wall models must model the momentum transfer to the wall without resolving the viscous scales. In an equilibrium analogy to the energy cascade, the turbulent momentum fluxes associated with large eddies away from the wall are transferred to smaller eddies near to the wall via a cascade which is eventually terminated by the viscous wall shear stress (Marusic et al., 2013). Therefore, akin to removal of energy by a model for the sub-grid scale energy dissipation, the core function of a wall model is to remove momentum from the flow at the wall. The wall modelling procedure therefore usually aims to explicitly model the viscous momentum flux which is left unresolved when coarse resolutions is chosen. This momentum flux is then applied at the wall by implementation of an artificial boundary condition.

Because of their importance in facilitating tractable LES simulations of wall-bounded flows, wall models have been identified as an important area of development by long-standing leaders in CFD such as NASA (Slotnick et al., 2014), and are currently in the infancy of their potential development (Piomelli, 2014). This report offers new perspectives on the wall modelling problem developed to further progress towards these targets. While wall models have mostly been successful at predicting mean statistics in equilibrium conditions (Bose and Park, 2018), the literature has collectively

identified key theoretical challenges which are faced in modelling wider conditions, alongside problematic numerical issues which limit practical usability.

Wall-modelled large eddy simulations (WMLES) have enabled the simulation of high-Reynolds number flows unachievable using wall-resolved techniques. Friction Reynolds numbers of up to the order 10^8 have been studied in channel flows and momentum thickness Reynolds numbers of up to 10^{12} have been investigated for boundary layers (Bose and Park, 2018). Agreement seen between WMLES and experimental and/or DNS results is good to low-order in these cases; mean velocity profiles are seen to match measurements and the empirical law of the wall where appropriate (Bose and Park, 2018). This is expected since the assumptions made in performing current WMLES are valid in such flows where the law of the wall is valid (Bose and Park, 2018). However, the accurate prediction of the fluctuating quantities is less well achieved. Whilst near-wall pressure fluctuations are found to be within a few percent of DNS results, the wall shear stress fluctuations are always significantly under-predicted (Iyer and Malik, 2020). Additional empirical models for estimation of the shear-stress fluctuations have been developed with reasonable success (Mathis et al., 2011; Inoue et al., 2012; Wang et al., 2021) based on the experimentally observed amplitude and frequency modulation of the small scales by large scale structures (Ganapathisubramani et al., 2012).

In application of WMLES to flows with complex geometries and pressure distributions, only qualitative agreement is seen (Bose and Park, 2018). Very few favourable quantitative comparisons can be made under strong pressure gradients. Bodart et al. (2013) performed analysis on a multi-element airfoil configuration, reporting a 10% discrepancy between the stall angle of attack predicted by WMLES and that measured experimentally. Iyer et al. (2016) made a comparative study of the main wall modelling techniques for the NACA4412 aerofoil near stall and the transonic bump and were only able to offer findings of "reasonable" qualitative agreement in the mean velocity profiles. However, pressure coefficients and their fluctuations are much more successfully predicted in general (Bose and Park, 2018) and this observation is explained by consistency with the high-Reynolds number approximation for the wall-normal momentum equation, $\frac{\partial p}{\partial y} = 0$, which suggests that the pressure fluctuations are imposed by the outer layer rather than the wall model (Bose and Park, 2018). Bose and Park (2018) also recognise that many of the more successful validation cases for complex geometries have involved features which result in sudden, "robust" separation (e.g. bluff bodies, backwards-facing step and shock-induced separation). Overall, there is a clear need in the literature for further investigation into the theoretical shortcomings of wall modelling in more complex flow cases featuring the sustained application of strong adverse pressure gradients which feature more complex history effects (Bobke et al., 2017).

In practice, wall models find a relation between a single-point measurement made at a chosen off-wall location and the local wall shear stress (Bose and Park, 2018) in a way that is similar to the explicit approach to LES modelling. This general goal has been achieved and implemented by many approaches of varying complexity. It is noted that a possible implicit approach to WMLES has, to the author's knowledge, not been investigated; the implicit methodology defined in the following chapter is potentially the first such attempt. In the context of the classical, explicit methodology, algebraic methods use relations often based on the log-law of the wall (Bose and Park, 2018). The operation of this kind of model is sketched in Figure 2.2(a).

Recent advances in the empirical modelling approach have also included data-driven and machine-learning LES frameworks, driven by increasing availability of high-fidelity data and improvement in learning algorithms. Wall flows with complex geometry or strongly inhomogeneous conditions have motivated the development of neural network based models that may learn non-linear closure relationships directly from DNS data (Choi et al., 2025; Beck et al., 2019). Such efforts have demonstrated a potential for improved correlations with exact closure terms (Beck et al., 2019), particularly in complex cases. Machine learning is therefore being integrated into wall models in an attempt to address shortcomings of traditional modelling correlations near wall boundaries, with findings highlighting both the potential for improvements in precision and the formidable challenges faced in ensuring generalisation to conditions unseen in the training data (Vadrot et al., 2023; Ma and Lozano-Durán, 2025). Overall, while data-driven LES models show promise, issues such as robust generalisation across flow conditions, physical consistency, and computational cost overheads remain significant challenges, emphasising the need to combine data-driven insights with new physical modelling principles for reliable LES in practical applications (Choi et al., 2025). These limitations remain particularly important for flow conditions such as the adverse pressure gradient boundary layers investigated in this thesis, where a consistent, empirical similarity relationship between conditions has not been established and so, at present, remains an area in which the generalisation of data-driven models cannot be guaranteed.

More elaborate physical models may also solve the thin boundary layer equations or even further reduced equations - similar to the RANS equations - on a separate, refined near-wall grid to which the LES provides a boundary condition at its outer edge (Larsson et al., 2016); this approach is represented in Figure 2.2(b). These so-called zonal approaches have the potential advantage that they can nominally incorporate effects of pressure gradients on the momentum balance as they resolve information about the inner layer which is unavailable in wall models which do not use a refined near-wall grid (Fowler et al., 2022). However, these methods suffer from greatly increased complexity in matching the transition between the RANS and LES solutions and increased cost which can approach wall-resolved LES due to spatial

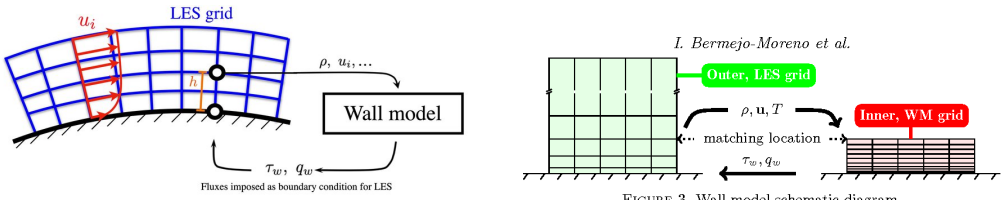

(A) Wall stress model (Lozano-Durán and Bae, 2020)

(B) Zonal wall model (Bermejo-Moreno et al., 2012)

FIGURE 2.2: Sketches of the working principles for zonal and RANS-free wall models.

resolution of the viscous sub-layer (Fowler et al., 2022). Furthermore, these methods have still been shown to give worse performance than simple algebraic models in some strong APG flows (Frère et al., 2019; Bose and Park, 2018) suggesting that they are not actually effective in incorporating pressure gradient information. Since the RANS inner solution theoretically describes the wall momentum balance but does not appear to be effective, a key open question is whether modelling of the local wall-stress is actually sufficient, or if broader forms of modelling are required. Therefore, a focus on the key assumptions and underlying issues experienced by wall models in general is maintained in order to guide the proposed methodology. A detailed taxonomy of particular wall modelling implementations can be found in (Larsson et al., 2016).

The current wall models typically rely on the same underlying set of assumptions (Bose and Park, 2018). A review of these is presented, relating the discussion to present challenges faced by WMLES and to key physical mechanisms involved in adverse pressure gradient boundary layers. Overall, adverse pressure gradient boundary layer conditions present various issues that make wall modelling more difficult. Firstly, the boundary layer is non-universal and history-dependent so that no unifying scaling laws are known to exist. Inner to outer layer interaction is stronger and not well understood (Han et al., 2024), invalidating classical approaches where equilibrium assumptions break down and making it problematic to adapt current zonal methodologies to these conditions.

The crucial physical assumption made by current wall models is the spatial and temporal decoupling of the inner and outer layers of the boundary layer (Piomelli, 2008). Decoupling means a causal disconnection of the small scales exists such that they may be explicitly discarded and modelled. In the popular framework for wall modelling, the LES grid size which scales with the boundary layer thickness is significantly larger than the inner viscous length scale and the LES time-step is far longer than the timescale of the near-wall eddies (Piomelli, 2008). Given equilibrium, the result is that outer layer, large scale structures are directly related to the behaviour of the inner layer through the wall shear stress. Under this assumption, the large scales should effectively be viewed as a modulating boundary condition, felt as a "footprint" on the wall which results in a frequency and amplitude modulation of the

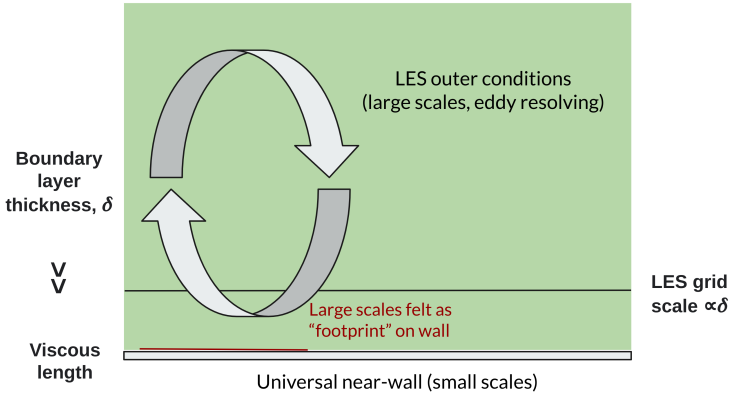

FIGURE 2.3: A sketch outlining the concept of scale separation in wall-modelled large eddy simulations.

wall fluctuations (Ganapathisubramani et al., 2012). The inner layer then responds purely based on this footprint of the large scales on the wall, and so is universal. This assumption is theoretically valid when there is a strong scale separation present in the boundary layer (Bose and Park, 2018), and there are no other effects which cause interaction from the inner to outer regions; the situation is sketched in Figure 2.3. It is well recognised that this concept facilitates accurate wall modelling in equilibrium conditions.

For spatial scale separation, the relevant parameter in equilibrium flows is the friction Reynolds number Re_τ which quantifies the ratio of the outer scale (the boundary layer thickness) to the inner, viscous length scale (Bose and Park, 2018). Re_τ should be sufficiently large to provide adequate scale separation and to make a Neumann boundary condition physically consistent when the grid resolution is taken to scale with the boundary layer thickness (Piomelli, 2008). However, most adverse pressure gradient test cases have examined rapid flow separation where the separation is induced by external factors to the boundary layer such as a shock or extreme wall curvature (Bose and Park, 2018). In these cases, scale separation can exist in the boundary layer before it rapidly detaches into a free shear layer, which does not then require wall modelling. In situations where pressure gradient is applied to the boundary layer over long stream-wise distances, or gradual separation occurs under very strong adverse pressure gradient, the wall shear stress and therefore Re_τ are reduced or gradually tend to zero approaching a separation point. This brings into question the scale separation assumption such that adverse pressure gradient situations prove more challenging and challenge assumptions of inner-outer decoupling. This type of flow is also a common and important scenario in many aerodynamic designs as separation is generally prolonged as far as possible by streamlined shapes for the purpose of drag reduction (Chaudhry et al., 2016).

Therefore, the scope of focus may be narrowed down to turbulent boundary layers which are subject to prolonged influence of an adverse pressure gradient (APG).

Now focusing on this area, very large-scale well-resolved numerical investigations have recently been carried out for such flows by Tanarro et al. (2020); these results are very useful to inform progress of wall modelling approaches. Firstly, it has been observed that APG causes the well-known outer peak in turbulence intensity to become more prominent (Tanarro et al., 2020). This is a usual indicator of strengthened scale separation (Morrill-Winter and Klewicki, 2013). Although there is an apparent scale separation under APG as suggested by the single-point statistics, the correlation between inner and outer regions is very low in terms of the linear coherence spectra, similar to the situation with reduced Re_τ (Tanarro et al., 2020). Therefore, the necessary direct relation between the outer flow and the wall shear is not present. This statistical result succinctly shows why explicit wall modelling where a correlation is required for the wall shear stress has not proven possible and may not be feasible under significant APG. The intensified outer peak must therefore be interpreted carefully. In fact, Tanarro et al. (2020) also show that APG energises all scales of turbulence without creating larger scales and that the small scales are preferentially energised. This comes in contrast to the result shown for increasing Re_τ, where the effect is principally to create larger scales, thus strengthening scale separation and creating a distinct "spectral ridge" in the 2-dimensional energy spectra (Tanarro et al., 2020).

Under APG, the key feature that can be identified to cause difficulties is an increased importance and non-universality of the small scales. The energisation of small scales in the outer layer is seen to become more extreme with larger values of the integrated Clauser parameter, which measures the cumulative strength of an adverse pressure gradient (Tanarro et al., 2020). Where the small scales gain non-universal characteristics, the inner layer is not decoupled and scales may not be explicitly separated and discarded. Therefore, APG conditions pose a fundamental challenge to the explicit LES wall modelling methodology. A solution to this problem is a crucial area of research which is developed in this thesis.

In terms of the wall-normal cascade, inner-outer coupling is embodied by intermittent transport of small scale energy and momentum away from the wall, against the prevailing cascade direction. Tanarro et al. (2020) observe that "flow history has an effect on the vertical displacement of the smallest scales". The transport of small scales away from the wall is clearly inconsistent with inner-outer decoupling assumptions relied upon by wall models and can therefore be identified as an important area of investigation for physical understanding and modelling of boundary layers away from equilibrium. This non-equilibrium effect known as bursting has been well studied in general and it has been recognised that the occurrence of bursts at the edge of the inner layer is the main process of turbulence production near the wall (Kim

et al., 1971; Rao et al., 1971). As expected, bursting frequency has been observed to increase under APG (Tillman and Kistler, 1996). This is because the development of a burst requires the wall-normal lifting of near-wall structures (Kim et al., 1971), which is aided by a larger wall-normal components of velocity. This situation is necessitated by mass conservation where APG decelerates the near-wall flow over a low-curvature wall. The larger concentration of energy in the near-wall, small scales under APG (Tanarro et al., 2020) also suggests a greater bursting energy is present. Since bursting is an intermittent feature of turbulence and acts as an inner-to-outer interaction (Rao et al., 1971), it is likely the primary process which results in damage to decoupling and equilibrium assumptions in APG boundary layers. Since the energisation of small scales in the outer layer is observed to become more extreme with larger values of the integrated Clauser parameter, the cumulative effect of adverse pressure gradient integrated along the boundary layer (rather than just the local strength of the pressure gradient) is the key feature which leads to breakdown of current assumptions and methodology. Because the non-equilibrium effects have direct dependence on pressure gradient history, and the history is unique to any particular problem, this introduces further complexity and non-universality which is highly problematic to capture empirically (Vinuesa et al., 2017).

Overall, adverse pressure gradient creates a distinctly difficult problem for wall modelling due to inner-outer coupling, which damages the key decoupling assumption relied upon in the current, explicit wall modelling methodology. Under the spatial scale-separation assumption which is pervasive in wall modelling, the specific small-scale details of the inner layer must not be important to the large scale dynamics; otherwise, the inner and outer layers are coupled. This is a reasonable expectation for equilibrium flows with high friction Reynolds number, but is highly questionable in adverse pressure gradient boundary layer flows, where the boundary layer accrues non-universal, problem-specific small scale properties. Feedback of the small scales near the wall into the large scales away from the wall through bursting can then be identified as a key mechanism which fundamentally undermines the explicit wall modelling methodology. Since there is substantial evidence to suggest that a sufficiently general empirical solution may not prove possible, it is not currently clear how the problem can be fully resolved, and this remains as a significant barrier to progress in the area. In the present work, the conceptual issues surrounding explicit wall modelling are considered, leading to the proposal of a novel, implicit method which aims to reduce the current reliance on empirical assumptions and data.

Given the absence of clear empirical correlations, it would be expected that zonal approaches solving an inner layer RANS-like equation would perform better, by incorporating pressure gradient information. However, as discussed above, this has been observed not to be the case. Physically, this issue can be understood by referring to a second key assumption used by wall modelling. In addition to spatial scale

separation, temporal scale separation is required by current wall modelling approaches (Piomelli, 2008). When a wall model is used in practice, it is applied on each LES time-step. Therefore, an assumption of equilibrium is being made and spatial decoupling must hold not only over long times but at all instants. In other words, it is necessary for variations in the outer flow (pressure gradient/wall shear footprint) to be much slower than the response timescale of the inner layer (Piomelli, 2008) so that the inner layer remains in a pseudo-equilibrium and correlations are effectively instantaneous. Physically, this is a reasonable assumption under equilibrium conditions because of the much shorter timescales of the eddies on the viscous scale compared to those in the outer layer (Piomelli, 2008). This is in part supported by the successes of wall models in channel flow and zero pressure gradient boundary layers (Bose and Park, 2018). It is worth remembering, however, that wall shear stress fluctuations are still under-predicted across the board (Iyer and Malik, 2020; Bose and Park, 2018).

Recently, the significance of "quasi-equilibrium" effects which break the equilibrium assumption have been recognised (Fowler et al., 2022). Similarly to the spatial picture, it is observed that APG enhances turbulent fluctuations at all scales near to the wall, with the effect being most significant for the smallest scales (Tanarro et al., 2020). Wall curvature has also been observed to augment high-frequency pressure fluctuations (Pargal et al., 2022). Therefore, increasingly rapid and larger amplitude velocity fluctuations are expected under APG conditions with complex geometry. In combination with the reduction in the mean wall shear stress caused by APG at a given momentum thickness Reynolds number (Tanarro et al., 2020), the effects of shear stress fluctuation are likely to be far larger under APG. Since zonal, RANS-like wall modelling methods rely on a temporal equilibrium assumption (Bose and Park, 2018), this perspective provides a clear justification for their weaker than expected performance under cumulative pressure gradient influence. Therefore, removing reliance on both spatial and temporal equilibrium/decoupling assumptions is of crucial importance to wall modelling for APG flows where the effects of non-equilibrium small scale behaviour must be captured.

Overall, scale separation permitted by equilibrium is the fundamental empirical feature which currently makes wall modelling and LES possible today. However, general turbulent boundary layers do not exhibit decoupled dynamics and the key adverse pressure gradient mechanisms outlined lead to the absence of a direct cascade which can be leveraged by empirical models. Therefore, the key gap in the literature is a framework for wall modelling that remains well-posed under flow conditions which do not conform with these classical assumptions. This requires models which do not rely in any way on scale separation and decoupling. In order to achieve this, this thesis provides a reinterpretation of the modelling problem from a new, geometric perspective.

Beyond these physical matters, further problems have been identified in the wall modelling literature relating to the numerical implementation of the physical models. Predominantly, these issues arise from the implementation of the boundary condition in wall-modelled LES. Wall models arise where the no-slip boundary condition is unresolved, and so wall models have been quite naturally treated as a modification to the boundary condition instead of forming a part of the SGS stress tensor (Bose and Park, 2018). However, this approach generates the so-called log-layer mismatch problem which plagues wall modelling (Yang et al., 2017; Piomelli et al., 2003; Lee et al., 2013). This refers to the general over-prediction of the wall shear stress, even with ideal physical models. The phenomenon is usually attributed to issues relating to the placement of the off-wall sampling location and to numerical error (Yang et al., 2017). In practical implementations of wall modelling, the near-wall solution is inherently poorly resolved and corrupted numerically (Kawai and Larsson, 2012). Bou-Zeid et al. (2005) have shown using the Schwartz inequality that wall shear stress over-prediction is guaranteed in a formulation local to the wall due to the LES velocity fluctuations. In essence, the LES is temporally and spatially unresolved near the wall, leading to uncontrolled numerical error. With clear sources of numerical error encountered when placing the sampling location at the first grid point from the wall, practitioners have been motivated to place the off-wall location further from the wall and to employ wall-parallel and temporal filtering on the sampling point to reduce numerical noise (Yang et al., 2017; Hosseinzade and Bergstrom, 2021; Bou-Zeid et al., 2005). These ad-hoc numerical techniques greatly improve accuracy of mean velocity profiles (Hosseinzade and Bergstrom, 2021) but such numerical compromises also artificially average the data used to determine the wall shear stress over time and space scales larger than those of the local LES. Consequently, significant under-prediction of the wall shear-stress fluctuations is observed. Furthermore, this leads to a reduction of the effective resolution where the velocity field is artificially smoothed over a length scale larger than the grid length scale.

As a result of this incompatibility at the wall, various studies have also shown that wall modelling approaches are very sensitive to the chosen LES sub-grid model (Frère et al., 2017; Whitmore et al., 2020). Again, with a wall boundary forming a sharp edge to the domain of the fluid, there is a region adjacent to the wall where quantities are not numerically well defined. This means that turbulent statistics are ill-defined or are unreliable and makes the SGS modelling fundamentally unreliable near to the wall. The ill-definition of the near-wall velocity field is supported by the results of Hosseinzade and Bergstrom (2021) who find that placing the sampling point 4 grid points from the wall eliminates much of log-layer mismatch. They also recognise that this solution to the problem is due to the compatibility of the sub-grid model with the LES resolution achieved away from the wall (Hosseinzade and Bergstrom, 2021), even though there is still a conflict next to the wall. Other efforts have suggested alternative handling of the issue through augmentation of the sub-grid model near the wall (Wu

and Meyers, 2013), an approach which also artificially smooths the fluctuations. As such, all of these ad-hoc corrections can be seen to have detrimental effects on the accuracy of simulations by reducing effective resolution and artificially damping fluctuations which have been established to be especially important under APG conditions.

It is also apparent, therefore, that the wall modelling problem presents not only a theoretical physical challenge but a numerical one in which it must be carefully considered how quantities are defined and measured near to the wall. While the artificial boundary condition approach to wall modelling has been taken since it greatly simplifies the modelling concept, it is limited in that it is only appropriate under certain conditions and produces numerical troubles. Most importantly, it is already known that numerical approaches which utilise a sharply-defined boundary condition are fundamentally incompatible with sub-grid scale modelling (Bou-Zeid et al., 2005). Therefore, it is essential that new approaches use different boundary conditions. In the present methodology, issues generated by the domain edge are addressed with the goal of ensuring regularity (controlled numerical error) at all positions.

In summary, WMLES shows great potential in that it has already facilitated the simulation of turbulent flows at Reynolds numbers inaccessible to wall-resolved methods. However, non-universal characteristics of adverse pressure gradient boundary layers pose a fundamental threat to the further application of the explicit WMLES methodology - particularly in conditions far from equilibrium. Serious numerical issues are also experienced due to the interaction between current wall-models and sub-grid scale modelling, suggesting a need for the integration of the two facets of the overall modelling problem under a unified description.

Together, these problems indicate a strong need for models developed to describe the sub-grid scales implicitly, in the sense that explicit scale separation is not necessitated by the LES filter or by the wall model. This approach is already well established for sub-grid scale modelling and has found various advantages, but it is not equipped with the tensor structure used by explicit LES which is essential to describe more complex flow conditions near to walls. An ideal model would therefore combine the unique advantages of the iLES method with the tensor structure of explicit LES - aiming to eliminate the dependence of explicit LES on empirical data and related equilibrium assumptions, while still preserving the ability to describe general conditions and unresolved momentum fluxes in wall bounded flows.

Chapter 3

Methodology

This chapter provides a theoretical approach to LES modelling which aims to preserve the universality of the turbulent cascade found under locally isotropic conditions. This is achieved by constructing a geometric description of the sub-grid scale velocity field in which conditions may always be considered locally isotropic and so modelling remains universal.

The conditions within a finite volume can be considered locally isotropic when the distribution of the velocity vector over the volume is isotropic. From another perspective, this means that a finite fluid packet behaves inertially in the sense that the motion of fluid in a volume may be characterised by a single velocity and an energy. In practice, where the velocity field may be faithfully characterised by a finite volume average, the momentum fluxes are fully resolved and so the finite volume scheme is valid in maintaining the conservation of momentum described by the Navier-Stokes equation. Hence, no sub-grid scale stress is required as long as energy conservation of the weak solution is maintained. Because the velocity distribution within a volume under locally isotropic conditions is locally indistinguishable from that found in homogeneous, isotropic turbulence, locally isotropic conditions allow for the consistent application of a universal iLES model for the local turbulent cascade mechanism.

This chapter takes an approach which reframes the modelling problem for conditions in which the finite volume resolution is not fine enough to resolve momentum fluxes and so cannot provide locally inertial conditions. This is achieved by making use of the fact that the local velocity distribution over a finite volume is reference-frame dependent. Instead of making modifications to the sub-grid scale model itself in an attempt to empirically account for deviations from locally isotropic conditions, special, local frames of reference are considered in which the conditions appear locally isotropic and a universal picture of energy conservation remains valid. The key observation is that the velocity distribution over a finite volume is reference-frame

dependent. In this sense, the components of the explicit sub-grid stress tensor may always be (locally) transformed into the identity matrix by a change of coordinate system or basis. In other words, the sub-grid scale velocity distribution can always (locally) be manipulated to appear isotropic given a special (locally inertial) choice of reference frame.

While a global change in reference frame is only a trivial change of coordinate choice, the power in this concept arises from requiring consistency between neighbouring positions. Assuming that the conditions are not homogeneous, there exists a different special reference frame at each point. Therefore, if it is required that inertial conditions are achieved at every position simultaneously, then a system of local reference frames is defined in which the sub-grid scale stress appears both homogeneous and isotropic, resulting in zero sub-grid scale force. Hence, inertial behaviour of the governing equations (without any sub-grid force) may be maintained by considering a system of local reference frames. Importantly, the required coordinate transformation which restores inertial behaviour at all positions is not global, but local. In other words, in order to eliminate the sub-grid scale force globally, a system of local reference frames must be constructed and equipped with a structure which describes how to consistently move between positions while maintaining locally inertial, universal behaviour. The mathematical structure which connects local frames of reference in this sense is a manifold.

The goal of the theoretical methodology described in this chapter is therefore to eliminate the sub-grid scale force from the LES equations by introducing a manifold structure. Overall, it is suggested that a geometric approach should be used which connects local reference frames in which turbulent behaviour appears inertial, such that the laws of physics remain locally universal. It is recognised that this concept is very similar in spirit to the geometrisation of the Newtonian gravitational force used by the theory of general relativity. Here, the explicit sub-grid scale force is geometrised, becoming an implicit effect of an induced non-Euclidean geometry. This approach generates a local, filter-free modelling problem for each finite volume in which strict locality greatly simplifies the possible approaches to modelling. Importantly, this leaves minimal need for empirical assumptions and data as input.

> When I meet God, I'm going to ask him two questions: why relativity? And why turbulence? I really believe he'll have an answer for the first. (Heisenberg)

3.1 Geometric framework

3.1.1 Definition

A method is defined which eliminates the sub-grid stress tensor from the equations used by explicit LES. In doing so, the explicit filter which generates the sub-grid stress tensor is also made redundant. The proposed methodology therefore provides a governing equation which describes sub-grid scale effects geometrically, maintaining the rich tensor structure of the classical LES methodology while eliminating the problematic explicit filter.

Based on the motivating arguments, it is chosen to treat the position space as a manifold. Non-Euclidean geometry of the manifold is then used to eliminate the sub-grid stress tensor from the LES equation. This serves as a mathematical method to eliminate the non-locality associated with explicit LES filtering and to facilitate a re-interpretation of the coarsely resolved velocity field and the sub-grid scale modelling problem in a strictly local sense. While the new approach is filter-free, it retains a tensor quantity which describes non-universality of the sub-grid scales. Therefore, the key advantages of implicit and explicit LES are combined.

The incompressible LES equation may be written in tensor form as

$$\partial_t \bar{u}^i = \nabla_j \left(\bar{\tau}_\nu^{ij} - \bar{u}^i \bar{u}^j - \tau_{\mathrm{SGS}}^{ij} \right) - g^{ij} \partial_j \bar{p} \tag{3.1}$$

along with the divergence-free constraint $\nabla_i \bar{u}^i = 0$ and where: $\bar{\cdot}$ is the LES filter operator; the vector $\nabla_j A^{ij}$ is the covariant divergence of a tensor A; $\bar{\tau}_\nu^{ij} = \nu \left(\nabla^i \bar{u}^j + \nabla^j \bar{u}^i \right)$ is the viscous stress tensor where $\nabla^i \bar{u}^j = g^{ik} \nabla_k \bar{u}^j$; and τ_{SGS}^{ij} is the sub-grid stress tensor. The position space is defined as a 3-dimensional manifold M with metric tensor g. In the Euclidean limit, the space is homogeneous and isotropic with $g_{ij} = \delta_{ij}$. In this case, the standard LES equation is recovered and the divergence operator takes its usual definition.

In order to eliminate the sub-grid stress tensor from the dynamical equation, it is required that $\nabla_j \tau_{\mathrm{SGS}}^{ij} = 0$. Subject to certain conditions, this constraint is satisfied by taking $g^{ij} = \tau_{\mathrm{SGS}}^{ij} / c^2$ where c is a constant velocity which produces a non-dimensional metric g; for now, $c^2 = 1$ is taken for simplicity of notation. The goal is therefore for the metric tensor to replace the sub-grid stress tensor in representing unresolved information. The necessary condition $\nabla_j g^{ij} = \nabla_j \tau_{\mathrm{SGS}}^{ij} = 0$ is ensured by the standard definition of a manifold with a compatible metric connection. Metric compatibility means that, as vectors are parallel transported on the manifold, the metric is respected such that the lengths of vectors and the angles between them are preserved. Given that τ_{SGS} is symmetric, the choice of the metric tensor is also constrained to be symmetric, requiring that the connection itself is torsion-free; the manifold does not

twist but may stretch and shear. The fundamental theorem of Riemannian geometry states that the Levi-Civita connection is the unique choice which satisfies both constraints (Lee, 2018). Therefore, in order to remain physically consistent, the position space under the new geometric turbulence framework takes the form of a 3-dimensional Riemann manifold.

The resultant governing equation for the large-scale velocity field is the Navier-Stokes equation on a manifold background

$$\partial_t \langle u^i \rangle = \nabla_j \left(\langle \tau_v^{ij} \rangle - \langle u^i \rangle \langle u^j \rangle \right) - g^{ij} \partial_j p \tag{3.2}$$

where the metric tensor describes the background geometry. The motion of the fluid is therefore universally inertial in the sense that motion occurs locally according to the observed forces and Newtonian laws (according to the Navier-Stokes equation without additional terms). Moreover, there is no problematic, unobservable sub-grid scale force which arises in LES.

Since LES filtering is no longer required to produce the SGS stress tensor, the operator $\langle \cdot \rangle$ which defines the large scale velocity field may now also be interpreted implicitly (in the iLES sense). The key role of the metric tensor is in the definition of the covariant derivative, which is defined from the perspective of a numerical implementation in Chapter 4. The originality of this modelling methodology is that it eliminates the divergence of the sub-grid stress tensor; this is unique because of the direct implication that no force arises from the sub-grid scales in this framework. Because it makes the explicit LES filter redundant, this key conceptual distinction has novel implications for the interpretation of the large scale velocity field, as discussed in Section 3.1.2.

Similar to the sub-grid scale stress tensor, the role of the metric tensor must be explained with reference to under-resolution of the velocity field. However, the metric tensor must be interpreted with distinct physical meaning due to its non-dimensionality, its geometric meaning, and the crucial differences between the explicit LES filter and implicit filtering. This distinction creates significant conceptual advantages for the new methodology. The metric's physical interpretation and its role in the equations is addressed in the following section.

3.1.2 Interpretation

In explicit LES, an effective (sub-grid scale) force appears under large observation scales where the Navier-Stokes equation breaks down. The new framework re-interprets the sub-grid effect through the appearance of an "effective metric" at coarse scales, rather than the true Euclidean one. In this picture, a key difference is

that the Navier-Stokes equation is preserved. The description can again be described as locally inertial in the sense that unobservable forces are not acting to produce anomalous accelerations which cannot be explained by the inertial mass and measured forces. This comes as a consequence of the fact that a manifold by definition locally resembles Euclidean space (over a small enough volume scale). The local preservation of the governing equation can be understood to represent the preservation of symmetries which are fundamental to conservation. Because the metric tensor does not form an explicit part of the dynamics, it is best interpreted as a constraint on the dynamics which becomes significant for large observation scales. This contrasts with the explicit LES framework, where the sub-grid scale stress provides a "hard" constraint by explicitly determining the dynamics. In the present description the fluid dynamics are free to evolve according to the Navier-Stokes equations and are not explicitly constrained by the metric. Instead, the shape of the manifold may be used to provide a "soft", statistical constraint which guides the dynamics.

The distance measure $ds^2 = g_{ij}dx^i dx^j$ creates a geometric structure to the space, a local portion of which is sketched in Figure 3.1 for a sheared geometry relevant to conditions of fluid shear. Here, coordinate directions which were previously independent in a Euclidean manifold are effectively coupled by off-diagonal components of the metric tensor. In the present study, this effect becomes important near to wall boundaries where displacements normal to the wall are statistically coupled with displacements parallel to the wall by turbulence effects. Under the simplified local geometry sketched by Figure 3.1 - assuming a simple, "laminar-like" shear condition - a perturbation along one coordinate direction induces motion in the other coordinate direction due to the directional coupling. When turbulent fluctuations are involved, or there is uncertainty in the measurement of the velocity field due to finite resolution, the geometry couples statistical fluctuations in the two directions. Equivalently, where the coordinate directions are coupled, with a distance measure such as $ds^2 = dx^2 + dy^2 - \frac{1}{4}dxdy$, distances in the compressed quadrants with $dxdy > 0$ are effectively reduced, while distances in the expanded quadrants $(dxdy < 0)$ are effectively increased.

By analogy, this local description mirrors the statistical coupling of velocity components described by the Reynolds or sub-grid stress tensors. Locally, the key originality in the present method is that a force is not explicitly applied and therefore does not require explicit modelling. Instead, random perturbations resulting from finite resolution and measurement uncertainty in capturing the underlying distribution of a turbulent velocity field are allowed to exist and form part of the theory. The impact of possible fluctuations is then guided by the geometrical structure as described above, rather than being directly prescribed via a forcing. In the proposed framework, as discussed, the model is a soft constraint on the local dynamics, which are left free to play out as governed by the Navier-Stokes equation.

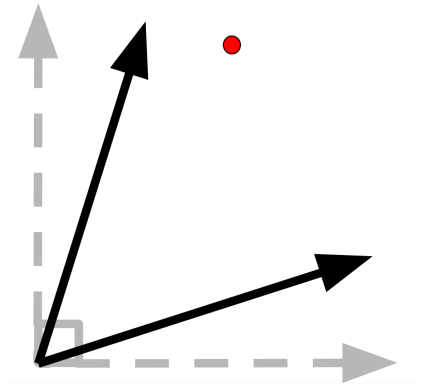

FIGURE 3.1: A conceptual sketch demonstrating the local effect of a modification to the off-diagonal components of the effective metric on the motions of fluid particles.

The new perspective contributed is that, while random fluctuations are free to occur, the metric changes the response of the system by creating statistical coupling between different directions. Overall, this philosophy contrasts strongly with the traditional methodology in which a force is imposed, representing an explicit collapse of the space of possible fluctuations into a single realisation which is dictated by a model. Therefore, a significant difference in practice is that the geometric framework preserves the statistical state of many possible unresolved perturbations, while the classical framework collapses it by forcing the choice of a single realisation of the statistical distribution describing the sub-grid stress tensor.

Expanding this local picture to examine the global structure of the manifold exposes further novelties in the geometric approach. Figure 3.2b sketches a feasible manifold structure which may be formed in a boundary layer flow where shear is varying with position. In the case with constant shear (Figure 3.2a), it is evident that local coordinate patches can be tiled together without issue to form a global manifold structure, showing that the manifold is in this case flat but sheared, with simple local statistical coupling of directions. However, where the shear is variable with position, tiling of local patches is not possible to represent on the Euclidean plane without distortion of either lengths or angles, as illustrated by Figure 3.2b. In the same sense that a map of the globe cannot be faithfully reproduced on paper, this is a visual illustration of the fact that the manifold under realistic flow conditions takes on non-Euclidean, curved properties. It is this global organisation which provides core mathematical structure to the geometric framework which is not available in existing methods. The major novel property of the geometric model with a curved manifold is that distances between positions are path-dependent. This feature, combined with the avoidance of an explicit collapse in the statistical state of possible fluctuations, creates a valuable property which can be exploited. Namely, because there is no explicit realisation of the statistical distribution describing the sub-grid scales, the dynamics may implicitly explore the true space of different possible trajectories with different, path-dependent outcomes. As discussed, path-dependent behaviour is a key property

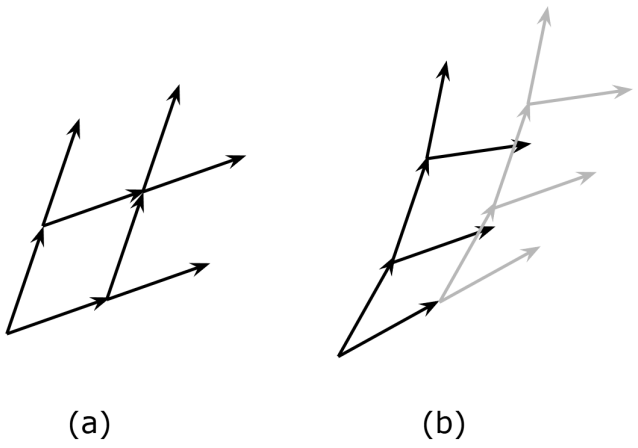

FIGURE 3.2: A conceptual sketch demonstrating: (a) flatness of the manifold with homogeneous shear in 2 dimensions; and (b) the effect of shear variation on the global properties of the manifold.

of non-equilibrium systems, including pressure gradient boundary layers, and any single realisation is not necessarily representative of the true statistical structure. The geometric framework therefore offers an original and unique mathematical property to describe this feature. Meanwhile, this rich, additional structure is explicitly discarded by current methods where a force or filtering operator is applied. Later, it is argued that path-dependency arising from curvature of the manifold is crucial to capture the modelling of pressure gradient boundary layers.

However, without an explicit filter, the metric interpretation is still wanting a definition for the large-scale velocity field under the (implicit) operator $\langle\cdot\rangle$. Therefore, an interpretation is provided for the large-scale velocity field which is consistent with the geometric description.

Let the velocity at position $x \in \mathbb{R}^3$ be represented by a vector-valued distribution $U(u)$ which takes on values in $u \in \mathbb{R}^3$. At each point, a configuration integral $Z(x)$ can be written for the possible states of the velocity vector U

$$Z(x) = \int \exp\left(-\frac{x_i U_i}{\nu_\Delta}\right) d^3u \tag{3.3}$$

which integrates over the velocity distribution.

The expectation value for the velocity vector is then defined by

$$\mathbb{E}\left[U_i\right] = \langle U_i \rangle = -\frac{\partial \log Z}{\partial x_i} \tag{3.4}$$

and the Hessian defines a Fisher information metric (Crooks, 2007)

$$g_{ij}(x) = -\frac{\partial^2 \log Z}{\partial x_i \partial x_j} = \langle (U_i - \langle U_i \rangle)(U_j - \langle U_j \rangle) \rangle. \tag{3.5}$$

Hence, a distribution-valued velocity field implies geometric structure equivalent to that used in the proposed geometric model. Uncertainty in the measurement of the velocity field creates geometric structure because different possible realisations of the velocity vector represent different paths for a finite fluid packet through space; the characteristics of these paths are governed by the metric tensor. Hence, the metric tensor can be understood to implicitly represent the sub-grid scale distribution of velocity across a finite volume. Notice that the metric tensor g that has been defined is in some sense similar to the LES sub-grid stress tensor in that it can also be viewed as a covariance matrix. However, its meaning is distinct and must be carefully interpreted because the operator $\langle \cdot \rangle$ here is not equivalent to an explicit LES filter.

The most natural interpretation is that the operator $\langle \cdot \rangle$ corresponds to an expectation value over a finite volume. Evidently, the underlying velocity field is not truly distribution valued, but is deterministic. However, uncertainty in the velocity vector can be framed in terms of the positional uncertainty associated with finite resolution. Where the position is measured to a precision of $\pm \Delta x/2$ with Δx being the discretisation length scale, the velocity field at any position is distribution-valued with values sampled uniformly over the finite volume. This interpretation is sketched in Figure 3.3 which illustrates that the velocity value for a finite volume is distribution-valued. Hence, a distribution of measured values for the velocity field appears as a natural result of discrete spatial resolution. Overall, the metric tensor should therefore be understood as a natural by-product of measurement uncertainty in LES. The origins of the geometric framework can therefore be described in terms of how statistical uncertainty induces geometrical structure. Note that the "filtering" process here is implicit where a finite volume scheme is used, because the scheme already represents a weak solution which by definition tracks the expectation (average) values for the velocity field over finite volumes. The metric then is a proxy for describing the first order, local statistical structure of the velocity field distribution across a finite volume of space.

Importantly, the implicit filtering is local in that it operates within a single unit of resolution (the finite volume). This is simply not possible in the explicit LES approach, because a numerical filter must be applied by convolving a discrete filter kernel with the velocity field. Hence, the LES filter kernel must have non-local support which spans multiple units of resolution (or grid points) in order to produce any filtering effect. Therefore, it is crucial to note that the new, geometric approach maximises locality of the statistical sampling involved in defining the large-scale velocity field and equivalently minimises artificial dissipation. No further locality can possibly be

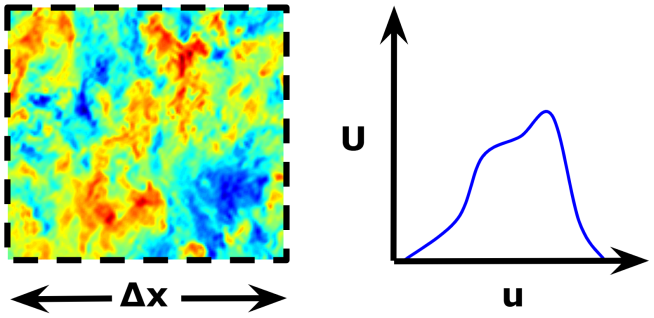

FIGURE 3.3: A conceptual sketch of the distribution U of the velocity u found over a finite volume with positional measurement uncertainty $\pm\Delta x/2$.

achieved due to the fundamental limits of the positional measurement uncertainty. Locality of the present description later brings strong implications for the universality of models constructed for the metric tensor.

Overall, this approach generates a framework in which the effects of anisotropy and inhomogeneity of different problems can be modelled locally in the strictest possible sense (to within measurement uncertainty defined by the chosen resolution). Because the new approach maximises locality, the local modelling problem treated in the following section is greatly simplified. Multiple positions are not sampled over and so the modelling problem depends only on the locally available pieces of information (the velocity gradient and pressure). In contrast, a compact LES filter kernel might sample over a single grid point either side of a central location, and in doing so introduces a cube of 27 grid points which have been sampled. At each position involved, the statistical properties will be different due to the particular flow conditions. These non-local statistics are then blended into a non-universal distribution which must be modelled for closure. This introduces an enormous potential for non-universality in the sampled distribution for the SGS tensor. All of this variation is totally problem-dependent, with an effectively unlimited range of possible anisotropic and inhomogeneous configurations. Even for such a compact 3-dimensional kernel, and with only 2 possible statistical states at each sample point, the non-locality of the sampling would introduce 2^{27} possible conditions under which the sub-grid scale stress tensor must be modelled in order for the model to apply in all possible conditions. While the real data is continuous, the essence of this observation is that the informational complexity exponentially increases with increasing non-locality (with the number of sample points under the kernel). It is therefore hugely significant that the proposed geometric formulation is able to absolutely minimise the excess non-locality and statistical variability/complexity.

Overall, a reduced potential for model complexity in the present framework is achieved by introducing a new mathematical description which avoids explicit filtering and provides the opportunity for a novel reinterpretation of the turbulence

modelling problem. All the while, clear parallels are maintained with the original LES approach. Despite this, exact equivalence between the new geometric approach and a traditional LES model is not possible because the minimal, implicit filtering applied in the present framework is impossible to reproduce explicitly. The key advantage of the new approach over current implicitly filtered frameworks is that it defines the metric tensor which provides rich tensorial structure with the potential for describing non-inertial conditions which cannot be represented by iLES dissipation alone. The following section addresses the modelling problem for the metric tensor, leading to a practical implementation of the new method which is defined numerically and tested in the following chapters.

3.2 Modelling

Given the interpretation of the metric tensor as a local description for the sub-grid scale velocity distribution over a finite volume, there is a clear path to writing down an expression for the metric. Namely, in the simplest possible model, anisotropy of the velocity distribution over a single finite volume is described by the resolved fluid shear stress. This holds true because the velocity distribution is approximately described by the velocity differences across the faces of a finite volume, and the strength of the resultant momentum fluxes which cause deviations from locally isotropic conditions are proportional to the fluid viscosity. Therefore, the resolved viscous stress tensor may be used locally to model the metric tensor in a way which consistently represents sub-grid scale momentum fluxes. In a similar way, the relative pressure may be used to provide a model for the sub-grid scale normal stress under inhomogeneous, pressure gradient conditions. In constructing the model, the viscous and pressure stresses are considered separately.

3.2.1 Shear model

This section describes the viscous effect on the metric tensor, which principally addresses unresolved momentum fluxes. In order to lay the foundation, the simplest possible model for the metric is adopted, where small perturbations around the Euclidean metric tensor are proportional to the viscous stress tensor. This amounts to assuming that the linear variation in velocity across the faces of a finite volume is the leading order component which describes the local anisotropy. This assumption is reasonable due to the fact that no better approximation for the velocity distribution is available given the choice of a particular resolution.

The proposed model can be written as

$$g^{ij} - \delta^{ij} = -\frac{2k\nu}{c^2} S^{ij} + O(|x|^2) \tag{3.6}$$

where S^{ij} is the contravariant form of the rate-of-strain tensor, ν is the physical viscosity, and the constant $k/c^2 = 3$. Note that this is a second-order, local approximation to the metric tensor because higher-order variation is possible across the finite volume. However, a numerical solver is chosen later which employs second-order finite differencing for the viscous diffusion term. Therefore, the current choice represents the most accurate order of approximation available. It is later demonstrated that perturbations around the Euclidean metric are in fact small, such that the linear order term chosen here dominates higher order terms.

Notably, this concept also leads to a familiar model which is similar in form to a traditional eddy-viscosity model. However, because the intended geometric deformation is strictly proportional to the rate-of-strain tensor, a constant coefficient is chosen. Again, it is argued that this simplification is made possible because the model is defined in a strictly local way such that conditions-dependence is minimised. The model therefore makes use of the fact that, locally, deviations from isotropy are best described by the rate-of-strain tensor, since no further relevant information is available.

In fact, any conditions-dependence in the new model must come from higher-order variations in the velocity field across a finite volume. Because these effects are known to be contained within the higher-order terms, the proposed model does not leave conditions-dependence as an unknown empirical factor, but makes it clear where the model is valid or not. Confidence can therefore be held that any specific order of approximation (where second order is chosen in this work) is truly the leading-order contribution to a description of the sub-grid scale velocity distribution. This can be explicitly validated by making sure that the perturbations made to the Euclidean metric tensor are small in magnitude, such that lower-order terms dominate. If higher-order accuracy is required, a higher-order approximation must be used for the rate-of-strain tensor. If precision needs to be adjusted, the length scale of discretisation must be changed.

The function of the model may be described through the fact that the metric tensor defines a distance measure $ds^2 = g_{ij} dx^i dx^j$ on the position space (where $g_{ij} = \delta_{ij}$ for Euclidean geometry). Differences in the metric from the Euclidean metric therefore represent discrepancies in the trajectories of fluid packets caused by sub-grid scale action. For example, a classical turbulent shear stress in the wall-fixed frame of reference may be represented by a non-zero off-diagonal component $g_{12} = g_{21} \neq 0$ as described above and sketched in Figure 3.1. In this case, motion in the x^1 (stream-wise) direction is coupled with motion in the x^2 (wall-normal) direction. Again, this mode

of operation is somewhat analogous to the correlation between velocity components described by the LES sub-grid stress tensor, but is distinguished by the fact that the metric tensor can be defined locally and therefore far more universally.

It is demonstrated that, when combined with a dissipative iLES scheme which represents universal, inertial energy dissipation, Equation 3.6 naturally functions as an "implicit" wall model by implicitly providing the appropriate momentum fluxes. The model is shown to converge into the regime where viscous scales are partially resolved, retaining effectiveness even for small grid length scales relative to the wall's viscous length scale. This contrasts with many explicit LES wall models which require the first grid point to be situated within the logarithmic-layer due to decoupling assumptions. Appropriately regularising numerical techniques are chosen such that the model does not exhibit numerical sensitivity because sharp interfaces between solution zones and artificial boundary conditions are both eliminated. Finally, the model is also capable of accurately predicting fluctuating statistics, as it applies minimal smoothing to the solution and so has less tendency to under-predict these quantities.

3.2.2 Pressure model

The shear model presented above is intended to represent unresolved, local momentum fluxes - especially the viscous wall shear stress - and to maintain the local momentum balance. However, it has been established that pressure gradient boundary layers see two effects: the local momentum balance; and an accumulated, history dependent energetic effect. In analogy to the shear model for local momentum fluxes as described by the anisotropy of the local stress tensor, the pressure effect may be described with regard to sub-grid scale energy and the inhomogeneity of the pressure (the other component of the total stress tensor). Where the shear model accounts for velocity differences across a finite volume, which produce non-inertial behaviour, pressure gradients directly produce non-inertial conditions through acceleration resulting from the pressure gradient.

The simplest possible model is investigated, where differences in the metric tensor compared to the Euclidean metric are proportional to the pressure. Including both viscous and pressure contributions, the overall model may now be written as

$$g^{ij} - \delta^{ij} = -\frac{2\kappa\nu}{c^2} S^{ij} + \frac{C_p}{c^2}(p - p_0)\delta^{ij} + O(|x|^3) \tag{3.7}$$

where $p(x)$ is the pressure, p_0 is the pressure at a free-stream reference location, δ_{ij} is the Euclidean metric tensor and the constant $C_p = 1/12$. Equation 3.7 is used to calculate values for the metric tensor at each time step of simulation, with the rate of

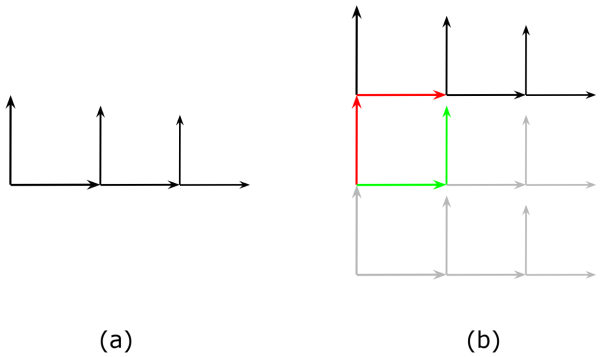

FIGURE 3.4: A conceptual sketch of the pressure model function as compression of the manifold along a coordinate direction.

strain tensor being calculated in the same way as it appears in the viscous stress tensor, via finite differences of the velocity field.

Where the shear component of the model has the effect of shearing the manifold geometry, the pressure component of the model has the effect of expanding or contracting the fabric of the manifold, proportional to the local pressure. This means an expansion/contraction of the distance measure in the direction of pressure gradient as visualised by Figure 3.4a. The impact of this effect on the global structure of the manifold is sketched in Figure 3.4b, which aims to explain the unique geometric effect in a similar way to how Figure 3.2 did for the shear modification. Figure 3.4b shows that, as the metric expands or contracts along one direction, it is no longer possible to draw the complete space on the Euclidean plane without distortion of either angles or distances. In the sketch, this is manifested in the appearance of disconnections, which cannot be closed without distorting angles or distances when drawn on the Eulerian plane. Hence, when a connection between local coordinate patches is formed as described by the metric, the resultant manifold is curved. Therefore, varying pressure directly results in non-Euclidean curvature of the manifold. The nature of the curvature created, however, is different to that found in the shear case and sketched in Figure 3.2. However, it also creates an effect whereby the distance between points is path-dependent. In the conceptual geometry illustrated by Figure 3.4, the green path is shorter than the red path for example due to shrinking of distances when moving horizontally to the right. Thus, the order of turbulent fluctuations matters in this model; a horizontal fluctuation followed by a vertical fluctuation is not equivalent to the same fluctuations but with their order reversed. Both varying pressure and varying shear stress create this non-classical property which is unique to the proposed geometric model. Such an effect cannot possibly be captured by applying an explicit forcing, because the force cannot act in more than one direction at once and so cannot capture the true statistical nature of the observed system.

Although the manifold is always locally Euclidean, when moving through the manifold under the effects of the model, motion in one direction begins to become "harder" due to an expanding distance measure, while motion in the other direction becomes "easier" due to a contracting distance measure. With motion in the direction of acceleration, the distance measure expands in such a way that the acceleration is cancelled out. Hence, the conditions may appear locally inertial. Therefore, this component of the model can be understood as a geometrisation of the acceleration effect on turbulence caused by pressure gradient. In other words, the proposed model once again represents a system of reference frames in which the conditions appear locally inertial in that they are locally indistinguishable from homogeneous, isotropic turbulence. In this case, this means finding a system of local frames of reference in which the pressure gradient acceleration is effectively not felt, in a similar sense to how the shear model may be viewed in terms of eliminating the appearance of sub-grid forces.

The interpretation for this component of the model is more subtle as it does not align so clearly with classical ideas of wall-stress modelling as the shear model, and it appears locally as a second-order rather than linear effect on the geometry. Broadly, rather than capturing shear effects which describe local momentum flux, it captures the energetic effects generated by the accumulative history of pressure gradients. While the local pressure gradient has a direct impact on the momentum balance, the effect of a large scale, mean pressure gradient on the momentum balance is well resolved even under a coarse LES resolution. The literature has identified an indirect and sub-grid scale, "history" effect described by an accumulation of the pressure gradient along a boundary layer. It is this accumulative history effect on the small scale energy of the fluctuations - not the local momentum balance - which is the target of the proposed pressure model. It can immediately be noted that the proposed model also falls in line with empirical observations, which suggest that the integrated pressure gradient (or relative pressure) is a key factor for describing this effect on the turbulent boundary layer structure.

Overall, a common theme is that both the shear and pressure aspects of the overall model also capture a crucial property of non-equilibrium statistical systems - path dependency. By defining a geometric structure, explicit choices are not made about turbulent fluctuations. For example, the fluid at a certain position may take many possible paths on the manifold depending on uncertainty in the local distribution of possible velocities. Therefore, modelling is achieved in this framework without explicitly making a choice between possible realisations and therefore without collapsing the full space of possibilities. This contrasts strongly with explicit LES in which a particular value for the sub-grid scale stress tensor must be chosen from a distribution. Instead, the current approach recognises that different possible underlying fluctuations exist as a result of measurement uncertainty; the possibilities

then all remain valid, and there is no need to insist on any particular explicit realisation. Conceptually, this is important for non-equilibrium flows since non-equilibrium systems are non-ergodic - meaning that any particular realisation is not representative of the overall statistical behaviour. This perspective, which is inaccessible to explicit LES, is the essence of history-dependence. The proposed geometric framework therefore has unique mathematical potential to remain consistent with the observed, history-dependent behaviour of APG boundary layers.

Chapter 4

Computational Setup

This chapter describes the computational methodology used to validate the theoretical methodology presented in the preceding chapter. The flow solver employed to generate simulation results is defined, including numerical implementation of the new geometric model and smooth numerical treatment of wall boundary conditions.

4.1 Flow solver

Simulations were carried out using a flow solver which is a significantly adapted version of Waterlily.jl (Weymouth and Font, 2025). The key modification is the implementation of the divergence theorem in the finite volume code. The method is adapted for non-Euclidean geometries described by a metric tensor which are required for the present modelling methodology. The solver supports both CPU and GPU hardware (Weymouth and Font, 2025). However, unless stated otherwise, all simulations are executed on GPU with single floating-point precision (FP32) and are performed using a uniform Cartesian grid for simplicity and efficiency of the computational code. This permits a pure focus on the scientific methodology, without adding unnecessary complexity to the numerical methods which might confound any results. The boundary data immersion method (BDIM) is used for a smooth treatment of wall boundaries (Maertens and Weymouth, 2015). This permits iLES energy conservation which is based on regularisation of the velocity field to function robustly near to walls, which are otherwise known to introduce numerical irregularities that are problematic in wall modelling. Furthermore, the use of an immersed boundary method means that all results and tools produced may also be applied to more complex and moving/morphing wall geometries without significant modification.

The solver is based on a finite volume scheme with staggered velocity-pressure variable placement and with pressure and viscous terms being discretised using

second-order central differences (Weymouth and Font, 2025). The solver is also equipped with a built in, iLES dissipation model given by a flux-limited quadratic upstream interpolation for convective kinematics (QUICK) discretisation of the non-linear, convective term (Weymouth and Font, 2025). This scheme is used throughout to calculate the advective fluxes. A geometric multigrid method is used to solve the pressure Poisson equation (Weymouth, 2022) and an explicit predictor-corrector scheme is used to integrate the Navier-Stokes momentum equation over time. The time-step is automatically adjusted to maintain the Courant-Friedrichs-Lewy (CFL) number.

Given the present theoretical methodology, modification is required to the solver in order to represent the effects of Riemannian geometry. This applies to the divergence operator as applied to the momentum flux, while the BDIM acts on the equation system as a whole and so remains unchanged as outlined later. In order to solve the governing Navier-Stokes equation

$$\partial_t \langle u^i \rangle = \nabla_j \left(\langle \tau_\nu^{ij} \rangle - \langle u^i \rangle \langle u^j \rangle \right) - g^{ij} \partial_j \langle p \rangle \tag{4.1}$$

on a manifold (M, g) and where $\langle u \rangle$ is the expectation value of the velocity distribution over a finite volume, the definition of the covariant divergence operator for the manifold needs to be incorporated into the numerical scheme. This is the only significant difference compared to the standard Waterlily.jl solver; many finite volume solvers could also be adapted in a similar way with relative ease.

The divergence theorem taking into account geometry of the manifold is given in terms of the covariant divergence as (Warner, 1983)

$$\int_V \nabla_j \Phi^{ij} \sqrt{|g|} d^3x = \int_{\partial V} n_j \Phi^{ij} \sqrt{|h|} d^2x \tag{4.2}$$

where: $\Phi^{ij} = \langle \tau_\nu^{ij} \rangle - \langle u^i \rangle \langle u^j \rangle$ is here the resolved momentum flux; $\sqrt{|g|} d^3x$ is the volume element of the manifold with $|g|$ being the determinant of the metric; and $\sqrt{|h|} d^2x$ is the surface element with

$$h_{ab} = g_{ij} \partial_a x^i \partial_b x^j \tag{4.3}$$

being the induced metric on the surface of the volume ∂V. The terms $\partial_a x^i$ and $\partial_b x^i$ are the partial derivatives of the coordinate along tangent vectors to the surface. The covariant normal $n_i = g_{ij} n^j$ is given in terms of the unit normal vector to the volume n^j and the metric. With Cartesian finite volumes, the normal vectors are simply the (signed) basis vectors, significantly simplifying calculations.

Numerically, first the metric tensor is calculated according to Equation 3.7. The rate of strain tensor is already calculated using second order finite differences to find the

viscous stress tensor τ_ν^{ij}, while the pressure field is used to modify the diagonal components of the metric tensor if the pressure model is activated. Otherwise, Equation 3.6 is used to calculate the metric tensor when only the shear model is active. With the summed indices being written out explicitly, the divergence of the momentum flux is calculated as the sum over the faces of a cubic finite volume and the components of the flux

$$\int_{\partial V} n_j \Phi^{ij} \sqrt{|h|} d^2x \approx \sum_{\text{faces}} \sum_{j=1}^{3} \sum_{k=1}^{3} g_{jk} n^k \Phi^{ij} \sqrt{|h|} \tag{4.4}$$

where here the metric tensor values are co-located with the momentum flux values on face centres. According to Equation 3.7, the metric tensor is calculated using the gradients of the velocity field involved in the rate-of-strain tensor, and using the pressure field. Therefore, its off-diagonal components are co-located with the major momentum flux components as required. Meanwhile, its diagonal components are co-located with the pressure at the cell centres.

The effect of the metric tensor on the numerical implementation may be visualised by considering, for example, a flux of x-momentum in the y direction as illustrated in Figure 4.1. In the standard, Euclidean geometry, the covariant (n_i) and contravariant (n^i) components of the face normal vectors are equivalent because the metric tensor is equal to the Kronecker delta. Therefore the fluxes of x momentum in the y coordinate direction are entirely determined by the faces orthogonal to the y coordinate axis such as the lower face in Figure 4.1. However, in the non-Euclidean case, the covariant components of the normal vectors are modified by the metric tensor $(n_i = g_{ij} n^j)$. For each face, in Euclidean geometry, two components of the momentum flux act to transport momentum tangentially along a finite volume face (such as the left face shown in Figure 4.1) and so do not add to the discrete momentum balance because they are orthogonal to the normal vector. Where the geometry (through the covariant normal vector components n_i) is modified by a non-Euclidean metric tensor, these fluxes become minor contributors to the momentum balance due to the geometry of the manifold. The result is that, in addition to the usual iteration over each of 3 momentum components (index i in Equation 4.4) and the summation of the major fluxes over each of 3 coordinate directions (index j), two additional, geometry-induced minor fluxes must also be incorporated for each face, corresponding with the summation over the index k in Equation 4.4. For example, when considering the x-momentum over a face with normal pointing along the y coordinate direction, the major flux is the Φ^{xy} component as illustrated in Figure 4.1, transporting x-momentum in the y direction with the coefficient $g_{yy} n^y \approx 1$. However, in the geometric model, the components Φ^{xz} and Φ^{xx} at this location must also be taken into account due to the manifold, with minor contributions $g_{zy} n^y \Phi^{xz}$ and $g_{xy} n^y \Phi^{xx}$ respectively induced by the cross-components in the metric tensor. Due to the

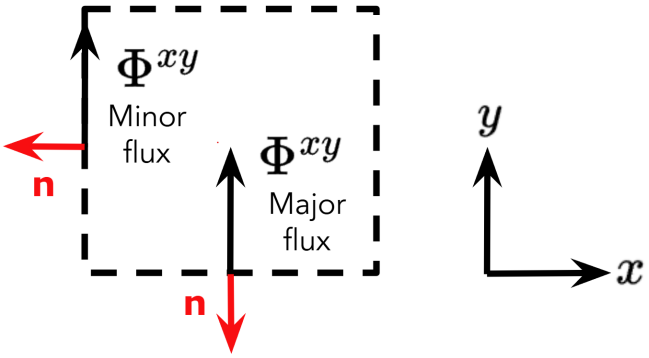

FIGURE 4.1: A sketch showing the major and minor finite volume momentum fluxes for the x momentum component in the y direction.

staggered location of the calculated momentum fluxes relative to the minor flux locations, the metric tensor and momentum flux values are linearly interpolated to determine the values when required at minor locations.

For the sake of comparison to existing methods, it is also tempting to attempt to reverse the divergence theorem, translating the modification to the finite volume fluxes back into a standard force term as used in the LES equations. An attempt to do so generates interesting conceptual observations which serve to further highlight the originality of the newly proposed methodology. As discussed in Chapter 1, the distortion of the numerical geometry can be viewed as a consequence of the finite volume scale of the numerical scheme, and the fact that a single velocity value averaged over a finite volume is not in fact a faithful representation of the true, underlying velocity distribution across that volume. Moreover, the use of a metric tensor as described fundamentally relies upon the existence of a velocity distribution across finite regions of space as argued in Chapter 3. Because no filter is ever formally applied, attempting to return to a point-wise solution from the integral form simply implies a return to the Navier-Stokes equation itself. Since no filtering operator has formally been applied, there is formally no force term generated. In fact, on the contrary, the mechanism by which the proposed geometric model functions is through the elimination of any sub-grid scale forces as demonstrated by Section 3.1.1. Thus, because the geometric model is decidedly founded upon elimination of the sub-grid scale forces, an attempt to translate its effect back into an equivalent sub-grid scale force term to be added to the point-wise Navier-Stokes momentum equations is not coherent with the new philosophy for turbulence modelling put forward.

In other words, the generation of a model in the present context arises from treating the velocity as distribution valued or uncertain, which is not a feature compatible with a point-wise solution. The generation of an artificial, sub-grid scale force term strictly requires the application of a filter operation constructed to average over uncertain degrees of freedom; this procedure is avoided in the current methodology. The

filter-free operation and zero sub-grid scale force which are characteristic of the new model are a key aspect of its contribution, and the avoidance of filtering or averaging over the unresolved degrees of freedom creates mathematical capacity for new structure not available in the classical methodology, as highlighted in Section 3.1.2. This observation highlights a fundamental tension in compatibility between the finite-scale description of turbulence in LES versus the point-wise description typically employed by the classical LES equations. It is argued that an integral description with finite scale and physically consistent measurement uncertainty is more realistic for numerical simulation than a point-wise description, since the point-wise description relies upon the formal application of a filter operation (implemented either implicitly or explicitly) in order to provide an approximation that is usable in the discrete numerical setting.

Following the calculation of the divergence of the fluxes, the boundary data immersion method (BDIM) is utilised to integrate the equations forward in time, ensuring the regularity of the velocity field in the proximity of the wall interface. This approach is necessary to avoid the uncontrolled numerical error and ill-defined velocity field caused by a sharp wall boundary condition under wall-modelled resolution. This is significant both due to the use of the iLES method for energy conservation - which relies on controlling the regularity of the velocity field - and due to the need to calculate the metric tensor and other quantities with minimum numerical noise at all positions. The goal is therefore to ensure that modelling may be performed consistently throughout the domain without numerical sensitivity and strong dependency on the numerics becoming a problem near the wall.

The BDIM makes use of the meta-equation concept (Weymouth and Yue, 2011) illustrated by Figure 4.2 where two sets of equations (the fluid equations and the body equations) F and B on their respective domains Ω_b and Ω_f, together with a boundary condition S on the boundary σ_s, are smoothed and assembled over the boundary so that the modified problem is governed by just one meta-equation M_ϵ on the unified domain $\Omega = \Omega_f + \Omega_b$. Because the goal of the BDIM is to combine the equations, which change normal to the boundary, the method only utilises smoothing normal to the boundary and only in the interfacial region in order to minimise the dissipative effects on the solution Maertens and Weymouth (2015). In the current work, the wall geometry is always stationary and so the body equation is trivial. Since only the fluid equation is modified by the addition of the metric tensor, no modification is made to the BDIM method in the present solver. Unless otherwise stated, all simulations are all carried out using the wall-normal smoothing length scale $\epsilon = 2\Delta x$, with this choice being made because it minimises the L_2 error in the velocity field (Maertens and Weymouth, 2015).

The time integration is carried out as in Maertens and Weymouth (2015) using an explicit Euler integration scheme with Heun's corrector, but substituting the

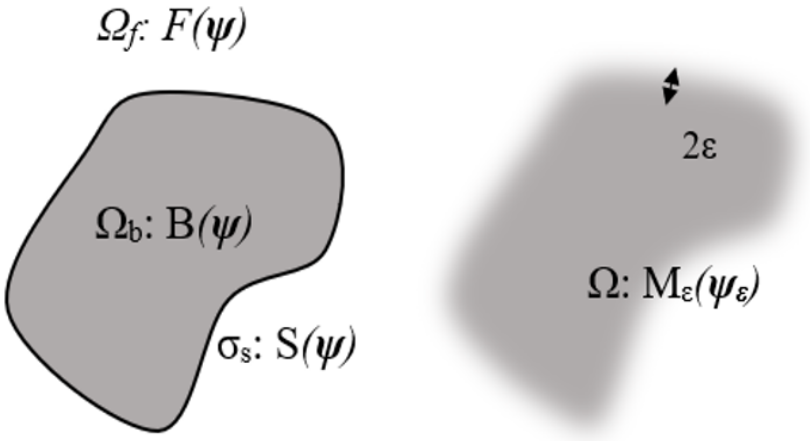

(A) Multi-domain problem 'P_0' (B) Single-domain, modified problem 'P_ϵ'

FIGURE 4.2: A sketch illustrating the meta-equation concept utilised by the boundary data immersion method (BDIM).

geometrically modified divergence of the momentum flux to form the momentum operator

$$r^i_{\Delta t}(u^i_0) = \Delta t \nabla_j \Phi^{ij} = \Delta t \left[\nabla_j \left(\langle \tau^{ij}_\nu \rangle - \langle u^i \rangle \langle u^j \rangle \right) \right]. \tag{4.5}$$

The BDIM is used to smooth the interface between the fluid and solid domains. In the setting of coarse resolution, this treatment maintains smoothness necessary for discrete operators to provide a robust approximation near to the wall. To achieve this, a kernel function with finite support is applied local to the wall as described by Maertens and Weymouth (2015). In the following, μ_0 is the zeroth moment of the BDIM kernel function over the fluid domain, defined by Maertens and Weymouth (2015) as

$$\mu_0(d) = \begin{cases} \frac{1}{2}\left[1 + \frac{d}{\epsilon} + \frac{1}{\pi}\sin\left(\frac{d}{\epsilon\pi}\right)\right] & \text{for} \quad |d| < \epsilon \\ 0 & \text{for} \quad d \leq -\epsilon \\ 1 & \text{for} \quad d \geq \epsilon \end{cases} \tag{4.6}$$

where d is the signed distance of a point from the wall boundary (with $d > 0$ inside the fluid and $d < 0$ inside the solid body). The second order BDIM treatment is used, which also employs the first moment of the BDIM kernel function over the fluid domain, defined as (Maertens and Weymouth, 2015)

$$\mu_1(d) = \begin{cases} \epsilon\left[\frac{1}{4} - \left(\frac{d}{2\epsilon}\right)^2 - \frac{1}{2\pi}\left(\frac{d}{\epsilon}\sin\left(\frac{d}{\epsilon}\pi\right) + \frac{1}{\pi}\left(1 + \cos\left(\frac{d}{\epsilon}\pi\right)\right)\right)\right] & \text{for} \quad |d| < \epsilon \\ 0 & \text{for} \quad |d| \geq \epsilon \end{cases} \tag{4.7}$$

with $\epsilon = 2\Delta x$ in the numerical implementation. The following set of equations are solved in order to calculate $u(t_0 + \Delta t)$ from $u_0 = u(t_0)$ and $p(t_0 + \Delta t)$ from $p_0 = p(t_0)$.

Euler integration with pressure correction

$$u^i_* = \mu_0(u^i_0 + r^i_{\Delta t}(u^i_0)) + \mu_1 \frac{\partial}{\partial n}\left(u^i_0 + r^i_{\Delta t}(u^i_0)\right) \tag{4.8}$$

$$\Delta t \nabla_i \left(\mu_0 \nabla^i p_0\right) = \nabla_i u^i_* \tag{4.9}$$

$$u^i_1 = u^i_* - \Delta t \mu_0 \nabla^i p_0 \tag{4.10}$$

Heun's corrector

$$u^i_{1*} = \mu_0(u^i_0 + r^i_{\Delta t}(u^i_1)) + \mu_1 \frac{\partial}{\partial n}\left(u^i_0 + r^i_{\Delta t}(u^i_1)\right) \tag{4.11}$$

$$\Delta t \nabla_i \left(\mu_0 \nabla^i p\right) = \nabla_i u^i_{1*} \tag{4.12}$$

$$u^i_2 = u^i_{1*} - \Delta t \mu_0 \nabla^i p \tag{4.13}$$

$$u^i = (u^i_1 + u^i_2)/2 \tag{4.14}$$

Again, note that this procedure is identical to that described by Maertens and Weymouth (2015), except for the modification to the operator $r_{\Delta t}$ as described above. The pressure Poisson equation is solved as usual, ensuring that the solution velocity is always divergence free at each time step. Because the pressure is a scalar field, it does not have components which transform under a change of basis, unlike the components of a vector field, and so its values are not directly altered by the geometry. However, it is understood that the pressure field is indirectly modified by the geometric sub-grid model's effect on the momentum fluxes. Therefore, while the time integration procedure remains the same as the base numerical code, it must be noted that the new model indirectly leads to modifications in the pressure field, as it now works to maintain the divergence-free constraint on the solution velocity field under the effects of the modified momentum fluxes. This is particularly relevant under the pressure model described by Equation 3.7 under which the trace of the metric tensor may deviate significantly from that of the Euclidean metric.

Chapter 5

Results

Turbulent boundary layers are simulated under a variety of conditions using coarse resolution which does not resolve the viscous wall momentum flux - referred to as "wall-modelled" resolution. A wide range of conditions are investigated, beginning with flat plate boundary layers. First of all, a zero pressure gradient (ZPG) condition is tested as a benchmark. This case isolates the expected effect of the shear model, which is principally on the mean momentum flux and therefore on the mean velocity field. In the ZPG case, the logarithmic law of the wall is valid and so the physics of the flow are mostly described by an equilibrium cascade of momentum flux towards the wall over the wall-normal length scales. Therefore, the shear model is applied alone for this case and the mean and fluctuating velocity statistics are investigated.

Progressing from the ZPG case, adverse pressure gradient (APG) conditions are investigated, with a pressure distribution being applied along the flat plate, imposed via a prescribed variation of the free-stream velocity. This provides a canonical case under which to investigate the effects of pressure gradient. The APG case is first simulated using the shear model alone, allowing assessment of the remaining errors. Subsequently, the pressure model is applied in addition and the results produced by the combined model are evaluated.

The model is lastly tested for an aerofoil case with the NACA4412 at 5 degrees angle of attack offering a very challenging test case which represents a realistic, practical problem. This case features curved wall geometry, a more complex pressure distribution and stronger local pressure gradient effects in absolute terms, including incipient separation near the trailing edge.

Overall, this range of test cases has been chosen to provide a representative sample of canonical scientific cases typically used to study boundary layers, as well as realistic practical applications.

5.1 Validation cases setup

The chosen validation cases are outlined including reference to the relevant datasets used for validation of the modelled simulations which test the geometric iLES methodology. As far as possible, the computational setup is constructed to match like-for-like with the reference simulations.

5.1.1 Zero pressure gradient, flat plate boundary layer

A zero pressure gradient (ZPG), flat plate boundary layer is simulated in a spanwise-periodic domain. The computational setup is chosen to match that investigated using DNS simulations and experiment by Schlatter et al. (2009). This case is also used as a baseline for comparison against adverse pressure gradient data by Bobke et al. (2017). To match the original presentation, all length scales are expressed in term of the displacement thickness δ_0^* of the laminar inlet velocity profile.

The lower edge of the domain is the wall boundary with no-slip boundary condition enforced by BDIM. The outlet is a convective outlet and, on the upper edge of the domain, a Neumann boundary condition is applied to all velocity components. The normal component enforces a zero pressure gradient distribution along the flat plate by conservation of mass with the Neumann condition

$$\frac{\partial v}{\partial y} = 0. \tag{5.1}$$

The resolutions used are far coarser than the original, wall-resolved simulations. As a result, the boundary layer tripping used in the reference, wall-resolved simulation is not resolvable. Therefore, a recycling-rescaling condition is used to generate turbulence at the tripping strip, which spans stream-wise positions $10 \leq x \leq 14$. In the present setup, a sample is taken at the downstream plane with $x = 250$. The developed boundary layer found at this plane is then scaled in the wall-normal direction and injected at the tripping location. The wall-normal scale factor is chosen to control for the correct momentum thickness at the tripping location compared to the reference data.

A range of resolutions are investigated to examine different resolution regimes. The resolution cases are described by Table 5.1 where the suffix (n) of the case ID ZPG-n identifies the resolution. The identifier n represents the relative size of the grid length scale compared to the reference length scale δ_0^* such that $n = \delta_0^*/\Delta x$.

Case ID	N_x	N_y	N_z	L_x	L_y	L_z	$\delta_0^*/\Delta x$
ZPG-1.00	768	48	96	768	48	96	1.00
ZPG-1.25	960	60	128	768	48	102	1.25
ZPG-1.5	1152	72	160	768	48	106	1.5
ZPG-1.75	1344	84	192	768	48	110	1.75

TABLE 5.1: Table of resolution cases used for each ZPG boundary layer case, showing number of computational grid points N and spatial extents L used across the stream-wise (x), wall-normal (y) and span-wise (z) directions respective.

5.1.2 Adverse pressure gradient, flat plate boundary layers

A flat plat case with adverse pressure gradient (APG) distribution is defined in a similar way to the ZPG flat plate case, matching the computational setup of Bobke et al. (2016) and Bobke et al. (2017). In order to apply an APG, the upper wall boundary condition is modified so that it imposes a prescribed external velocity profile $U_\infty(x)$ by setting

$$\frac{\partial v}{\partial y} = -\frac{\partial U_\infty}{\partial x}. \tag{5.2}$$

The external velocity profile $U_\infty(x)$ is defined with a ZPG inlet region, before application of APG downstream from the inlet. Therefore, the inlet region is identical to the ZPG case. The free-stream velocity distribution is given by $U_\infty = 1$ for $x < 350$, and

$$U_\infty(x) = \left(1 + \frac{(x - 350)}{60}\right)^m \quad \forall \quad x \geq 350. \tag{5.3}$$

Different APG velocity distributions are plotted in Figure 5.1. Note that the laminar boundary layer equations under a power-law U_∞ distribution provide the Falkner-Skan similarity solutions (Falkner and Skan, 1931). With $m \lesssim -0.2$, separation occurs in the laminar case over a flat wall, providing a reference point which shows that the pressure gradients investigated here are very significant in strength.

The same recycling-rescaling condition is applied as for the ZPG simulation as the sample plane $(x = 250)$ is located well within the ZPG inlet region, and so is unaffected by changes to the external velocity distribution. The region $0 \leq x \leq 350$ is therefore treated as an inflow region for the APG "test section" over $x \geq 350$.

For the computational domain, spatial extents are expanded relative to the ZPG case in the span-wise and wall-normal directions to accommodate for the thicker boundary layer produced under APG conditions. The resolution cases are described by Table 5.2 where again the suffix (n) of the case ID APG-m-n refers to the resolution relative to the reference length scale δ_0^* such that $\delta_0^* = n\Delta x$ and the m digit refers to the exponent governing the strength of the applied pressure gradient. For each case, the span-wise extent is at least four times the boundary layer thickness over the domain.

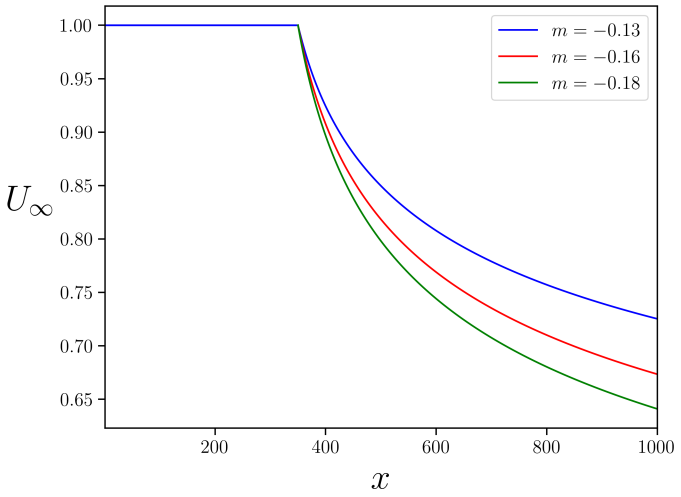

FIGURE 5.1: Free-stream velocity distributions defined according to the different exponents m.

Case ID	N_x	N_y	N_z	L_x	L_y	L_z
APG-13-1.00	768	96	96	768	96	96
APG-13-1.25	960	128	128	768	102	102
APG-13-1.5	1152	160	160	768	107	107

TABLE 5.2: Table of resolution cases used for each APG boundary layer case, showing number of computational grid points N and spatial extents L used across the stream-wise (x), wall-normal (y) and span-wise (z) directions respective.

The computational domain plotted is sketched in Figure 5.2. Key stream-wise locations are marked and the stream-wise is visualised for the case APG-13-1.25.

FIGURE 5.2: Side view of the computational domain for the APG flat plate with: trip strip $(10 \leq x \leq 14)$; recycling plane $(x = 250)$; pressure gradient application location $(x = 350)$; and sampling plane for statistics $(x = 614)$ marked.

5.1.3 Wing boundary layers

Lastly, wing boundary layers are investigated for a spanwise-periodic NACA4412 geometry at 5 degrees angle of attack. The NACA4412 geometry is investigated at a Reynolds number $Re_c = cU_\infty/\nu = 4 \times 10^5$ where c is the chord length and U_∞ is the free-stream velocity. The computational setup is constructed to match that described by Tanarro et al. (2020) as closely as is feasible.

Artificial tripping is achieved on both the suction and pressure sides of the aerofoil at 10% of the chord. Since the tripping of the original, wall-resolved simulations is again

unresolvable, a physical trip is used with geometry which is as small as possible without becoming unresolvable given the simulation resolution. The minimum resolvable 2-dimensional feature on the Cartesian grid has length scale $L_t = \sqrt{2}(\Delta x/c)$ in terms of the Cartesian grid scale Δx and the chord c. The height h of the tripping geometry relative to the aerofoil surface is then given by a step function

$$h = \begin{cases} +L_t & \text{if} \quad -L_t < (x/c - 0.1) < 0 \\ -L_t & \text{if} \quad 0 \leq (x/c - 0.1) < +L_t \end{cases}. \tag{5.4}$$

In order to add 3-dimensional irregularity, the value of L_t is perturbed at each grid location by adding a random uniform distribution over the range $\pm\Delta x/2$. The random roughness perturbation is then resampled every $4L_t$ units of time.

As well as the tripping itself, another important consideration for the transition region with a coarse grid is the resolution of the initial laminar boundary layer prior to the tripping location at $x/c = 0.1$. It is ensured that the laminar boundary layer thickness is reasonably well captured at the tripping location. This is required so that the momentum inflow to the turbulent region can be expected to remain in agreement with the reference simulations. To enforce this condition, it is required that there are at least 5 grid points across the laminar boundary layer thickness δ_{99} at $x/c = 0.1$. This condition provides minimal resolution of the laminar boundary layer so as not to significantly inflate the eventual turbulent boundary layer thickness further downstream.

The laminar boundary layer thickness scales approximately like

$$\delta_{99} \sim \sqrt{\frac{\nu x}{U_\infty}} \tag{5.5}$$

and so the minimal resolution that may be used scales with $Re^{0.5}$. For example, in the case with Reynolds number of 4×10^5 a resolution is chosen with 512 grid points along the chord. Where $\nu = UL/Re = 1 \times 512/400,000 = 0.00128$, the boundary layer thickness at the tripping location is approximately $\delta_{99} = \sqrt{0.00128 \times 0.1} \approx 0.01c$ or approximately 1% of the chord. Therefore, the laminar boundary layer is minimally resolved by the grid cells which have a length scale of approximately 0.2% of the chord. The requirement outlined here is in accordance with estimates for wall-modelled LES which recognise that simulations have a cost that scales like $Re^{0.5}$ (Reynolds, 1990).

The NACA4412 simulation case is described by Table 5.3 where the cases are labelled by Reynolds number. The span-wise extent of the domain is 10% of the chord, matching the original wall-resolved study.

Case ID	N_c	N_x	N_y	N_z	L_x/c	L_y/c	L_z/c
NACA4412-400k	512	768	768	48	1.5	1.5	0.1

TABLE 5.3: Table showing number of computational grid points N and spatial extents L used where N_c is the number of grid points along the chord of the aerofoil geometry.

5.2 ZPG flat plate boundary layer results

The ZPG case is intended to display the basic function of a model in removing momentum from the flow at the wall where unresolved, sub-grid scale viscous shear stress is significant at the boundary. The desired outcome is therefore that the mean velocity profiles collapse to the reference data even when using coarse, wall-modelled resolution. In this case, the off-diagonal components of the metric tensor which represent coupling between the wall-normal and stream-wise directions are dominant in the wall-fixed frame of reference. The differences from the Euclidean metric tensor replace the classical sub-grid shear stresses which transfer stream-wise momentum in the wall-normal direction throughout the boundary layer.

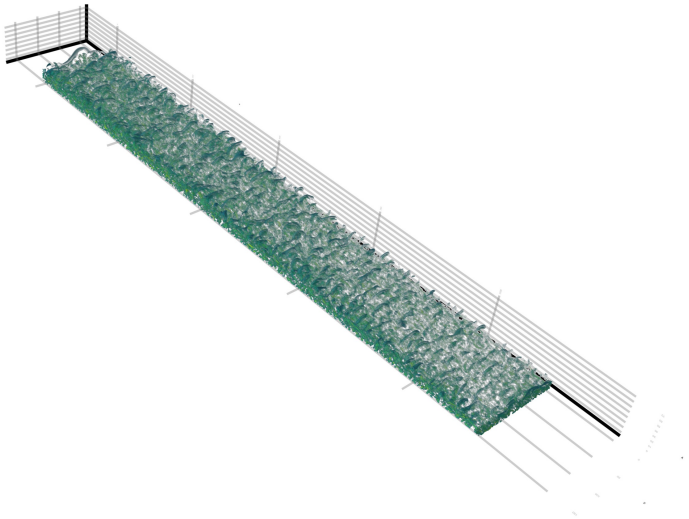

FIGURE 5.3: Iso-surfaces of the λ_2-criterion, visualising the 3-dimensional vortex structure along the flat plate under zero pressure gradient conditions.

Figure 5.3 presents a visualisation of the flow for the ZPG flat plate boundary layer case, showing turbulent transition tripping and the development of coherent, multi-scale structures as the boundary layer thickens down-stream. For all simulations, unless stated otherwise, the simulation is allowed to settle for 10 flow-through times $T_{\text{f-t}} = L_x/U_\infty$ to an equilibrium state from a uniform initial condition. Next, the mean velocity field is averaged over 2 flow-through times before the fluctuating statistics are converged over 8 further flow-through times. Four different resolutions are investigated, with wall-normal grid spacing spanning from

$12 \leq \Delta y^+ \leq 21$ in wall units for the stream-wise location $x = 614$ at which the velocity profile is sampled. In terms of the outer scale, the number of grid points across the 99% boundary layer thickness at this location spans the range $16 \leq \delta_{99}/\Delta y \leq 28$. This moderate Reynolds number case has been selected because it allows the results to span this full range between the two extremes of possible resolution choice within the computational constraints of the study. At one extreme, around 20 grid points across the boundary layer $(\delta_{99}/\Delta y \approx 20)$ is often considered a minimum requirement in order to sufficiently capture boundary layer structure (Bose and Park, 2018; Bose and Moin, 2014). This provides a minimum resolution bound to approach and test based on the outer length scale. The opposite end of the resolution spectrum sits where viscous dynamics begin to become partially resolved, yet the flow is still not fully resolved. This begins to become significant for $\Delta y^+ < 15$; at the wall-normal location $y^+ \approx 10$, approximately half of the shear is carried by viscous stresses and half by turbulent stresses. Hence, the resolution cases with finer grid resolution serve to demonstrate that the model continues to function effectively even when the first grid point is well below the self-similar, logarithmic law regime and resolved viscous influence is relatively strong.

First of all, the simulation is run without the geometric model applied, so that baseline errors may be assessed. These cases rely on iLES dissipation only. Figure 5.4 shows the mean velocity profiles produced by these simulations over the range of resolutions investigated and at the stream-wise location $x = 614$. At this location, the friction Reynolds number $Re_\tau = 340$. Note that the present simulation data is scaled throughout using the friction velocity u_τ taken from the reference data for direct comparison. Thus, the coarsely resolved profiles match the reference data away from the wall due to the identical, prescribed external velocity. Any discrepancy in the coarsely-resolved results is shown in absolute terms.

As might be expected, some marginal improvement in the result can be seen with improving resolution, but since the viscous scales are never well resolved, convergence is very modest with iLES dissipation only and errors in the mean velocity profile are large. It is, however, noteworthy that the velocity profile follows an almost perfect logarithmic profile with the standard von-Karman slope coefficient of approximately 2.5. This implies a constant momentum flux across the boundary layer which is produced by resolved turbulent transfer, since it is known that the turbulent transfer of momentum with negligible viscous effect produces this kind of logarithmic behaviour in the mean velocity profile. According to Bae et al. (2019), the slope of the logarithmic law produced in the simulation is mainly a result of the choice of sub-grid scale model. Therefore, the correct slope is a strong indication here that correct turbulence behaviour and an appropriate dissipation model are in place. Bae et al. (2019) also found that the vertical shift in the profile is mainly controlled by the wall model in traditional wall-modelled LES simulations. Since the error between the

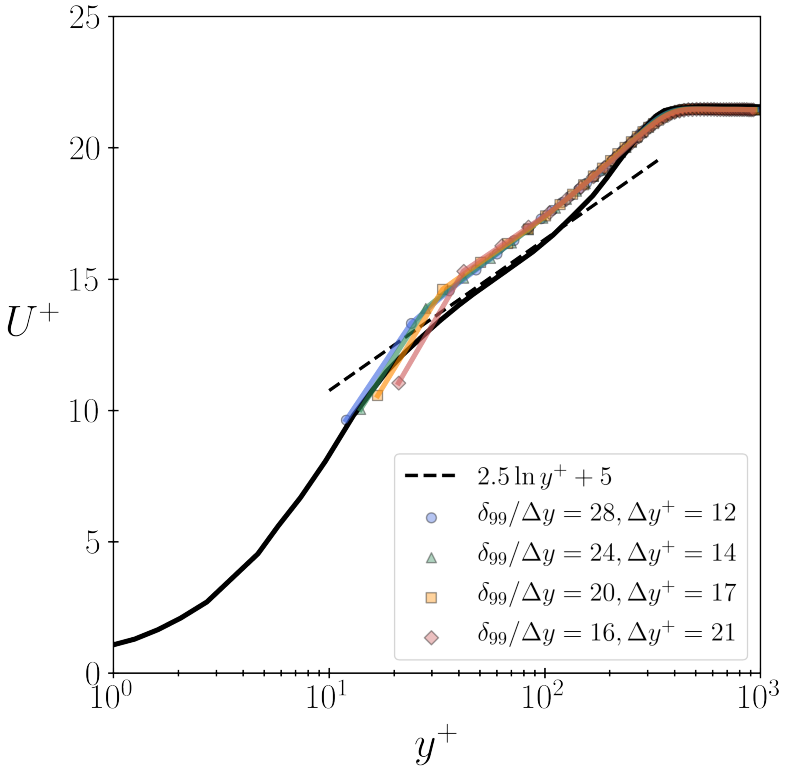

FIGURE 5.4: Time-averaged, wall-normal profiles of stream-wise velocity plotted in wall units for each resolution case (ZPG-1.00 -red; ZPG-1.25 - orange; ZPG-1.50 - green; ZPG-1.75 - blue) with iLES modelling only and at friction Reynolds number $Re_\tau = 340$. The reference data from Schlatter et al. (2009) is plotted in a solid black line.

coarsely resolved profiles and the reference data in Figure 5.4 can mainly be described by a vertical shift in the profile near to the wall, this is the clear error that must be addressed by addition of the geometric shear model.

Figure 5.5 shows the Reynolds stresses for the corresponding iLES-only cases, revealing an under-prediction of the stream-wise fluctuations, while the other components are, surprisingly, in relatively close agreement with the reference data. This is likely due to the prediction of a robust logarithmic law which is correct in its slope, indicating the presence of realistic fluctuations and turbulent momentum transfer. The under-prediction of the stream-wise component may relate to the incorrect shift of the mean velocity profile by demonstrating an incorrect formation of stream-wise coherent structures in the boundary layer without appropriate modelling of the momentum flux at the wall.

To address the errors principally found in the mean velocity profile, the shear model defined in Equation 3.6 is applied to each resolution case. Figure 5.6 shows the mean velocity profiles obtained, revealing improved agreement with the reference data. The wall-normal velocity profiles are now collapsed on top of the reference data, demonstrating accurate representation of the resolved momentum distribution in the boundary layer as intended, and implying correct momentum flux to the wall.

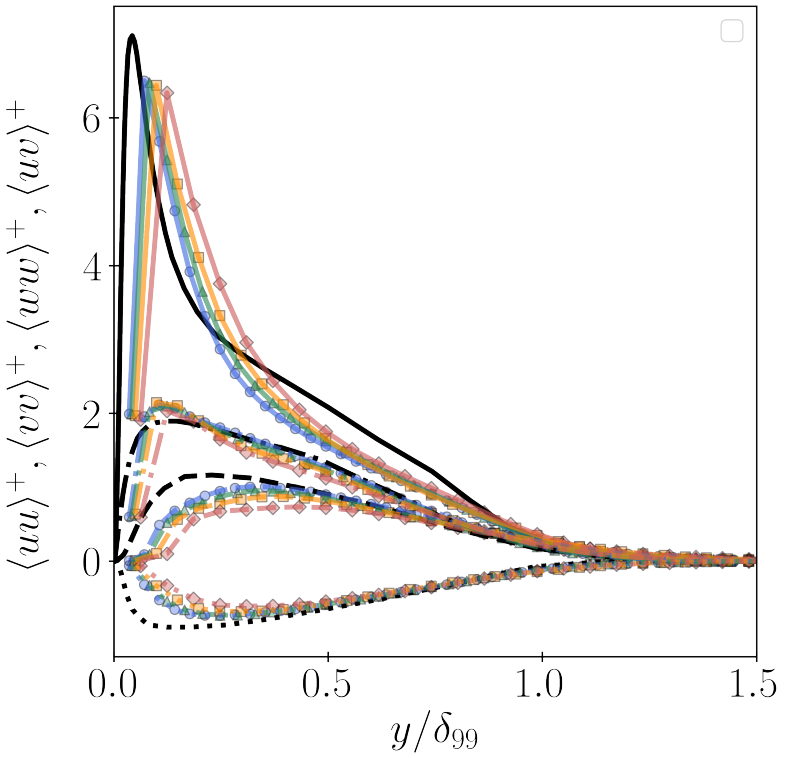

FIGURE 5.5: Wall-normal Reynolds stress profiles for each resolution case with iLES modelling only (ZPG-1.00 -red; ZPG-1.25 - orange; ZPG-1.50 - green; ZPG-1.75 - blue). The Reynolds stress components are identified by line-styles: $\langle uu\rangle^+(-)$; $\langle vv\rangle^+(--)$; $\langle ww\rangle^+(-.)$; and $\langle uv\rangle^+(..)$. The reference data from Schlatter et al. (2009) is plotted in black.

Furthermore, the simulation is insensitive to the resolution chosen for $\delta_{99}/\Delta y > 20$. In the extreme range of coarse resolution relative to the outer length scale with $\delta_{99}/\Delta y = 16$, some discrepancy may be observed in the velocity profile, especially at the first few grid points nearest the wall. The results therefore suggest that the threshold of $\delta_{99}/\Delta y \geq 20$ is appropriate as a large-scale bound on resolution. However, for the small-scale end of the resolution spectrum with $\Delta y^+ = 12$ the results remain robust where partial resolution of viscous forces becomes significant. Note that where the data point nearest to the wall falls below the reference data this is due to the fact that each data point represents a volumetric average. The point nearest the wall therefore takes on half of its value from locations nearer to the wall such the mean value falls below the un-averaged profile of the reference data at this location.

In order to confirm that perturbations around the Euclidean metric tensor are indeed small, the components of the metric tensor are also investigated. The metric tensor is examined at the sample location $x = 614$ and where the shear effect is strongest - at the first grid point away from the wall ($y^+ = 17$ for resolution case ZPG-1.25). In the wall-fixed frame of reference, the metric tensor has time-averaged components

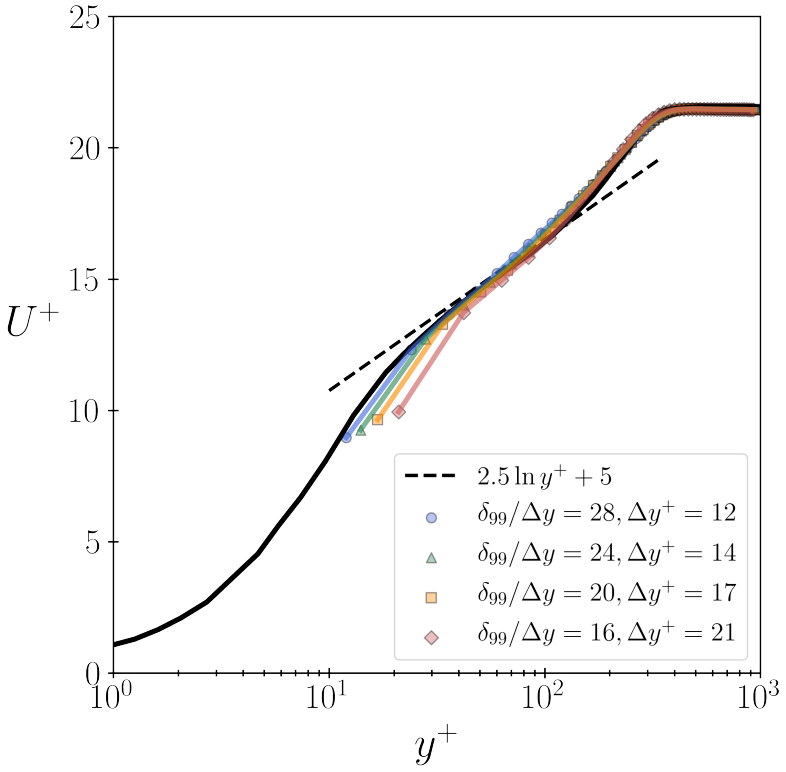

FIGURE 5.6: Time-averaged, wall-normal profiles of stream-wise velocity plotted in wall units for each resolution case (ZPG-1.00 -red; ZPG-1.25 - orange; ZPG-1.50 - green; ZPG-1.75 - blue) with geometric shear model applied and at friction Reynolds number $Re_\tau = 340$. The reference data from Schlatter et al. (2009) is plotted in a solid black line.

$$g_{ij} = \begin{pmatrix} 1.00 & -1.15 \times 10^{-3} & -9.83 \times 10^{-6} \\ -1.15 \times 10^{-3} & 1.00 & 3.03 \times 10^{-5} \\ -9.83 \times 10^{-6} & 3.03 \times 10^{-5} & 1.00 \end{pmatrix}. \tag{5.6}$$

The components involving the wall-normal and stream-wise directions ($g_{xy} = g_{yx}$) are the dominant deviations from the Euclidean metric as expected. These components are also small in magnitude, indicating that the second order treatment proposed in Equation 3.6 remains justified.

For the Reynolds stress under the shear model, Figure 5.7 also reveals an increase in accuracy for the important stream-wise component. The stream-wise structure of fluctuations is now correctly predicted, with discrepancies found only near to the sharp inner-peak which is smoothed out by the coarse resolution. The Reynolds shear stress component is also well-predicted, but span-wise and wall-normal fluctuations are damped to some extent by the model. While the stream-wise structures found in the boundary layer tend to be large-scale, coherent structures, the damped (span-wise and wall-normal) Reynolds stress components tend to be higher-frequency in character. Hence, as the grid scale and therefore the time-step are coarsened, filtering

out certain temporal frequencies such that a larger portion of the energetic content is not observable in the LES.

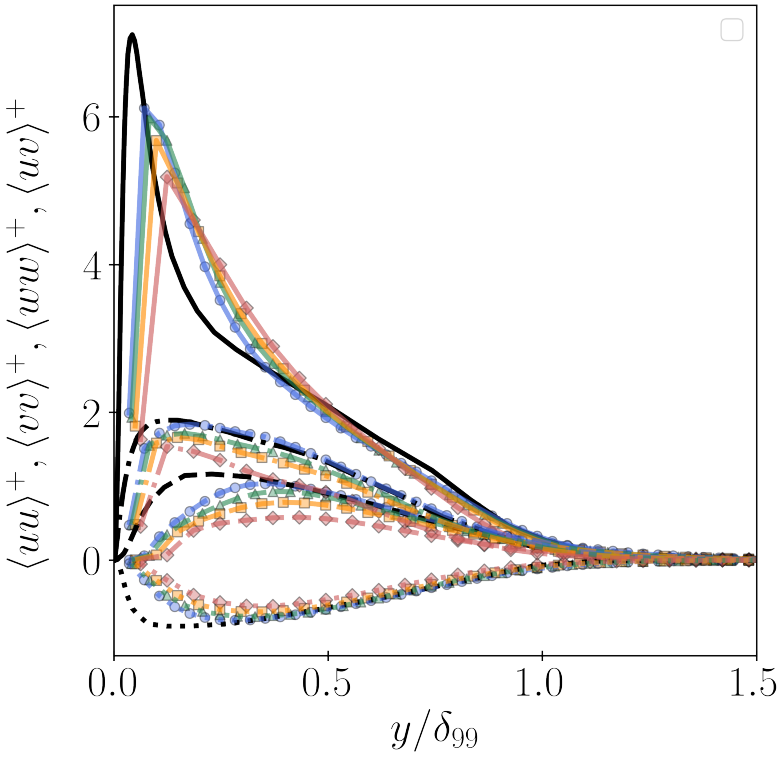

FIGURE 5.7: Wall-normal Reynolds stress profiles for each resolution case with geometric shear model applied (ZPG-1.00 -red; ZPG-1.25 - orange; ZPG-1.50 - green; ZPG-1.75 - blue). The Reynolds stress components are identified by line-styles: $\langle uu\rangle^+(-)$; $\langle vv\rangle^+(--)$; $\langle ww\rangle^+(-.)$; and $\langle uv\rangle^+(..)$. The reference data from Schlatter et al. (2009) is plotted in black.

Figure 5.8 visualises the effects of the shear model on the stream-wise structure of the boundary layer by plotting the stream-wise velocity field on a wall-parallel plane at a height of 30 wall units above the wall (when measured at the location $x = 614$ wall-normal velocity profiles are sampled). The top figure (with shear model) shows a distinctly higher level of large-scale organisation, matching the augmentation of the stream-wise Reynolds stress caused by the shear model. In fact, the appearance of the shear-modelled velocity structure is very similar to a zoomed in version of the un-modelled field, with the model acting like a lens. It was found when experimenting with the model that the sign of the model coefficient controls the "direction" of this zoom effect, while the coefficient determines the strength.

In summary, the shear model demonstrates the appropriate actuation over the mean velocity field, removing momentum from the flow in the vicinity of the wall. Resolution sensitivity has also been ruled out for the model over a complete range between inner- and outer-scaled frontiers of the possible resolution. Fluctuating quantities are also generally well predicted, although span-wise and wall-normal fluctuations are somewhat damped by the model, perhaps as a result of temporal

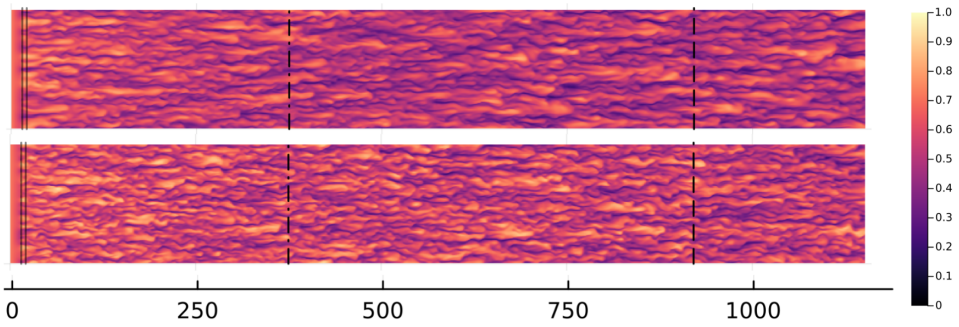

FIGURE 5.8: Stream-wise velocity plotted on a wall-parallel plane at $y^+ = 30$ (measured at $x = 614$) for resolution case ZPG-1.5 with shear model (top) and with iLES model only (bottom). The tripping strip, recycling sample plane and the sample point for the wall normal profiles are marked.

filtering provided by the coarse LES time-step. All results are achieved using a single, constant model coefficient and so exhibit a minimum requirement for empirical data input.

5.3 APG flat plate boundary layer results

Having demonstrated that the shear model produces the intended actuation over the flow under ZPG conditions, the model is now applied to APG boundary layers. The results demonstrate that the transfer of momentum and the associated modelling of the unresolved, viscous shear does not represent the full picture under these flow conditions. Rather, errors are still present which are possible to address under the current perspective by application of separate (pressure) modelling.

First of all, the pressure gradient cases with exponent $m = -0.13$ are investigated over the stated range of resolutions. Figure 5.9 presents a visualisation of the flow for the APG flat plate boundary layer condition, showing the rapid expansion in the boundary layer thickness after the stream-wise location at which APG is applied. Simulations are once again run initially without the application of the geometric model, with modelling provided by iLES dissipation only. The resultant velocity profiles shown in Figure 5.10 show that, in relative terms, the errors in the mean velocity profiles are much larger for the APG case than for the equivalent ZPG case. Regardless, a similar qualitative effect is present in that the profile tends towards a logarithmic profile which is shifted vertically above the canonical logarithmic law. However, the influence of the outer region which departs from logarithmic behaviour is far stronger as is characteristic of APG boundary layers. At the sampled location with $x = 614$, the Clauser pressure gradient parameter $\beta = 1.62$ and the friction Reynolds number $Re_\tau = 317$.

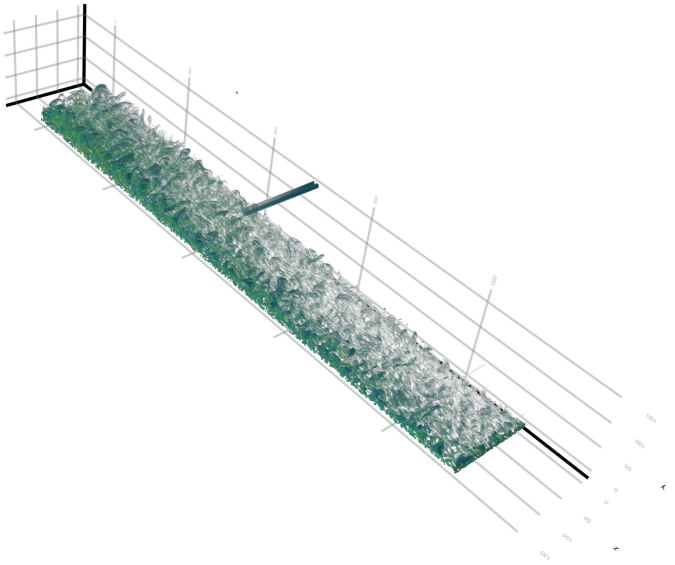

FIGURE 5.9: Iso-surfaces of the λ_2-criterion, visualising the 3-dimensional vortex structure along the flat plate under the adverse pressure gradient conditions.

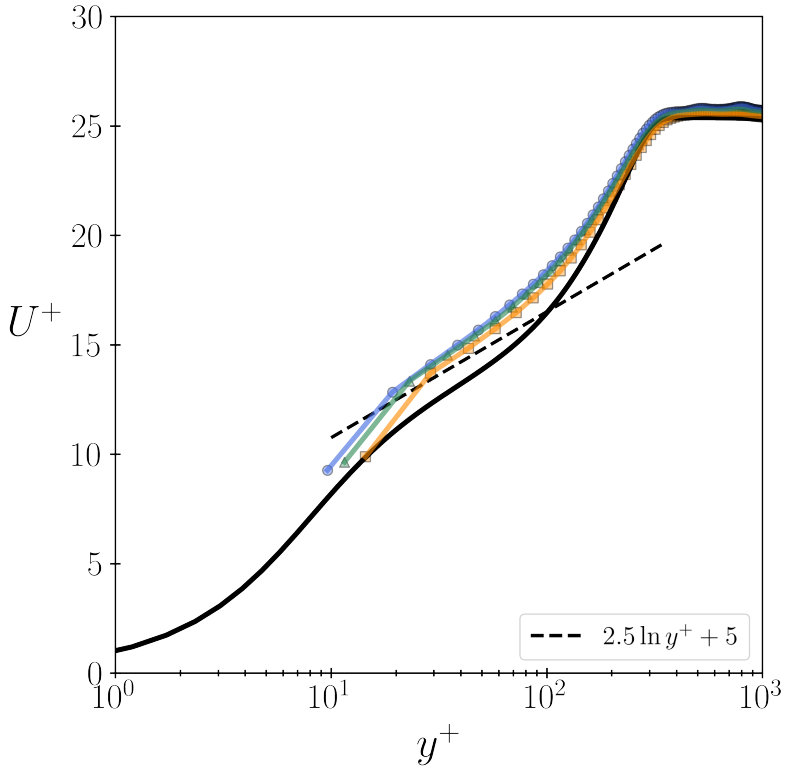

FIGURE 5.10: Time-averaged, wall-normal profiles of stream-wise velocity plotted in wall units for each resolution case with $m = -0.13$ (APG-13-1.0 - orange; APG-13-1.25 - green; APG-13-1.5 - blue) and with iLES modelling only at friction Reynolds number $Re_\tau = 317$. The reference data from Bobke et al. (2016) is plotted in a solid black line.

For the corresponding Reynolds stresses shown in Figure 5.11, errors are again large, with severely under-predicted energy of the fluctuations - especially away from the

wall. In fact, the iLES-only Reynolds stress profiles are more similar in shape to those found in the ZPG reference data than the APG reference data, with no evidence of the distinct outer peak expected under APG. Errors are especially marked for the span-wise and wall-normal fluctuations, indicating a clear lack of the characteristic outer peak turbulent energy which is a key feature of APG flows and a lack of turbulent fluctuations across the boundary layer and in all fluctuation directions.

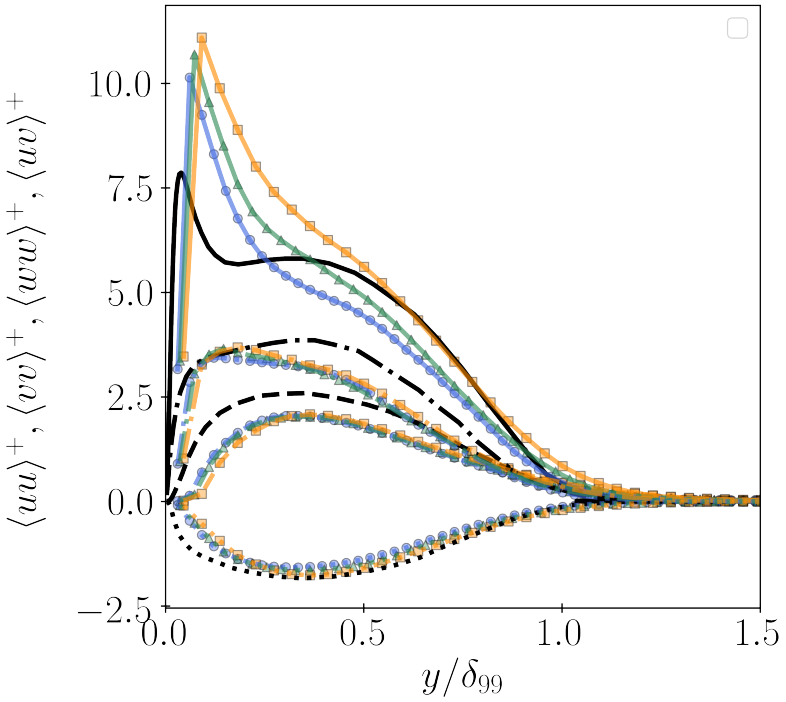

FIGURE 5.11: Wall-normal Reynolds stress profiles for each resolution case with $m = -0.13$ (APG-13-1.0 - orange; APG-13-1.25 - green; APG-13-1.5 - blue) and with iLES modelling only. The Reynolds stress components are identified by line-styles: $\langle uu\rangle^+(-)$; $\langle vv\rangle^+(--)$; $\langle ww\rangle^+(-.)$; and $\langle uv\rangle^+(..)$. The reference data from Bobke et al. (2016) is plotted in black.

To begin accounting for the errors found in the case without geometric modelling, the geometric shear model is first applied as it was for the ZPG case. Any remaining error is then assessed before applying the pressure model. Figure 5.12 shows the mean velocity profiles produced with the geometric shear model applied. Again, the effect of introducing the model is qualitatively similar to that produced in the ZPG case, with the velocity profile nearer to the wall being shifted vertically downward, indicating an augmented removal of stream-wise momentum from the flow by the model.

However, the mean velocity profiles remain vertically shifted across the entire profile compared to the reference data, suggesting that the shear model does not fully represent the APG conditions. For the lowest-resolution case, the error caused by improperly coarse resolution has also been exaggerated by the pressure-gradient effects, with the results of this case deviating more significantly from the other

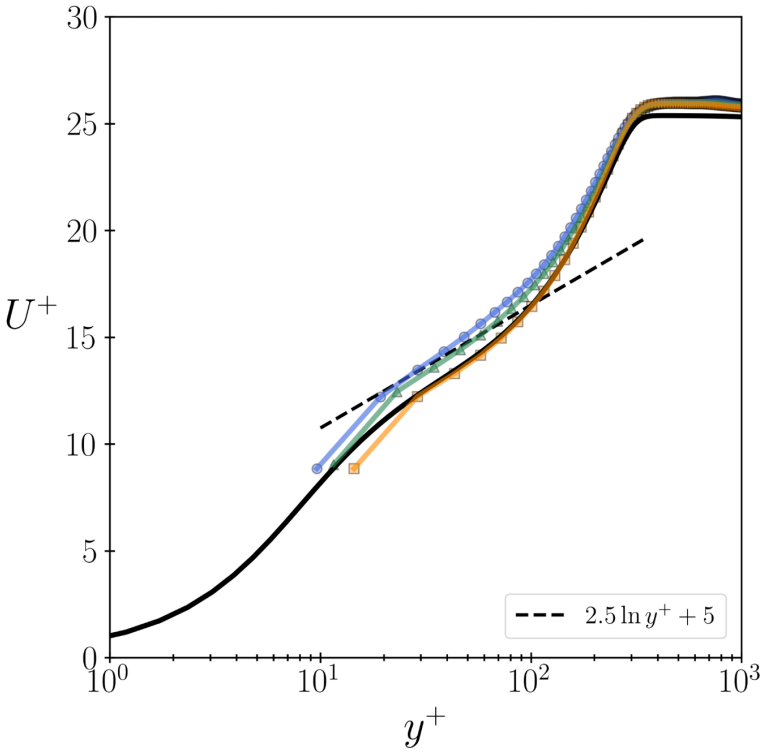

FIGURE 5.12: Time-averaged, wall-normal profiles of stream-wise velocity plotted in wall units for each resolution case with $m = -0.13$ (APG-13-1.0 - orange; APG-13-1.25 - green; APG-13-1.5 - blue) and with geometric shear model applied. The reference data from Bobke et al. (2016) is plotted in a solid black line.

resolution cases. This suggests that the number of grid points across the boundary layer thickness is of increased importance for the APG case, perhaps as a result of the increased intensity of turbulence in the outer layer.

The discrepancies found can be further analysed by examining the Reynolds stresses shown in Figure 5.13. Overall, the fluctuations are relatively well predicted apart from in the stream-wise component. The stream-wise component does not exhibit a distinct outer peak to match the reference data and is significantly exaggerated in magnitude.

As anticipated, while the shear model provides a significant improvement in accuracy in this case, it does not fully capture the effects of the pressure gradient. Heuristically, the Clauser pressure gradient parameter at this location is $\beta = 1.62$, indicating that the relative local importance of the wall shear and the pressure gradient is approximately balanced, with a slight dominance of the pressure gradient effect. This is reflected in the mean velocity profiles shown in Figure 5.12, where the shear model corrects approximately half of the error in the mean velocity profile when compared to the results relying on iLES dissipation only shown in Figure 5.10.

Having applied the shear model alone, the full model defined in Equation 3.7 is applied, including the hypothesised pressure effects. Figure 5.14 shows the result of

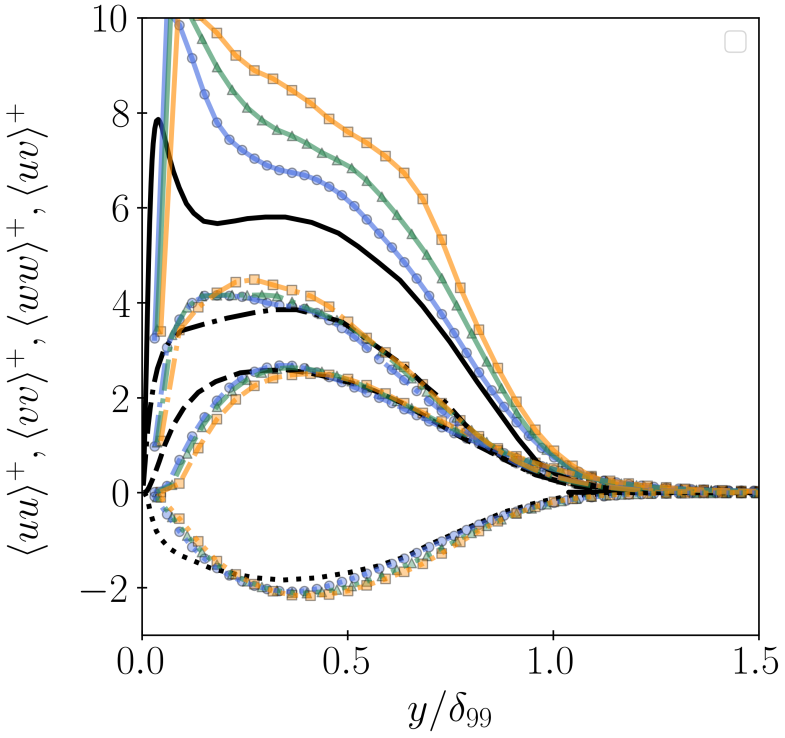

FIGURE 5.13: Wall-normal Reynolds stress profiles for each resolution case with $m = -0.13$ (APG-13-1.0 - orange; APG-13-1.25 - green; APG-13-1.5 - blue) and with geometric shear model applied. The Reynolds stress components are identified by line-styles: $\langle uu\rangle^+(-)$; $\langle vv\rangle^+(--)$; $\langle ww\rangle^+(-.)$; and $\langle uv\rangle^+(..)$. The reference data from Bobke et al. (2016) is plotted in black.

applying the combined model on the mean velocity profiles produced. With the inclusion of the pressure model, the mean velocity profiles have predominantly collapsed onto the reference data. Relative to the shear modelled results, the mean velocity profiles have been shifted downwards across the entire range of wall-normal distances. A minor discrepancy still exists in the under-resolved case as expected, although the error is relatively minor given the extremely coarse resolution chosen for this case.

For the Reynolds stress, application of the pressure model also generates significant change, especially in the stream-wise component as shown in Figure 5.15. The stream-wise profiles now take on the expected shape with a well-defined outer peak and show significantly reduced resolution-dependence. However, the magnitude of the stream-wise component remains over-predicted relative to the reference data. Meanwhile, the other components of the Reynolds stress remain in good agreement with the reference data.

The momentum thickness along the boundary layer is also plotted over the APG section in order to confirm the correct spatial evolution of the momentum in the boundary layer. As expected from the accuracy of the velocity profiles, the momentum thickness also matches well with the reference data.

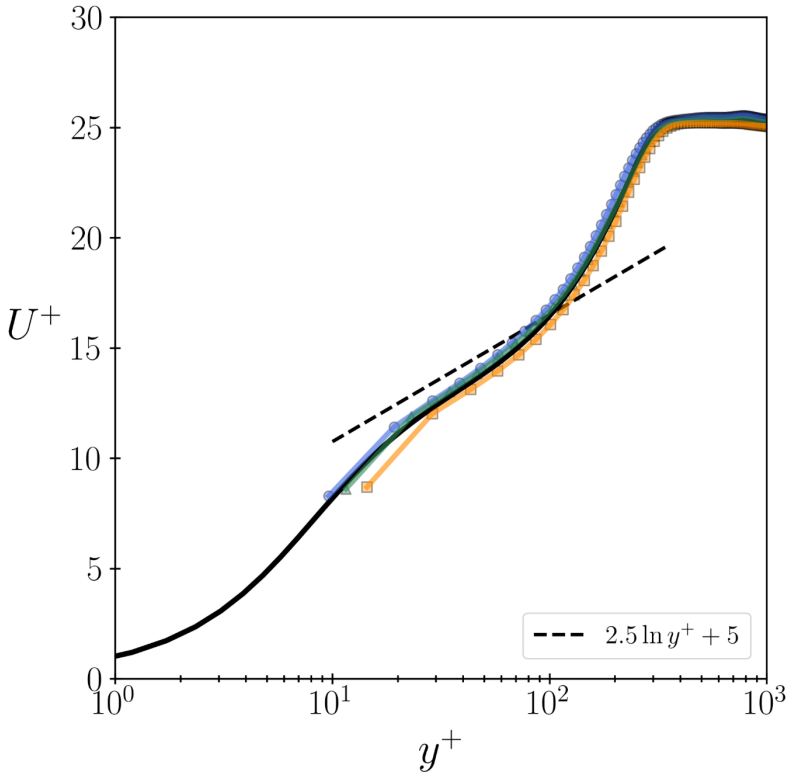

FIGURE 5.14: Time-averaged, wall-normal velocity profiles plotted in wall units for each resolution case with $m = -0.13$ (APG-13-1.0 - orange; APG-13-1.25 - green; APG-13-1.5 - blue) and with both geometric shear and pressure models applied. The reference data from Bobke et al. (2016) is plotted in a solid black line.

Finally, the diagonal components of the metric tensor are investigated. At the sample location, due to the cumulative effect of the pressure gradient, the effect of the pressure model is significant, with the diagonal components of the metric being perturbed by approximately 2%. The change created by the pressure model therefore may still be considered a small perturbation around the Euclidean metric.

Overall, the results provide confidence that the model is able to account for pressure gradient effects, especially since no empirical assumptions are made about the form of the pressure distribution in the model. In order to evaluate the model's viability under a more complex pressure gradient distribution, the NACA4412 case is investigated in the following section. This provides an important case with a more arbitrary and realistic free-stream velocity distribution which contrasts with the analytical power-law distribution studied so far.

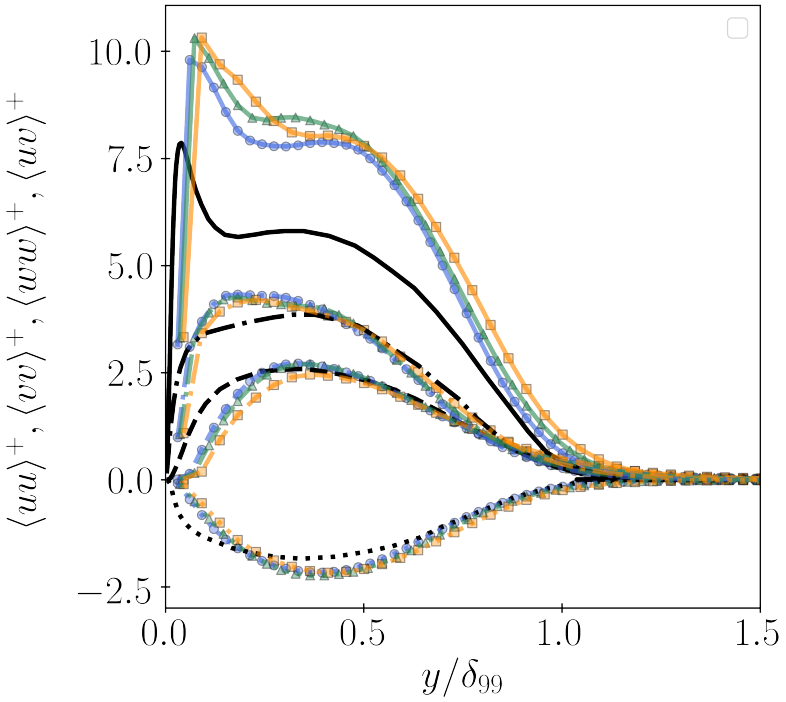

FIGURE 5.15: Wall-normal Reynolds stress profiles for each resolution case with $m = -0.13$ (APG-13-1.0 - orange; APG-13-1.25 - green; APG-13-1.5 - blue) and with both geometric shear and pressure models applied. The Reynolds stress components are identified by line-styles: $\langle uu\rangle^+(-)$; $\langle vv\rangle^+(--)$; $\langle ww\rangle^+(-.)$; and $\langle uv\rangle^+(..)$. The reference data from Bobke et al. (2016) is plotted in black.

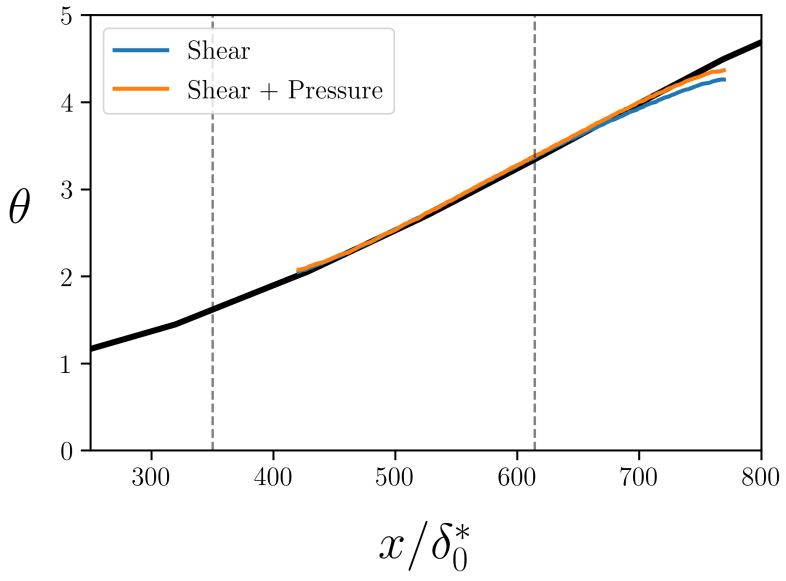

FIGURE 5.16: Boundary layer momentum thickness θ plotted against stream-wise position for the geometric modelled cases with resolution case APG-13-1.25 and with $m = -0.13$.

5.4 NACA4412 aerofoil results

Having validated modelling with pressure gradient a case is called for which represents practical applications with more complex conditions. Figure 5.17 presents a visualisation of the flow in which the foil geometry has been cut away to view the flow on both sides. The visualisation shows turbulent transition tripping at $x/c = 0.1$ and the marked difference in the boundary layer character between suction and pressure sides of the aerofoil, as well as the formation of a turbulent wake. The NACA4412 aerofoil at 5 degrees angle of attack and at high Reynolds number is a case of very high complexity in which accurate wall modelled LES results are considered challenging to produce (Bose and Park, 2018). Wall models aside, Vinuesa et al. (2018) show that appreciable differences can even be found between solutions computed using DNS and solutions using wall-resolved LES. Especially in the Reynolds stress, discrepancies of up to 10% are found using LES even when the wall is fully resolved (Vinuesa et al., 2018). Therefore, a reasonable goal for the present geometric iLES simulation is to predict the mean velocity profile to within an error of 5%. Application to a more complex wall geometry is possible without any adaptation to the model already tested because the model is defined locally, and so does not depend on variations in the wider conditions. Because BDIM is used, the wall geometry is also naturally handled without alteration.

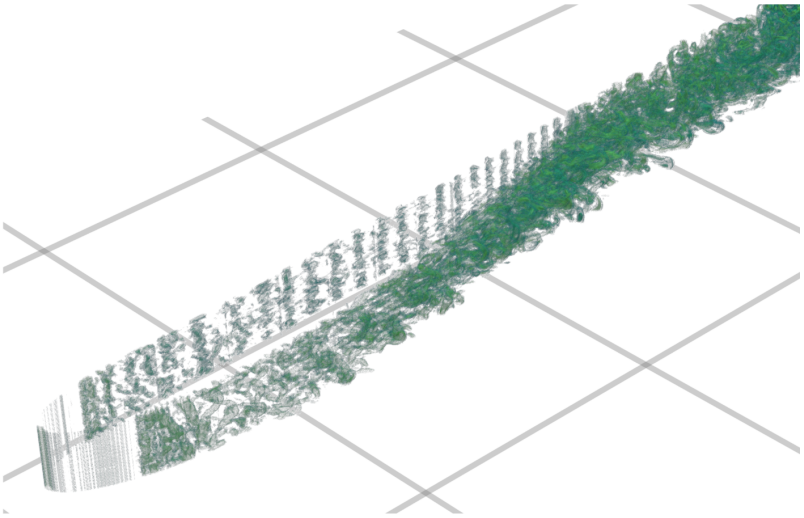

FIGURE 5.17: Iso-surfaces of the 3-dimensional λ_2 vortex structure around both sides of the NACA4412 aerofoil at 5 degrees angle of attack and at a Reynolds number of 400,000. The suction side of the aerofoil is the one in the foreground of this image.

Once again, a simulation is initially run using iLES dissipation only, before the geometric shear model is applied. Figure 5.18 shows the difference between the iLES-only and geometric shear modelled velocity fields over the aerofoil at Reynolds number of 4×10^5. This image shows that the modelled boundary layer is significantly thinner over the mid portion of the aerofoil (reaching the free-stream

velocity at shorter distances from the wall). In addition, the flow near to the wall is relatively slower as expected.

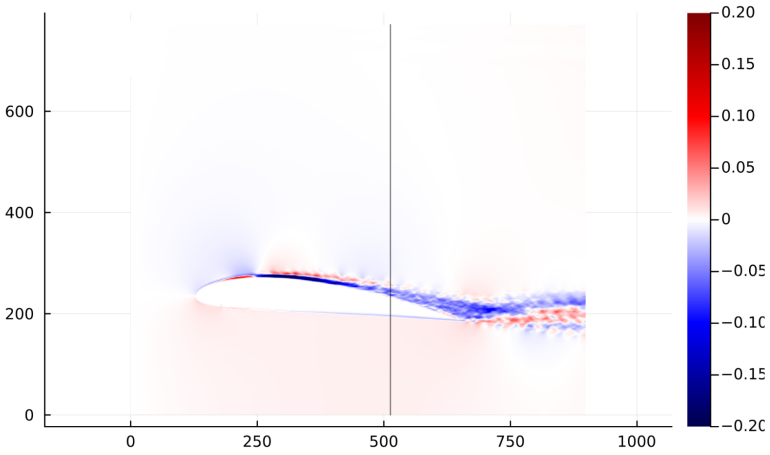

FIGURE 5.18: Image showing the difference between the span-wise and time-averaged velocity fields achieved with and without the geometric shear model for case NACA4412-400k. The difference is plotted as the velocity field with geometric modelling minus the velocity field without geometric modelling.

Wall-normal velocity profiles are investigated at two different positions along the chord with $x/c = 0.4$ and $x/c = 0.75$ where c is the chord length. At $x/c = 0.4$, $Re_\tau = 239$ and the boundary layer is under mild local APG with $\beta = 0.6$, with a history of very strong favourable pressure gradient upstream of $x/c = 0.2$. At $x/c = 0.75$, $Re_\tau = 364$ and the local $\beta = 3.6$ indicates a strong pressure gradient effect locally, with complex pressure gradient history featuring an increasingly strong adverse pressure gradient as the boundary layer moves downstream.

Figure 5.19 compares mean velocity profiles at $x/c = 0.4$ with iLES only and with the geometric model applied. At this location, the differences in momentum of the boundary layer are extreme, with the iLES-only simulation making errors of greater than 30% in the mean velocity profile. This is likely due to the very high wall shear stress upstream and local to the sample location, which is very poorly represented without the geometric shear model. In addition, the grid resolution in wall units is coarse compared to the flat plate results previously studied. Therefore, it can be observed, as expected, that the importance of the shear model grows with the wall-normal resolution length scale measured in wall units. However, the geometric shear modelled profile shows good agreement with the reference data, suggesting effective modelling is still provided by the geometric shear model over stream-wise positions up to $x/c = 0.4$.

Further downstream, Figure 5.20 investigates the mean velocity profile at $x/c = 0.75$. The error in the iLES-only profile here is more modest, likely as a result of better resolution at this location when measured in wall units. The modelled profile is again in good agreement with the reference data, showing that the shear model has

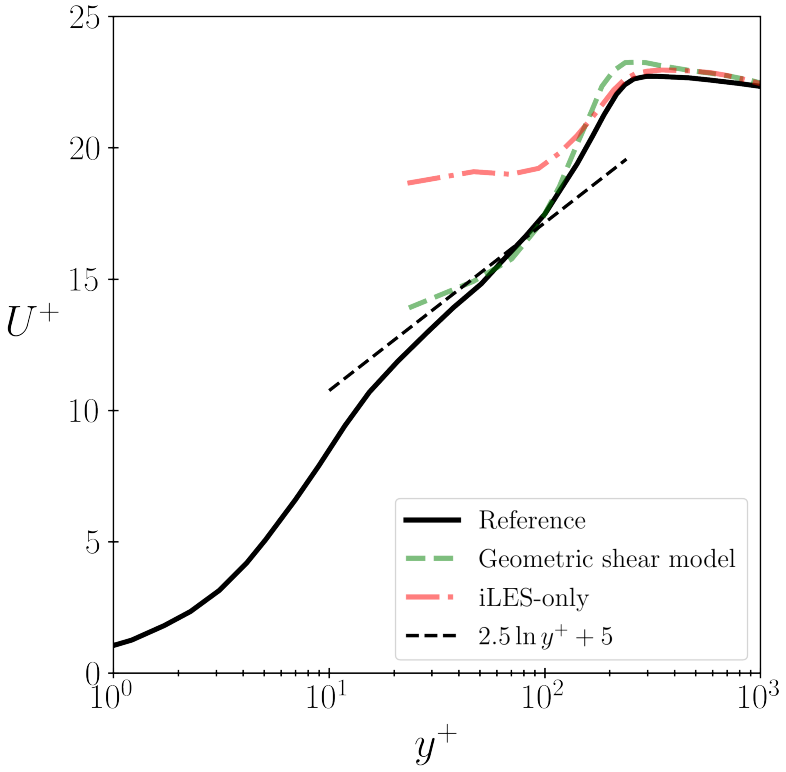

FIGURE 5.19: Time-averaged, wall-normal velocity profiles of wall-parallel velocity measured in wall units and sampled at $x/c = 0.4$ for the NACA4412 aerofoil at Reynolds number of 4×10^5 and at angle of attack 5 degrees. The reference data from Tanarro et al. (2020) is plotted in a solid black line.

maintained effective modelling under the conditions. In comparison to the flat plate APG boundary layer case, the local β value is significantly larger. Therefore, the accuracy of this result without pressure modelling is potentially surprising. However, the APG has persisted for a far shorter stream-wise distance relative to the boundary layer thickness. Hence, the integrated effect of the pressure gradient is actually weaker, significantly reducing the potential significance of the pressure model in this case.

The accuracy of the shear model for this stream-wise location is perhaps surprising and highlights key properties of the proposed model and the physical pressure gradient effects. Namely, the local momentum balance depends on the local pressure gradient and the shear model. Therefore, it can be argued that the shear model itself is adaptive to conditions with local pressure gradient (in the sense that is maintains the local momentum balance). As suggested previously, the impact of the pressure model is not tied to the local pressure gradient, which directly impacts the local momentum balance, but is tied to the accumulated effect of pressure gradient history on the boundary layer. This represents a higher-order effect on the energy of turbulent fluctuations. In the NACA4412 case, where the pressure gradient varies relatively rapidly and is applied over relatively short stream-wise distances, this leads to a

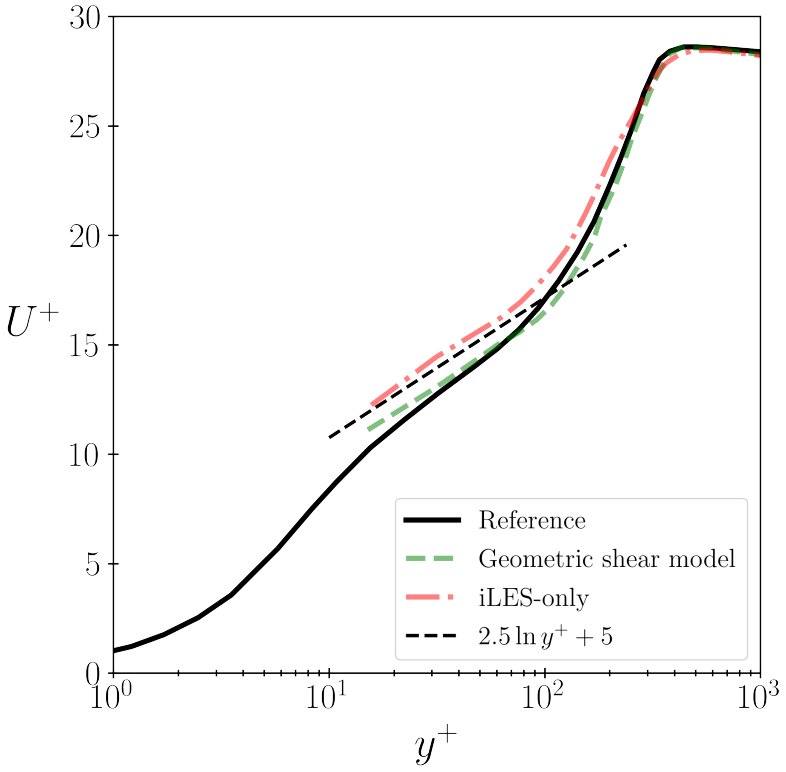

FIGURE 5.20: Time-averaged, wall-normal profiles of wall-parallel velocity measured in wall units sampled at $x/c = 0.4$ for the NACA4412 aerofoil at Reynolds number of 400,000 and at angle of attack 5 degrees. The reference data from Tanarro et al. (2020) is plotted in a solid black line.

reduced importance of the pressure model up to $x/c = 0.75$. However, it can still be expected that the pressure model will have a strong impact yet further downstream where the integrated pressure gradient effect becomes more significant.

5.5 Computational Performance

The relative computational performance of the code is assessed with and without activation of the geometric model in order to assess the model's computational overhead. Relative computational cost is quantified in terms of the average CPU cost per time step (CPS) and the average time step size (Δt). These quantities measured while the geometric model is active (Δt_{geom}, CPS_{geom}) are compared with their values while running the base iLES solver without the geometric model (Δt_{iLES}, CPS_{iLES}) in Table 5.4. The relative computational cost is defined as the ratio of CPS between cases divided by the ratio of the time step sizes. Table 5.4 summarises the overall computational performance for each case at a representative resolution and converged over 1 flow-through time of the domain in each case.

Case ID	$\Delta t_{\text{geom}} / \Delta t_{\text{iLES}}$	$\text{CPS}_{\text{geom}} / \text{CPS}_{\text{iLES}}$	Relative cost
ZPG-1.25	1.000	1.316	1.316
APG-13-1.25 (shear only)	0.985	1.279	1.298
APG-13-1.25 (combined model)	0.978	1.280	1.309
NACA4412-400k	1.003	1.304	1.301

TABLE 5.4: Table of relative cost per time step (CPS), relative time-step size and relative cost incurred by the geometric model over a representative sample of the validation cases.

For classical LES models, the baseline, static Smagorinsky model is known to introduce negligible computational cost overheads of approximately 1-5%. Meanwhile, more advanced static models such as the anisotropic minimum dissipation (AMD) produce overheads of approximately 10% (Gadde et al., 2021). Dynamic models such as the Lagrangian-averaged scale-dependent (LASD) model or dynamic Smagorinsky model generate overheads in the region of 20-80% depending on the specific setup and complexity of operations performed (Gadde et al., 2021; Chow et al., 2005), or even higher for the most expensive of models. Therefore, the present model with an overhead of approximately 30% as shown by Table 5.4 has performance comparable to the faster dynamic models. The result falling in the range of dynamic models is expected due to the adaptive nature of the present model as well as its utility in predicting near-wall flow behaviour. It can also be observed in Table 5.4 that the shear model dominates computational overhead of the geometric model itself, with the addition of the pressure model having negligible impact. Therefore, the results are encouraging in that the computational overhead created by the proposed model is reasonable by established standards. If further work were to be carried out on computational optimisation of the implementation, it is likely that the computational overheads may be reduced to around 20% relative to the base solver.

Chapter 6

Discussion

This chapter aims to discuss the advantages and limitations of the proposed methodology both in theoretical and practical terms. Further interpretation and perspectives on the methodology are also presented in light of the results, providing direction for future research and wider applications of the new concept.

The key advantage of the proposed model is that it defines a tensor structure which is used to describe non-universality of the sub-grid scale dynamics without introducing the requirement for explicit filtering. This is particularly useful conceptually because it avoids introducing non-locality into the theory and avoids explicit collapse of the full space of possibilities for the sub-grid scale statistics. The consequence is that the resultant modelling problem has minimal conditions-dependence.

This is only possible in the implicit geometric formulation because it does not sample data over different positions under a filter kernel. In general conditions, different positions have different statistical properties and so strong non-universality is introduced into the classical LES sub-grid scale closure problem. In contrast, the local modelling problem may be approximated in a strongly universal form which can only depend on the locally available velocity and pressure field. While it is recognised that higher-order description is possible, it is shown that the chosen metric model at second order dominates higher-order contributions. This contrasts strongly with explicit models in which non-locality under the sampling is accompanied with an exponential increase in possible modelling complexity.

This conceptual expectation for increased universality of the geometric model is supported by the effective modelling it provides under a large range of boundary layer conditions. All results are achieved using a simple model without any empirical parameter or model adjustment. Furthermore, the present model integrates the traditional wall model and sub-grid scale roles into a single framework. Therefore, there is no need for complex, zonal solutions, artificial boundary conditions or

separate “inner layer” numerical meshes used by other methodologies. Instead, the modelling procedure is applied uniformly at all positions and wall-boundary interfaces are treated smoothly. As a result, numerical sensitivities have not been experienced even when using the light-weight FP32 numerical representation.

In practical terms, these features are a significant advantage as they avoid a large amount of numerical complexity and lack of robustness associated with many present WMLES approaches. This property is similar to and inherited from the convergence advantages of iLES schemes over explicit LES schemes. In general, explicit LES applies only where the grid scale is large compared to the viscous scales and scale separation is possible. In contrast, iLES schemes are able to converge to DNS with refined resolution. Similarly, where WMLES approaches are specific to a situation where the grid scale is coarse relative to the viscous scales, the proposed geometric iLES model is both expected and observed to converge towards DNS with refined resolution. This behaviour arises from the fact that empirical assumptions are not made about scale separation, inner-outer decoupling or equilibrium. Instead, the implicit model is locally universal and is able to gracefully “switch off” as resolution is improved.

The results also provide evidence to suggest that the traditional picture of wall-stress modelling may be incomplete. While the pressure gradient does have a significant impact on the local momentum balance, this is not its only important effect. It is observed that the local effect of pressure gradient on the momentum balanced can be accounted for by the geometric shear model, which adapts to different shear conditions and whose purpose is to maintain local momentum conservation. After all, the pressure gradient impact on the momentum balance remains well-resolved in WMLES, since the mean pressure field generally only features large scale variations.

Moreover, it is argued that the accumulated (non-local) effect of the pressure gradient on the boundary layer structure is a separate issue and should be modelled separately from the local momentum balance using the proposed pressure model. While the shear model is always relevant locally and increases in importance with the magnitude of the unresolved shear stress, the pressure model as defined gains importance with integrated pressure gradient, not the local pressure gradient strength. The relative importance of the two components must therefore be quantified by the integrated Clauser parameter. This perspective is in agreement with the empirical observations made in the literature quantifying the pressure gradient history effect.

As a result, it has been observed that the pressure model was relatively more important under the flat-plate APG conditions than under the NACA4412 conditions, even at $x/c = 0.75$ with strong local pressure gradient. The pressure model appears to have a more significant effect under the flat-plate condition because a moderate APG is sustained for a very long stream-wise distance, compared to the NACA4412 case where the local pressure gradient effect is far stronger, but extent of the history effect

is weaker. This indicates an important distinction to be made in modelling both the local (momentum balance, wall shear) and history-dependent (energy, pressure) effects which both emerge from pressure gradients. While the modelling of the local momentum balance is foundational to wall modelling, the proposed concept for modelling the impact of the accumulated pressure gradient is not available in the current wall modelling literature. Therefore, this is an important new conceptual outcome of this work.

While the local momentum component may be framed in terms of the local anisotropy, the non-local pressure/energy component of the model is framed in terms of the (non-local) inhomogeneity of the pressure field. From the geometric perspective, this leads to two very different effects which must both be recognised. It is therefore suggested that current LES wall modelling, which focuses on the modelling of the wall shear stress may be incomplete. However, the proposed solution to the cumulative pressure gradient problem (using an inhomogeneous Riemann geometry) may not be one which is possible to implement in the context of explicit modelling due to the unique mathematical structure provided by the manifold. This leaves open questions on whether explicit wall modelling and sub-grid scale modelling is truly appropriate for application to general conditions featuring this accumulated pressure gradient history effect.

Aside from the aforementioned successes of the present methodology, limitations may also be found. The key error in predictions made by the model is the stream-wise Reynolds stress component for the APG flat plate boundary layer cases. While the modelled simulations have predicted the other components well, the stream-wise component is over-predicted in magnitude under APG conditions. It must be considered why this does not appear to have been an issue under ZPG conditions. It is therefore argued that - under APG conditions - there is a greater sensitivity to the upstream turbulent fluctuations due to the known history-dependence of the boundary layer. Therefore, it is likely that the simulation results under APG are significantly more sensitive to the conditions produced by the ZPG inflow region. Resultantly, it is most feasible that inadequacy in the inflow condition produces discrepancies in the APG Reynolds stresses, without appearing as a in issue in the ZPG simulations. If the turbulent fluctuations at the end of the ZPG inlet region are not entirely accurate, discrepancies can be expected to be inherited by the entire downstream evolution of the APG boundary layer due to history-dependence. The appearance of this problem reflects difficulties experienced in the practicalities of the modelled simulations - namely the impossibility of resolving the tripping and transition. The sensitivity of the solution to these “initial conditions” of the boundary layer and the worsening of the issue with coarser resolution under APG highlights that transition of the boundary layer is a key area for further investigation and one which is limiting for the present methodology.

A similar limitation is found in the NACA aerofoil case, where it is accepted that the thin laminar boundary layer on the nose region of the aerofoil is not modelled by the proposed methodology (which handles turbulence effects only), and so must be resolved. This means that the present methodology (similar to other wall models) does not eliminate Reynolds number scaling for this common kind of external flow problem (Reynolds, 1990). While the Reynolds number scaling of the laminar boundary layer is relatively weak relative to the scaling of turbulence, modelling of the laminar boundary layer and transition is, overall, a significant area which must be investigated in order to totally eliminate Reynolds number scaling of practical problems and to provide accurate initial boundary layer states.

Where a clear method for recycling-rescaling is not available for the NACA4412 case (due to the absence of a ZPG region), a "minimum resolvable" physical trip method was used. While the mean velocity profiles found downstream were consistent with the reference data, further investigation is required to confirm whether the geometric model is naturally able to align its behaviour with the transitional boundary layer, especially in cases which do not feature a robust, bypass transition. The effect of the geometric model on naturally evolving transitional instabilities has been left unresolved. Because the effective turbulent stresses produced by the model are directly proportional to the resolved fluid stresses, it is feasible that the model has a natural tendency to amplify disturbances in a laminar boundary layer. The minimal filtering provided by the implicit approach also offers an advantage over explicit methods, which tend to smooth out boundary layer instabilities more strongly.

For the NACA4412 case, further investigation is also required into the velocity field nearer to the trailing edge and into the fluctuating components of the velocity field, where the integrated effect of pressure gradient is larger. In this case, refinement to the pressure model may be required for cases with a more complex, 2- or 3-dimensional pressure field, compared to the simpler 1-dimensional variation present in the flat plate APG case.

A limitation of the current numerical methodology is the inefficient resolution provided by a Cartesian grid. Although this direction was chosen in order to provide robust and simple numerical methods for testing of the key scientific method, a generalisation to the numerical method would be extremely valuable in practical use cases if grid resolution can be adapted such that available computational effort is focused on the spatio-temporal regions in which it is most required. This would allow a wider investigation of yet more complex cases with further generalised 3-dimensional structure and higher Reynolds number. Such changes could also be combined with modern higher-order discretisation schemes if required in which it would also be appropriate to describe the metric tensor perturbation at higher-order in Equation 3.6. Furthermore, the extension of the computational code to multi-GPU

operation is necessary in order to avoid some computational limits on the problem size experienced in the current study.

Another further limitation that may be important for different classes of flows is that only the conservation of energy and momentum has been considered. In the present study, they are the only relevant conserved quantities for the flows considered. However, in very high Reynolds number flows which are nearly inviscid, or flows with strong mean rotational character (i.e. turbo-machinery, geophysical vortices), helicity conservation is also significant and may add additional complexity which is not yet considered in the proposed methodology. Where helicity is an important factor, the topological invariant may need to be considered as a further constraint when constructing the topological space used to model turbulence (the manifold). It can tentatively be suggested that this would require an interesting modification introducing asymmetry to the metric tensor in order to encode chirality, where the antisymmetric part of the metric describes orientation and linking of flow structures.

The interpretations of the proposed model are also discussed in further detail in order to aid potential future investigation following the present methodology. The notion that the Navier-Stokes equations are always valid given a small enough volume scale (fine enough resolution) is foundational to computational fluid dynamics. This property is embedded within the new geometric framework because a manifold is a topological space that locally resembles Euclidean space $\mathbb{R}^n$. Moreover, the (Euclidean and Newtonian) Navier-Stokes equation always remains valid locally - over sufficiently small volumes where the manifold appears flat. This universal, local behaviour may be termed “locally inertial” in the sense that the Navier-Stokes equation takes the balance of locally observed fluid forces and applies Newton’s laws to determine the temporal evolution.

The proposed geometric framework then recognises that, when observed at relatively larger volume scales (relatively coarse resolution), the Euclidean Navier-Stokes equations are no longer appropriate (due to the sub-grid scales). Over larger volumes, the manifold can no longer be approximated as flat, and so its non-Euclidean structure comes into play. The metric tensor and the manifold geometry then represent the connection between local, inertial frames of reference on the manifold as illustrated by Figure 6.1. With a connection consistent with locally inertial behaviour provided by the metric, modelling for the universal energy cascade mechanism can then be applied.

The key interpretation for the effect of the metric is therefore that it provides a resolution-independent geometric structure (the shape of the manifold) in which sub-grid forces vanish. This structure is not locally noticeable with very small volume scales, but is significant for coarser resolutions. Consequently, the dynamics of the present method are governed locally by the Navier-Stokes equations everywhere, all

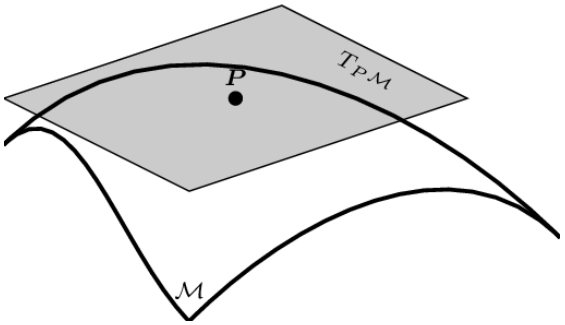

FIGURE 6.1: A manifold M (here 2-dimensional) is locally Euclidean, as represented by the tangent space T_pM which may be found at any point p. Sketch from (Faraki et al., 2014)

the time and regardless of resolution or local conditions. However, the Navier-Stokes equations are seen to evolve on a non-Euclidean background geometry determined by the metric model which describes non-inertial global behaviour. The resolution-independence of this background structure and the universal preservation of the Navier-Stokes equation has significant implications for the generality of the description under arbitrary conditions. This situation is strongly distinct from explicit LES, in which the closure problem is only defined under a specific filter choice and so cannot be resolution- or conditions-independent.

While the local modelling problem for the metric tensor is simplified compared to explicit LES, it also leads to the suggestion that two separate effects may exist - one describing the local momentum balance and one describing global inhomogeneity of the sub-grid scale energy. The validity of separating the shear model effect on the local momentum from the pressure model effect on energy can also be geometrically analysed. In the neighbourhood of any point p on a Riemann manifold (M, g), preferred "geodesic normal" coordinates can be found such that the metric components are approximated by the Euclidean metric in the specific sense that

$$g_{ij} = \delta_{ij} + O(|x|^2) \quad \text{and} \quad \frac{\partial g_{ij}}{\partial x^k}(p) = 0. \tag{6.1}$$

This means that the linear, shear model effect on the metric may be separated, being cancelled out in geodesic normal coordinates, and a quadratic correction may be analysed independently. In other words, the geometric shear transformation is linear, so a choice can always be made to locally align the coordinate system with the shear in order to examine the leading order non-linear correction.

This perspective also distinguishes the two components of the proposed model geometrically. The shear model locally creates linear (shearing) distortion of the manifold at each point, with components being bi-linear (coupling two coordinate directions). While the local geometry is non-Euclidean, it is intrinsically flat. In contrast, the pressure model produces a non-linear, self-coupling of coordinate

directions, resulting in a distortion which is quadratic in nature and represents an intrinsic curvature of the space. This geometrically explains why the shear model pertains to the (linear) momentum conservation of the fluid, while the pressure model pertains to the (quadratic) energy of turbulent fluctuations. This geometric distinction between the shear component of the model and the pressure component component aids in the physical interpretation and allows a new conceptual separation between the LES modelling of the momentum fluxes and energy in APG boundary layers. Furthermore, the non-linear, curvature effect of pressure provides strong justification for why it may not be possible to represent under classical, Euclidean frameworks.

Because typical LES wall models aim to model the momentum flux only, it is the non-linear effect of the pressure here which is unique. Because the shear effect does not involve intrinsic curvature of the manifold, it is feasible to approximate its effects as an explicit force (described by the LES sub-grid stress tensor) in the Euclidean setting. However, the pressure effect is described by intrinsic curvature, which is unique to the non-Euclidean manifold structure defined by the geometric model. Hence, it is fundamentally infeasible to represent this effect in the classical, Euclidean framework because the appropriate mathematical structure does not exist. From another perspective, explicit LES methods provide no way to represent the observed, path-dependent behaviour of pressure gradient boundary layers as non-equilibrium systems, as they explicitly choose a single realisation. However, motion on curved manifold geometries is inherently path-dependent. This non-classical property of the proposed model is therefore arguably an essential feature which unlocks potential which is not available in present methodologies. This may lead to a more advanced understanding of turbulence under general conditions where the classical picture is no longer appropriate due to the emergence of the distinctly non-classical effects of non-equilibrium.

The effects of manifold curvature can be further discussed by investigating its effect on volume scaling. Curvature causes volumes to scale differently with length scale compared to Euclidean spaces. This can be visualised, for example, by considering a circle on the surface of a sphere (a positively curved manifold). As the radius of the circle grows, the area contained within the circle grows more slowly than it does on a Euclidean manifold. This is a principal feature of Riemann manifolds in general. Specifically, the rate of growth in volume of a ball with radius ϵ at point p on a manifold M relative to that in Euclidean space is described by

$$\frac{\mathrm{Vol}(B_\epsilon(p) \subset M)}{\mathrm{Vol}(B_\epsilon(0) \subset \mathbb{R}^n)} = 1 - \frac{R}{6(n+2)}\epsilon^2 + O(\epsilon^3) \tag{6.2}$$

where R is the Ricci scalar (a function of the metric describing the average curvature) and n is the number of dimensions. Hence, the geometry of the manifold described by the metric tensor has a direct impact on the effective volumetric scaling.

This effect is relevant to the finite volume method which relies on describing the behaviour in the bulk of a 3-dimensional volume based on information present on the 2-dimensional volume boundary. In the context of turbulence, it is natural to ask the question: if there is unresolved detail of the velocity field within the volume, how can it still be encoded on the boundary?

This question can be answered by noting that a numerical scheme stores information with a certain density, which is proportional to the length scale of discretisation L. The information that may be stored on a closed 2-dimensional surface therefore scales with L^2 and the information that may be stored in a closed 3-dimensional volume scales with L^3. Therefore, in order for a surface (boundary of the volume) to encode the information present within a volume, the information density within the volume must scale like $L^{2/3}$. Otherwise, there is more information within the volume than can possibly be encoded on its boundary.

This observation that volumetric information can be encoded on a 2-dimensional boundary surface given a certain scaling aligns with the Kolmogorov scaling described by the structure function

$$\left\langle (\delta u(r))^2 \right\rangle = C_2 \left(\epsilon r\right)^{2/3}. \tag{6.3}$$

The Kolmogorov structure function represents energy present at separations of length scale r (such as the distance between opposite faces of a finite volume). The turbulence cascade therefore lies at a critical point of information density at which it is only just possible to describe volumetric information on a 2-dimensional boundary. This observation is very similar to the association between the Kolmogorov structure function and the Onsager conjecture provided in Chapter 2, which shows that the inertial turbulent cascade sits at critical point for energy conservation.

Under curved geometry, Equation 6.2 shows that the volume scales differently against area. Therefore, curvature provides a mechanism which control the quantity of information and energy locally present in a finite volume. This aligns with the impact of the pressure model, which is principally on the turbulent fluctuations and pressure field.

The interpretation of the large-scale velocity field in terms of Fisher information geometry may also be discussed further and interpreted as a soft (statistical) constraint on the dynamics. The key concept behind Equation 3.4 is that the (observed) expectation value of the velocity vector is held constant, while accounting for the fact that there are in fact many possibilities for the underlying configuration of the velocity field. These possibilities are (implicitly) integrated over (Equation 3.3), rather than considering just a single possible realisation as in an explicit LES. Given the constraints of a fixed expectation value (the observed velocity for a finite volume) and probability normalisation, the distribution which maximises entropy is the one

where possible fluctuations cancel out. This makes the expected value the best statistical representation of the system, in the sense that entropy can only decrease if the system moves away from that value. This is what is expressed by the partition function, and leads to the Fisher information metric, which describes a local cancellation of the sub-grid stress tensor.

The configuration integral (Equation 3.3) measures the relative volume occupied by the turbulence in phase space (x, u). This means that it measures the relative number of possible states, the relative entropy or the information density associated with the turbulent fluctuations. More specifically, the quantity $\log Z(x)$ represents the relative energy density of a state of the distribution-valued velocity vector. It's Hessian (Equation 3.5) being large in magnitude implies that energy changes are sharpy distinguishable at a position x. This case has high Fisher information and means that small changes in x cause large changes in U. In other words, observed data about U provides a lot of information about the coordinate parameter x and it is therefore easier to distinguish between x values. In other words, with a relatively high Fisher information and a strongly curved energy landscape, the system occupies tightly restricted regions of phase space and has relatively low entropy. On the contrary, with low Fisher information and where the energy landscape is relatively flat then the system is more loosely constrained in phase space and may explore it further, taking on larger fluctuations.

This demonstrates how the metric geometry may be viewed as a soft (statistical) constraint on the dynamics, guiding the trajectory of the dynamical system through phase space without forming a direct part of the dynamical evolution itself. The metric adjusts to the flow, being determined at each instant, but does not explicitly determine the dynamical evolution of the flow. Instead, it provides a background on which the flow dynamics play out, determining their own path while being guided by the geometry.

Armed with an understanding of the geometry as a statistical constraint on the fluctuations, further insight can be gained by considering how the redundant degrees of freedom (the unresolved fluctuations) behave. For a physical description to be considered well-posed, degrees of freedom which do not correspond to observable quantities must not affect the observed dynamics and so must be dealt with appropriately. These degrees of freedom, known as gauge degrees of freedom, have associated gauge symmetries which reflect the freedom to choose multiple mathematical configurations that describe the same physical situation. By defining the velocity field statistically, a range of possible distributions of the underlying velocity field are allowed for that lead to the same physical observation (the same expectation value for the velocity field). Again, the value for the expectation can be held fixed, even though the underlying configuration may vary in some complex way which is not actually relevant to the observed dynamics. This perspective on the problem

deviates strongly from explicit LES, in which a realisation is explicitly chosen amongst many possibilities, leading to a collapse of the full statistical state.

A simple example of gauge symmetry can already be found in incompressible flows where the pressure field exhibits gauge symmetry in that any constant scalar can be added globally to the pressure field without affecting the physical situation. This single, global gauge degree of freedom expresses mass conservation. For turbulence, the gauge degrees of freedom are in the unresolved velocity fluctuations which can take on many underlying configurations which lead to the same averaged values for the velocity field over finite volumes. Where we implicitly allow for all physically equivalent possibilities, the corresponding gauge symmetry is local and far more complex, being described by a tensor field with 6 independent gauge degrees of freedom per position and per point in time. The geometric framework expresses this local gauge symmetry (which eliminates any force emerging from the unobservable sub-grid scales) using the metric tensor. In other words, the metric tensor makes sure that unobservable, gauge degrees of freedom do not affect the locally observed dynamics. From this perspective, the geometric iLES concept can be understood to provide a "soft", statistical constraint on the dynamics such that the large-scale velocity field remains consistent with possible configurations of the unobservable degrees of freedom.

This view of the model as an implicit constraint on the dynamics, rather than as an explicit, forcing part of the dynamics is consistent with the iLES philosophy. This philosophy has proven important for robust application to non-universal conditions because it accepts that, although an explicit description of the dynamics may not always be possible, implicit mathematical constraints may still be put in place which maintain consistency of a weak solution with the underlying solution. The key conceptual progression is that the dynamics of the flow do not need to be explicitly modelled and enforced; instead, it is only necessary to constrain the dynamics in a way which retains consistency between what is observed and the underlying Navier-Stokes dynamics. Overall, the geometric model achieves this connection, forming a rich structure which provides a resolution-independent link between locally universal, inertial behaviour and non-universal, large-scale structure which can in principle be used to describe the anisotropy and inhomogeneity of general flow conditions.

Chapter 7

Conclusions

A novel, geometric model is provided which is intended for application to LES simulation of non-universal turbulent flows, especially those in which non-equilibrium precludes a robust empirical description of the statistics. The model has been validated for a range of turbulent boundary layer conditions from a zero pressure gradient flat plate to a NACA4412 aerofoil at 5 degrees angle of attack. The predictions made for the mean velocity profiles are accurate over the significant range of conditions investigated. Prediction of the Reynolds stress is also generally in good agreement with the reference data, aside from specific discrepancies which have been discussed. Furthermore, model adaptation is not required between conditions with identical, constant coefficients being used in all cases. The methodology also remains functional over the full range of reasonable resolution regimes. At the extremes of coarse resolution, it is found that results are accurate with greater than 20 grid points across the 99 percent boundary layer thickness, in agreement with previous studies. At the other extreme, the model is also validated where the grid length scale is as a small as approximately 10 wall units and viscous scales are partially resolved. This demonstrates insensitivity of the model to both resolution choice and conditions. Overall, the goal of producing a model which avoids the limiting, empirical assumptions required by explicit wall models and explicit LES has been achieved, with the model demonstrating minimal dependence both on conditions and on resolution.

While the chosen validation cases cover a relatively wide range of conditions, further investigation is called for under conditions near boundary layer separation. Due to the simplicity of the proposed shear model, it is highly likely that its behaviour will remain robust under such conditions, where the influence of sub-grid scale shear stress is reduced to zero. It can be seen from Equation 3.6 that where the shear stress reduces, the model naturally “turns off” as required for a wall model which is robust to separation. However, it is also possible that refinement of the pressure component

of the model may be necessary for flows with more complex, 3-dimensional pressure fields which are not validated in the present study.

Boundary layer transition both through artificial tripping (bypass transition) and through natural transition must also be studied further. While turbulent fluctuations were mostly predicted accurately, the results for the stream-wise fluctuations under adverse pressure gradient flat plate boundary layer conditions reveal a shortcoming in this area. This issue was only observed under non-equilibrium conditions, suggesting that sensitive dependence on the initial developmental history of the boundary layer is significant. Therefore, it is likely that the initial transition and development of the boundary layer has an impact on the stream-wise fluctuations further downstream. As a result, while the model appears to be effective in modelling the boundary layer evolution itself, more detailed theoretical and practical analysis of transition is required in order to ensure the development of consistent "initial conditions" for the boundary layer at its inception. Although transition is often treated as a separate subject from the LES modelling itself, experience suggests that the history-dependency of non-equilibrium boundary layers acts to intertwine all possible factors, and so future investigation into transition for adverse pressure gradient conditions is important.

The work overall implies that modelling of the sub-grid scales can be made more universal by maintaining strict locality of the theory through avoiding explicit filtering. While implicit LES has already been established, the present contribution significantly develops the filter-free methodology by introducing a powerful, tensor structure with unique properties that are beneficial for the prediction of turbulent flows under general conditions. The implicit, mathematical formulation used may be more appropriate under non-equilibrium conditions than traditional methods using explicit closures due to the fundamental difficulties being faced in describing non-universal and non-equilibrium boundary layer statistics in an explicit, empirical manner. While parallels to the classical LES approach are visible and help guide the methodology, the new approach creates a greatly simplified, local modelling problem with a distinct physical interpretation and with a clearly defined solution which is not achievable using the traditional approach due to fundamental differences in the filter definition.

Furthermore, the findings suggest that wall-stress modelling may not represent the complete picture for LES modelling of wall-bounded flows. Moreover, it is argued that the effect of pressure gradient is not only on the local momentum balance so that the cumulative (history) effect of pressure gradients on turbulent energy must also be modelled independently as a second-order effect. The thesis therefore provides evidence to suggest that the scope of LES wall modelling must be widened, and a methodology is proposed and tested which achieves this. Since this pressure-dependent feature is not present in current wall-stress modelling, which

models the local momentum balance only, the suggestion that models must directly incorporate cumulative pressure effects on other aspects of the flow structure is new. The proposed model highlights mathematical features resulting from curvature of the manifold which are unique to the geometric model and so are unlikely to appear as a possibility within the classical modelling frameworks. The distinctly non-classical features of the current methodology represent an opportunity to capture the crucial path/history-dependency of non-equilibrium turbulent flows in a way which is not feasible in the classical setting.

The theoretical and numerical results presented are therefore significant in that they provide an alternative to the explicit wall modelling approach taken by a large proportion of studies. Significant difficulties have been faced in empirically describing non-universal and non-equilibrium boundary layer conditions over multiple decades, and so an approach which eliminates dependence on the limiting assumptions used is valuable. In particular, the problematic definition of empirical ensembles under non-equilibrium suggests that the present approach which reframes the modelling problem in a locally universal setting is essential to progress modelling of these complex flows. The novel methodology for representing the sub-grid scales proposed by the present study is therefore a contribution which opens new avenues of research, with different challenges to those being faced by the current framework. The general modelling problem may now be attacked from a new perspective specifically designed to remain consistent under non-equilibrium conditions.

From a broader perspective, the newly proposed methodology may be adopted in future to help progress towards the socio-economic goals outlined in Chapter 1. The geometric framework directly opens new avenues for advances in aerodynamic design and prediction, with widespread potential applications in the industries of transport, energy generation and climate science among others. Because the approach is conditions-agnostic being minimally reliant on empirical correlations, it lends itself particularly well to future work on aerodynamic design and optimisation problems. Often, with strong reliance on empirical data, aerodynamic design tends to cluster closely around well-known, empirically tested shapes as frequently observed in industry. With an empirically tuned CFD model, it is extremely challenging to perform a satisfactory exploration of the full design space away from the status quo. To this end, the geometric model opens up new possibilities for how we think about predictive design and optimisation of fluid technology. In the geometric framework proposed, the turbulent fluid carries with it an associated internal geometry; it is now possible to consider how this interacts with the external geometry of boundary conditions imposed by design decisions. Moreover, flow characteristics are directly induced by the boundary conditions themselves, with quantities like shear stress, turbulent energy and friction all being encoded within the deformation of the modelled manifold. Because the manifold itself is non-Euclidean, it may take on

properties describing the transport of energy and momentum in a flow which are not obvious, or not intuitive, without the novel geometric context. Future work may therefore leverage the geometric framework as a tool which facilitates predictive exploration of the design space for fluid dynamics problems, making use of its unique structure to inform design decisions.

The concept that measurement uncertainty may induce effective geometrical structure is also a potentially impactful scientific contribution which has a strong potential to be generalised to many problems. The solution of under-resolved sets of equations is a generally important problem in a wider sense, implying that interesting applications also exist outside of fluid dynamics. Because of the lack of reliance on empirical phenomenology, the core idea of geometric sub-grid scale modelling presented in this thesis also creates possibilities for efficient simulation of various other physical phenomenon. Future work on generalising the methodology to similar, multi-scale problems in which full resolution is impossible could have much wider implications for the study and design of multi-scale dynamical systems in general. In many of these cases, the scaling of complexity is even less favourable than for the Navier-Stokes equations and the behaviour yet more complex such that empirical laws are unavailable for the processes of interest. In large, well developed fields of study such as fluid dynamics, developments have already proven hugely influential; at present, due to the enormous scale, even small improvements in simulation technology can have a large socio-economic impact. However, in less developed technologies where reliable empirical models and simulation methods are less available, methods such as the geometric modelling framework may prove yet more important, presenting an opportunity for rapid progress and growth in new industries and frontier technology. For example, a particularly interesting case study is the simulation of kinetic plasma dynamics crucial to understanding and designing stability of fusion plasma requires a 6-dimensional position-velocity phase-space solution; the much stronger 6-dimensional scaling means that problems become intractable much more rapidly, rendering even small-scale investigations impossible without strong models. Meanwhile, modelling and simulation technology are far less mature and face serious challenges. Nevertheless, there exists an under-resolved field to which the proposed geometric modelling framework can in principle be directly applied. On balance, the scope is wide for future work in generalising the core conceptual contribution presented here to other physical systems, some of which have the potential for significant impact.

Overall, this study presents a geometric framework for implicit LES that advances turbulence modelling by avoiding explicit filtering and empirical closure, while introducing a powerful new form of tensor structure used to describe general conditions. The central contribution is a novel interpretation of sub-grid modelling that maximises locality and minimises corresponding dependence on spatial

variations in statistical properties to within measurement uncertainty. A key result is the significant simplification of the resultant geometric modelling problem and its validated efficacy over a range of flow conditions. The implication is that the local and implicit model is inherently consistent with general conditions in which history-dependence strongly undermines the possibility of robust empirical treatments. Conceptually, the model also provides a new methodology for modelling the cumulative effects of pressure gradient in addition to the traditional focus on the local momentum balance. The geometric construction naturally captures relevant path-dependent effects, by avoiding the explicit choice of specific realisations. The impact is embodied by strongly non-classic features tied to the manifold geometry that cannot emerge within classical frameworks. Overall, the results suggest that future progress in modelling complex, non-universal boundary layers may lie in re-framing the sub-grid modelling problem geometrically such that it remains locally universal.

References

Hussein Aluie and Gregory L. Eyink. Localness of energy cascade in hydrodynamic turbulence. ii. sharp spectral filter. *Physics of Fluids*, 21(11):115108, 2009. .

Scott Atchley, Christopher Zimmer, John Lange, David Bernholdt, Veronica Melesse Vergara, Thomas Beck, Michael Brim, Reuben Budiardja, Sunita Chandrasekaran, Markus Eisenbach, Thomas Evans, Matthew Ezell, Nicholas Frontiere, Antigoni Georgiadou, Joe Glenski, Philipp Grete, Steven Hamilton, John Holmen, Axel Huebl, Daniel Jacobson, Wayne Joubert, Kim Mcmahon, Elia Merzari, Stan Moore, Andrew Myers, Stephen Nichols, Sarp Oral, Thomas Papatheodore, Danny Perez, David M. Rogers, Evan Schneider, Jean-Luc Vay, and P. K. Yeung. Frontier: Exploring exascale. In *Proceedings of the International Conference for High Performance Computing, Networking, Storage and Analysis*, SC '23, New York, NY, USA, 2023. Association for Computing Machinery. ISBN 9798400701092. . URL https://doi.org/10.1145/3581784.3607089.

Hyunji Jane Bae, Adrián Lozano-Durán, Sanjeeb T. Bose, and Parviz Moin. Dynamic slip wall model for large-eddy simulation. *Journal of Fluid Mechanics*, 859:400–432, 2019. .

Riccardo Balin, Kenneth E. Jansen, and Philippe R. Spalart. *Wall-Modeled LES of Flow over a Gaussian Bump with Strong Pressure Gradients and Separation*. . URL https://arc.aiaa.org/doi/abs/10.2514/6.2020-3012.

Andrea Beck, David Flad, and Claus-Dieter Munz. Deep neural networks for data-driven les closure models. *Journal of Computational Physics*, 398:108910, 2019. ISSN 0021-9991. . URL https://www.sciencedirect.com/science/article/pii/S0021999119306151.

Iván Bermejo-Moreno, Johan Larsson, Laura M. Campo, Julien A. Bodart, David Benjamin Helmer, Frank E. Ham, and John K. Eaton. Wall-modeled large-eddy simulations of shock/turbulent-boundary layer interaction in a duct. *Bulletin of the American Physical Society*, 2012.

A. Bobke, R. Vinuesa, R. Örlü, and P. Schlatter. History effects and near equilibrium in adverse-pressure-gradient turbulent boundary layers. *Journal of Fluid Mechanics*, 820:667–692, 2017. .

Alexandra Bobke, Ricardo Vinuesa, Ramis Örlü, and Philipp Schlatter. Large-eddy simulations of adverse pressure gradient turbulent boundary layers. *Journal of Physics: Conference Series*, 708(1):012012, 2016. .

Julien Bodart, Johan Larsson, and Parviz Moin. *Large eddy simulation of high-lift devices*. 2013. . URL https://arc.aiaa.org/doi/abs/10.2514/6.2013-2724.

S. T. Bose and P. Moin. A dynamic slip boundary condition for wall-modeled large-eddy simulation. *Physics of Fluids*, 26(1):015104, 2014. . URL https://doi.org/10.1063/1.4849535.

Sanjeeb T. Bose and George Ilhwan Park. Wall-modeled large-eddy simulation for complex turbulent flows. *Annual Review of Fluid Mechanics*, 50(1):535–561, 2018. . URL https://doi.org/10.1146/annurev-fluid-122316-045241.

Elie Bou-Zeid, Charles Meneveau, and Marc Parlange. A scale-dependent lagrangian dynamic model for large eddy simulation of complex turbulent flows. *Physics of Fluids*, 17(2):025105, 2005. . URL https://doi.org/10.1063/1.1839152.

Lydia Bourouiba. The fluid dynamics of disease transmission. *Annual Review of Fluid Mechanics*, 53(Volume 53, 2021):473–508, 2021. ISSN 1545-4479. . URL https://www.annualreviews.org/content/journals/10.1146/annurev-fluid-060220-113712.

J. G. Brasseur and S. Corrsin. Spectral evolution of the navier-stokes equations for low order couplings of fourier modes. In Geneviève Comte-Bellot and Jean Mathieu, editors, *Advances in Turbulence*, pages 152–162, Berlin, Heidelberg, 1987. Springer Berlin Heidelberg. ISBN 978-3-642-83045-7.

Tony Burton, Nick Jenkins, David Sharpe, Ervin Bossanyi, and Michael Graham. Wind energy handbook / tony burton, nick jenkins, david sharpe, ervin bossanyi, michael graham., 2021.

J. S. Carlton. *Marine propellers and propulsion*. Butterworth-Heinemann, Kidlington, Oxford, fourth edition. edition, 2019. ISBN 9780081003749. URL https://login.eux.idm.oclc.org/login?url=https://www.sciencedirect.com/science/book/9780081003664.

Tuncer Cebeci. Chapter 4 - general behavior of turbulent boundary layers. In Tuncer Cebeci, editor, *Analysis of Turbulent Flows with Computer Programs (Third Edition)*, pages 89–153. Butterworth-Heinemann, Oxford, third edition edition, 2013. ISBN 978-0-08-098335-6. . URL https://www.sciencedirect.com/science/article/pii/B9780080983356000045.

Dean R. Chapman. Computational aerodynamics development and outlook. *AIAA Journal*, 17(12):1293–1313, 1979. . URL https://doi.org/10.2514/3.61311.

Ishtiaq Chaudhry, Tipu Sultan, Farrukh Siddiqui, Muhammad Farhan, and Muhammad Asim. The flow separation delay in the boundary layer by induced vortices. *Journal of Visualization*, 20:1–11, 10 2016. .

Haecheon Choi, Chonghyuk Cho, Myunghwa Kim, and Jonghwan Park. Perspective on machine-learning-based large-eddy simulation. *Phys. Rev. Fluids*, 10:110701, Nov 2025. . URL https://link.aps.org/doi/10.1103/bxcn-rmdv.

Fotini Katopodes Chow, Robert L. Street, Ming Xue, and Joel H. Ferziger. Explicit filtering and reconstruction turbulence modeling for large-eddy simulation of neutral boundary layer flow. *Journal of the Atmospheric Sciences*, 62(7):2058 – 2077, 2005. . URL https://journals.ametsoc.org/view/journals/atsc/62/7/jas3456.1.xml.

Gavin E. Crooks. Measuring thermodynamic length. *Phys. Rev. Lett.*, 99:100602, Sep 2007. . URL https://link.aps.org/doi/10.1103/PhysRevLett.99.100602.

Lars Davidson. Large eddy simulations: How to evaluate resolution. *International Journal of Heat and Fluid Flow*, 30(5):1016 – 1025, 2009. ISSN 0142-727X. . URL https://doi.org/10.1016/j.ijheatfluidflow.2009.06.006. The 3rd International Conference on Heat Transfer and Fluid Flow in Microscale.

J. Andrzej Domaradzki and Robert S. Rogallo. Local energy transfer and nonlocal interactions in homogeneous, isotropic turbulence. *Physics of Fluids A: Fluid Dynamics*, 2(3):413–426, 1990. . URL https://doi.org/10.1063/1.857736.

Gregory L. Eyink and Hussein Aluie. Localness of energy cascade in hydrodynamic turbulence. i. smooth coarse graining. *Physics of Fluids*, 21(11):115107, 2009. .

V. M. Falkner and S. W. Skan. Solutions of the boundary layer equations. *Philosophical Magazine*, 12:865–896, 1931.

Masoud Faraki, Maziar Palhang, and Conrad Sanderson. Log-euclidean bag of words for human action recognition. *IET Computer Vision*, 9, 06 2014. .

N. Fehn and V. John. From anomalous dissipation through euler singularities to stabilized finite element methods for turbulent flows. *Flow, Turbulence and Combustion*, 115(1):347–388, 2025. . URL https://link.springer.com/article/10.1007/s10494-025-00639-6.

Mitchell Fowler, Tamer A. Zaki, and Charles Meneveau. A lagrangian relaxation towards equilibrium wall model for large eddy simulation. *Journal of Fluid Mechanics*, 934:A44, 2022. .

Ariane Frère, Corentin Carton de Wiart, Koen Hillewaert, Philippe Chatelain, and Grégoire Winckelmans. Application of wall-models to discontinuous galerkin les. *Physics of Fluids*, 29(8):085111, 2017. . URL https://doi.org/10.1063/1.4998977.

Ariane Frère, Koen Hillewaert, Philippe Chatelain, and Gregoire Winckelmans. *High Reynolds Number Airfoil: From Wall-Resolved to Wall-Modeled LES*, pages 381–387. 01 2019. ISBN 978-3-030-04914-0. .

Srinidhi N. Gadde, Anja Stieren, and Richard J. A. M. Stevens. Large-eddy simulations of stratified atmospheric boundary layers: Comparison of different subgrid models. *Boundary-Layer Meteorology*, 178(3):363–382, Mar 2021. ISSN 1573-1472. . URL https://doi.org/10.1007/s10546-020-00570-5.

B. Ganapathisubramani, N. Hutchins, J. P. Monty, D. Chung, and I. Marusic. Amplitude and frequency modulation in wall turbulence. *Journal of Fluid Mechanics*, 712:61–91, 2012. .

Nigel Goldenfeld and Hong-Yan Shih. Turbulence as a problem in non-equilibrium statistical mechanics. *Journal of Statistical Physics*, 167(3-4):575–594, 2017. .

Fernando F. Grinstein and Dimitris Drikakis. Computing turbulent flow dynamics with implicit large eddy simulation. *Journal of Fluids Engineering*, 129(12):1481–1482, 12 2007. ISSN 0098-2202. . URL https://doi.org/10.1115/1.2822659.

Mingze Han, Mingze Ma, and Chao Yan. Consistent outer scaling and analysis of adverse pressure gradient turbulent boundary layers. *Journal of Fluid Mechanics*, 982: A17, 2024. .

W. Heisenberg. Zur statistischen theorie der turbulenz. *Zeitschrift für Physik*, 124: 628–657, 1948. .

H. Hosseinzade and D. J. Bergstrom. Time-averaging and temporal-filtering in wall-modeled large eddy simulation. *Physics of Fluids*, 33(3):035108, 2021. . URL https://doi.org/10.1063/5.0039651.

W Hucho and G Sovran. Aerodynamics of road vehicles. *Annual Review of Fluid Mechanics*, 25(Volume 25, 1993):485–537, 1993. ISSN 1545-4479. . URL https://www.annualreviews.org/content/journals/10.1146/annurev.fl.25.010193.002413.

Yongyun Hwang. Statistical structure of self-sustaining attached eddies in turbulent channel flow. *Journal of Fluid Mechanics*, 767:254–289, 2015. .

M. Inoue, R. Mathis, I. Marusic, and D. I. Pullin. Inner-layer intensities for the flat-plate turbulent boundary layer combining a predictive wall-model with large-eddy simulations. *Physics of Fluids*, 24(7):075102, 2012. . URL https://doi.org/10.1063/1.4731299.

Prahladh S. Iyer and Mujeeb Malik. Wall-modeled les of the nasa juncture flow experiment. 01 2020. .

Prahladh S. Iyer, George Park, and Mujeeb Malik. A comparative study of wall models for les of turbulent separated flow. *Center for Turbulence Research Proceedings of the Summer Program*, 12 2016. .

Soshi Kawai and Johan Larsson. Wall-modeling in large eddy simulation: Length scales, grid resolution, and accuracy. *Physics of Fluids*, 24(1):015105, 2012. . URL https://doi.org/10.1063/1.3678331.

H. T. Kim, S. J. Kline, and W. C. Reynolds. The production of turbulence near a smooth wall in a turbulent boundary layer. *Journal of Fluid Mechanics*, 50(1):133–160, 1971. .

A. Kolmogorov. The Local Structure of Turbulence in Incompressible Viscous Fluid for Very Large Reynolds' Numbers. *Akademiia Nauk SSSR Doklady*, 30:301–305, January 1941. URL https://doi.org/10.1098/rspa.1991.0075.

Robert H. Kraichnan. On kolmogorov's inertial-range theories. *Journal of Fluid Mechanics*, 62(2):305–330, 1974. .

Johan Larsson, Soshi Kawai, Julien Bodart, and Ivan Bermejo-Moreno. Large eddy simulation with modeled wall-stress: recent progress and future directions. *Mechanical Engineering Reviews*, 3(1):15–00418–15–00418, 2016. .

John M. Lee. *Introduction to Riemannian Manifolds*. Springer, Cham, Switzerland, 2nd edition, 2018. ISBN 978-3-319-91755-9.

Jungil Lee, Minjeong Cho, and Haecheon Choi. Large eddy simulations of turbulent channel and boundary layer flows at high reynolds number with mean wall shear stress boundary condition. *Physics of Fluids*, 25(11):110808, 2013. . URL https://doi.org/10.1063/1.4819342.

Kenneth E. Lilly. On the application of the eddy viscosity concept in the inertial sub-range of turbulence. 1966.

Bo Liu, Huiyang Yu, Haibo Huang, Nansheng Liu, and Xiyun Lu. Investigation of nonlocal data-driven methods for subgrid-scale stress modeling in large eddy simulation. *AIP Advances*, 12(6):065129, 06 2022. ISSN 2158-3226. . URL https://doi.org/10.1063/5.0094316.

Adrián Lozano-Durán and H. Jane Bae. Self-critical machine-learning wall-modeled les for external aerodynamics. 12 2020.

Hao Lu, Christopher J. Rutland, and Leslie M. Smith. A priori tests of one-equation les modeling of rotating turbulence. *Journal of Turbulence*, 8:N37, 2007. . URL https://doi.org/10.1080/14685240701493947.

Rong Ma and Adrián Lozano-Durán. Machine-learning wall-model large-eddy simulation accounting for isotropic roughness under local equilibrium. *Journal of Fluid Mechanics*, 1007:A17, 2025. .

Y. Maciel, T. Wei, and A. G. Gungor. Non-equilibrium effects in turbulent boundary layers with pressure gradient. *Journal of Fluid Mechanics*, 822:5–24, 2017. .

Audrey P. Maertens and Gabriel D. Weymouth. Accurate cartesian-grid simulations of near-body flows at intermediate reynolds numbers. *Computer Methods in Applied Mechanics and Engineering*, 283:106 – 129, 2015. ISSN 0045-7825. . URL https://doi.org/10.1016/j.cma.2014.09.007.

Atharva Mahajan, Rahul Deshpande, Taygun R. Gungor, Yvan Maciel, and Ricardo Vinuesa. Upstream history quantification and scale-decomposed energy analysis for weak-to-strong adverse-pressure-gradient turbulent boundary layers. *International Journal of Heat and Fluid Flow*, 117:110004, 2026. ISSN 0142-727X. . URL https://www.sciencedirect.com/science/article/pii/S0142727X25002620.

Len Margolin. Finite scale theory: The role of the observer in classical fluid flow. *Mechanics Research Communications*, 57, 01 2013. . URL https://doi.org/10.1016/j.mechrescom.2013.12.004.

Ivan Marusic and Jason P. Monty. Attached eddy model of wall turbulence. *Annual Review of Fluid Mechanics*, 51(1):49–74, 2019. . URL https://doi.org/10.1146/annurev-fluid-010518-040427.

Ivan Marusic, Jason P. Monty, Marcus Hultmark, and Alexander J. Smits. On the logarithmic region in wall turbulence. *Journal of Fluid Mechanics*, 716:R3, 2013. .

R. Mathis, N. Hutchins, and I. Marusic. A predictive inner–outer model for streamwise turbulence statistics in wall-bounded flows. *Journal of Fluid Mechanics*, 681:537–566, 2011. .

C. Morrill-Winter and J. Klewicki. Influences of boundary layer scale separation on the vorticity transport contribution to turbulent inertia. *Physics of Fluids*, 25(1): 015108, 2013. . URL https://doi.org/10.1063/1.4775361.

F.T. Nieuwstadt and H. Van Dop. *Atmospheric Turbulence and Air Pollution Modelling: A Course held in The Hague, 21–25 September, 1981*. Atmospheric and Oceanographic Sciences Library. Springer Netherlands, 2012. ISBN 9789401091121. URL https://books.google.co.uk/books?id=ebXVBgAAQBAJ.

A. M. Obukhov. Spectral energy distribution in a turbulent flow. *Akademiia Nauk SSSR Doklady*, 32(1):22–24, 1941.

L. Onsager. The distribution of energy in turbulence. *Phys. Rev.*, 68:286, 1945.

L. Onsager. Statistical hydrodynamics. *Il Nuovo Cimento (1943-1954)*, 6(2):279–287, 1949. ISSN 1827-6121. . URL https://doi.org/10.1007/BF02780991.

Saurabh Pargal, Hao Wu, Junlin Yuan, and Stéphane Moreau. Adverse-pressure-gradient turbulent boundary layer on convex wall. *Physics of Fluids*, 34(3):035107, 2022. . URL https://doi.org/10.1063/5.0083919.

Norbert Peters. *Turbulent Combustion*. Cambridge Monographs on Mechanics. Cambridge University Press, 2000.

U. Piomelli. Large eddy simulations in 2030 and beyond. *Philosophical Transactions of the Royal Society of London Series A*, 372(2022):20130320–20130320, July 2014. . URL https://doi.org/10.1098/rsta.2013.0320.

Ugo Piomelli. Wall-layer models for large-eddy simulations. *Progress in Aerospace Sciences*, 44(6):437–446, 2008. ISSN 0376-0421. . URL https://www.sciencedirect.com/science/article/pii/S037604210800047X. Large Eddy Simulation - Current Capabilities and Areas of Needed Research.

Ugo Piomelli, Elias Balaras, Hugo Pasinato, Kyle D. Squires, and Philippe R. Spalart. The inner–outer layer interface in large-eddy simulations with wall-layer models. *International Journal of Heat and Fluid Flow*, 24(4):538–550, 2003. ISSN 0142-727X. . URL https://www.sciencedirect.com/science/article/pii/S0142727X03000481. Selected Papers from the Fifth International Conference on Engineering Turbulence Modelling and Measurements.

K. Narahari Rao, R. Narasimha, and M. A. Badri Narayanan. The 'bursting' phenomenon in a turbulent boundary layer. *Journal of Fluid Mechanics*, 48(2): 339–352, 1971. .

W. C. Reynolds. The potential and limitations of direct and large eddy simulations. In J. L. Lumley, editor, *Whither Turbulence? Turbulence at the Crossroads*, pages 313–343, Berlin, Heidelberg, 1990. Springer Berlin Heidelberg. ISBN 978-3-540-47032-8. URL https://doi.org/10.1007/3-540-52535-1_52.

Philipp Schlatter, Ramis Örlü, Qiang Li, Geert Brethouwer, Jens H. M. Fransson, Arne V. Johansson, P. Henrik Alfredsson, and Dan S. Henningson. Turbulent boundary layers up to $re_\theta = 2500$ studied through simulation and experiment. *Physics of Fluids*, 21(5):051702, 2009. .

Emil Simiu and Robert H. Scanlan. *Wind effects on structures : fundamentals and applications to design*. John Wiley, New York, 3rd ed edition, 1996. ISBN 0471121576; 9780471121572.

Jeffrey P. Slotnick, Abdollah Khodadoust, Juan J. Alonso, David L. Darmofal, William Gropp, Elizabeth A. Lurie, and Dimitri J. Mavriplis. Cfd vision 2030 study: A path to revolutionary computational aerosciences. 2014.

Bjorn Stevens and Donald H. Lenschow. Observations, experiments, and large eddy simulation. *Bulletin of the American Meteorological Society*, 82(2):283 – 294, 2001. . URL https://journals.ametsoc.org/view/journals/bams/82/2/1520-0477_2001_082_0283_oeales_2_3_co_2.xml.

R. Stoffer, C. M. van Leeuwen, D. Podareanu, V. Codreanu, M. A. Veerman, M. Janssens, O. K. Hartogensis, and C. C. van Heerwaarden. Development of a large-eddy simulation subgrid model based on artificial neural networks: a case study of turbulent channel flow. *Geoscientific Model Development*, 14(6):3769–3788, 2021. . URL https://gmd.copernicus.org/articles/14/3769/2021/.

Á. Tanarro, R. Vinuesa, and P. Schlatter. Effect of adverse pressure gradients on turbulent wing boundary layers. *Journal of Fluid Mechanics*, 883:A8, 2020. .

T. G. Tillman and A. L. Kistler. Scaling of the bursting frequency for turbulent boundary layers approaching separation. *AIAA Journal*, 34(5):1070–1072, 1996. . URL https://doi.org/10.2514/3.13189.

Aurélien Vadrot, Xiang I. A. Yang, and Mahdi Abkar. Survey of machine-learning wall models for large-eddy simulation. *Phys. Rev. Fluids*, 8:064603, Jun 2023. . URL https://link.aps.org/doi/10.1103/PhysRevFluids.8.064603.

John C. Vassilicos. Beyond scale-by-scale equilibrium. *Atmosphere*, 14(4), 2023. ISSN 2073-4433. . URL https://www.mdpi.com/2073-4433/14/4/736.

R. Vinuesa, P.S. Negi, M. Atzori, A. Hanifi, D.S. Henningson, and P. Schlatter. Turbulent boundary layers around wing sections up to rec=1,000,000. *International Journal of Heat and Fluid Flow*, 72:86–99, 2018. ISSN 0142-727X. . URL https://www.sciencedirect.com/science/article/pii/S0142727X17311426.

Ricardo Vinuesa, Ramis Örlü, Carlos Sanmiguel Vila, Andrea Ianiro, Stefano Discetti, and Philipp Schlatter. Revisiting history effects in adverse-pressure-gradient turbulent boundary layers. *Flow, Turbulence and Combustion*, 99(3):565–587, 2017. . URL https://link.springer.com/article/10.1007/s10494-017-9845-7.

P. S. Volpiani et al. A comprehensive study about implicit/explicit large-eddy simulations with implicit/explicit filtering. *Flow, Turbulence and Combustion*, 114(1): 1–25, 2024. . URL https://link.springer.com/article/10.1007/s10494-024-00577-9.

Limin Wang, Ruifeng Hu, and Xiaojing Zheng. A scaling improved inner–outer decomposition of near-wall turbulent motions. *Physics of Fluids*, 33(4):045120, 2021. . URL https://doi.org/10.1063/5.0046502.

Frank W. Warner. *Foundations of Differentiable Manifolds and Lie Groups*, volume 94 of *Graduate Texts in Mathematics*. Springer, 1983. ISBN 978-0-387-90894-6. .

Gabriel D. Weymouth. Data-driven multi-grid solver for accelerated pressure projection. *Computers & Fluids*, 246:105620, 2022. ISSN 0045-7930. . URL https://www.sciencedirect.com/science/article/pii/S0045793022002213.

Gabriel D. Weymouth and Bernat Font. Waterlily.jl: A differentiable and backend-agnostic julia solver for incompressible viscous flow around dynamic bodies. *Computer Physics Communications*, 315:109748, 2025. ISSN 0010-4655. . URL https://www.sciencedirect.com/science/article/pii/S0010465525002504.

G.D. Weymouth and Dick K.P. Yue. Boundary data immersion method for cartesian-grid simulations of fluid-body interaction problems. *Journal of Computational Physics*, 230(16):6233 – 6247, 2011. ISSN 0021-9991. . URL https://doi.org/10.1016/j.jcp.2011.04.022.

Michael Whitmore, Adrián Lozano-Durán, and Parviz Moin. Requirements and sensitivity analysis of rans-free wall-modeled les. *Centre for Turbulence Research Annual Briefs*, 12 2020.

Cameron Witkowski, Stephen Brown, and Kevin Truong. On the precise link between energy and information. *Entropy*, 26(3), 2024. ISSN 1099-4300. . URL https://www.mdpi.com/1099-4300/26/3/203.

Peng Wu and Johan Meyers. A constraint for the subgrid-scale stresses in the logarithmic region of high reynolds number turbulent boundary layers: A solution to the log-layer mismatch problem. *Physics of Fluids*, 25(1):015104, 2013. . URL https://doi.org/10.1063/1.4774344.

Xiang I. A. Yang, George Ilhwan Park, and Parviz Moin. Log-layer mismatch and modeling of the fluctuating wall stress in wall-modeled large-eddy simulations. *Phys. Rev. Fluids*, 2:104601, Oct 2017. . URL https://link.aps.org/doi/10.1103/PhysRevFluids.2.104601.

H. Yao, P. K. Yeung, T. A. Zaki, and C. Meneveau. Forward and inverse energy cascade in fluid turbulence adhere to kolmogorov's refined similarity hypothesis. *Phys. Rev. Lett.*, 132:164001, Apr 2024. . URL https://link.aps.org/doi/10.1103/PhysRevLett.132.164001.